Investigation of natural halogenated volatile organic compounds in the Amazon rainforest

Dissertation

Zur Erlangung des akademischen Grades

“Doctor rerum naturalium” (Dr. rer. nat.)

der Fachbereiche:

08 – Physik, Mathematik und Informatik

09 - Chemie, Pharmazie, Geographie und Geowissenschaften

10 - Biologie

Universitätsmedizin

verfasst und vorgelegt von

Simon Christoph Hartmann

geb. in Remscheid

Mainz, 02.10.2024

MAX PLANCK INSTITUTE FOR CHEMISTRY

JOHANNES GUTENBERG UNIVERSITÄT MAINZ

Max Planck Graduate Center mit der Johannes Gutenberg-Universität

Date of the oral exam: 29.11.2024

I hereby declare that I wrote the dissertation submitted without any unauthorized external assistance and used only sources acknowledged in the work. All textual passages which are appropriated verbatim or paraphrased from published and unpublished texts as well as all information obtained from oral sources are duly indicated and listed in accordance with bibliographical rules. In carrying out this research, I complied with the rules of standard scientific practice as formulated in the statutes of Johannes Gutenberg-University Mainz to ensure standard scientific practice.

Mainz, 02.10.2024 _____

Throughout most parts of this work, I used ChatGPT[1], DeepL[2], and Grammarly[3] for language and structure-related assistance. In compliance with the guidelines of Johannes Gutenberg University Mainz[4], I have consulted with my supervisor and the institute's ombudsperson to ensure that all AI usage in this work adheres to good scientific practice. I have not used AI tools for generating ideas or original content. Instead, I employed the mentioned AI tools solely for linguistic improvements, paraphrasing, editing, translation of text passages, and assistance with text structure. Fully aware of the strengths and limitations of AI tools, I used them responsibly, ensuring the integrity of my work by not relying on their content-related output. When ChatGPT was consulted on specific topics, its outputs were carefully compared with my own research in the same manner as traditional internet research.

[1] **ChatGPT**: OpenAI. (2023). *ChatGPT* (GPT-4). Retrieved from https://chat.openai.com/
[2] **DeepL**: DeepL SE. *DeepL Translator and DeepL Write*. Retrieved from https://www.deepl.com/translator and https://www.deepl.com/de/write
[3] **Grammarly**: Grammarly Inc. *Grammarly for MS Office*. Retrieved from https://www.grammarly.com/
[4] **JGU Mainz**: *KI in der Hochschulbildung | Digitale Lehre*. https://digitale-lehre.uni-mainz.de/lehren-pruefen/ki-in-der-hochschulbildung/ and https://acrobat.adobe.com/id/urn:aaid:sc:EU:8de9f7ca-06f4-4f99-8cdf-9117f56c9698, last access: 23 September 2024.

I have not failed. I've just found 10,000 ways that won't work.

Thomas Alva Edison (1847-1931)

Abstract

Halogenated volatile organic compounds (XVOCs) form a compound class that impacts our atmosphere on many different scales. From a global perspective, the most important aspects of XVOCs are their ability to deplete stratospheric ozone and their global warming potential. While the most dangerous compounds in this respect, chlorofluorocarbons (CFCs), are exclusively of anthropogenic origin (i.e. produced by human activities) and their production has now been banned, the focus of research has shifted to naturally formed XVOCs.

The Amazon rainforest is of great importance for natural XVOCs in several respects: first, tropical plants are considered the largest source of some XVOCs, including chloromethane (CH_3Cl), the most important naturally formed XVOC. Secondly, the XVOCs emitted in the tropics are particularly important as they can reach the upper troposphere and subsequently the stratosphere relatively quickly due to frequent deep convection. This makes them relatively more harmful for stratospheric ozone depletion than if emitted at higher latitudes. Thirdly, the fact that local anthropogenic influences and emissions can be excluded when measuring XVOCs in a remote location such as the Amazon rainforest is added to the reasons already mentioned. On one hand, this ensures that detected changes in XVOC abundances can be traced back to natural emissions or sinks. On the other hand, it enables monitoring of the atmospheric background of long-lived anthropogenic XVOCs such as CFCs and thus complements existing global monitoring networks such as those of the Advanced Global Atmospheric Gases Experiment (AGAGE) or the National Oceanic and Atmospheric Administration (NOAA).

In this dissertation, XVOCs in the Amazon rainforest ecosystem are considered from different perspectives. A first study investigated the triple-element stable isotope composition (^2H, ^{13}C, ^{37}Cl) of chloromethane formed and degraded by plants. Experiments with the royal fern (*Osmunda regalis*) provided the first complete isotopic fingerprint of chloromethane emissions of this kind. At the same time, isotopic analysis of chloromethane precursors relevant for formation by plants indicated minimal changes in hydrogen and chlorine isotopic ratios during formation, simplifying future isotopic predictions. This is an important finding as determining the isotopic composition of an XVOC offers the potential to differentiate between different sources and sinks and to quantify their respective strengths. In the case of chloromethane, there are large uncertainties in its global budget with reported sinks outweighing the sources, which indicates that the formation and degradation processes are not fully understood yet. This is supported by the fact that degradation experiments with a club moss (*Selaginella kraussiana*) revealed substantial isotopic fractionation across all three elements, suggesting a previously unrecognized biotic degradation mechanism. The findings from this study offer valuable insights for isotope-based models aimed at improving the accuracy of the global chloromethane budget.

The second study presented in this dissertation investigated two halogenated very short-lived substances (VSLSs), chloroform and bromoform, at the Amazon Tall Tower Observatory (ATTO) research site in central Amazonia. The underlying method was ambient air sampling on adsorbent-filled tubes and subsequent thermodesorption and analysis with a GC-ToF-MS setup. Chloroform abundances within the canopy showed comparable medians throughout three different seasons, with significant spikes in abundance observed during the transitional and wet seasons. Elevated tower measurements (80 m and 320 m) indicated that emissions follow a diel pattern, peaking at midday and decreasing overnight and that these emissions originate from ground level. Soil flux measurements confirmed the soil to be a chloroform source throughout all seasons. Bromoform levels displayed weaker local source indications compared to chloroform. Nonetheless, slight diel

cycles and occasional spikes point to potential local bromoform sources. In summary, this study hypothesizes chloroform levels of the ambient air in the Amazon rainforest to be primarily influenced by local sources, while bromoform levels are more affected by long-range transport. The detected seasonal variations emphasize the need for further investigations on the impact of El Niño-Southern Oscillation (ENSO) anomalies on local emissions.

The third part of this dissertation describes the method development and resulting setup of a cryogen-free air preconcentration unit coupled to a GC-MS system at ATTO. This is the first attempt to implement such a setup in the middle of a tropical rainforest, and it serves several objectives. First, it enables the acquisition of long-term in situ XVOC data in the Amazon rainforest. Secondly, the abundance of a whole range of XVOCs at different heights of the ATTO tower can be measured, from ground level up to 320 m above ground. It therefore provides the potential to identify local sources and sinks, to determine diel and seasonal fluctuations, and to estimate the net fluxes of the Amazon rainforest ecosystem. Thirdly, the setup aims to complement campaign-based measurements of single XVOC sources and sinks. First results are presented as a proof of concept and method validation, potential sources of error are discussed in detail, and future modifications and applications are suggested.

Zusammenfassung

Halogenierte flüchtige organische Verbindungen (XVOCs) bilden eine Stoffklasse, die unsere Atmosphäre auf vielen verschiedenen Ebenen beeinflusst. Aus globaler Sicht sind die wichtigsten Aspekte der XVOCs ihre Fähigkeit, stratosphärisches Ozon abzubauen, sowie ihr Treibhauspotenzial. Während die in dieser Hinsicht gefährlichsten Verbindungen, die Fluorchlorkohlenwasserstoffe (FCKW), ausschließlich anthropogenen Ursprungs sind (d. h. durch menschliche Aktivitäten erzeugt werden) und ihre Herstellung inzwischen verboten wurde, hat sich der Schwerpunkt der Forschung inzwischen auf natürlich gebildete XVOC verlagert.

Der Amazonas-Regenwald ist für natürliche XVOCs in mehrfacher Hinsicht von großer Bedeutung: Erstens gelten tropische Pflanzen als die größte Quelle einiger XVOCs, einschließlich Chlormethan (CH_3Cl), dem wichtigsten natürlich gebildeten XVOC. Zweitens sind die in den Tropen emittierten XVOCs von besonderer Bedeutung, da sie aufgrund der hier häufig auftretenden Tiefenkonvektion relativ schnell die obere Troposphäre und anschließend die Stratosphäre erreichen können. Dadurch sind sie für den stratosphärischen Ozonabbau relativ schädlicher, als wenn sie in höheren Breiten emittiert werden. Drittens kommt zu den bereits genannten Gründen die Tatsache hinzu, dass bei der Messung von XVOCs an einem abgelegenen Ort wie dem Amazonas-Regenwald lokale anthropogene Einflüsse und Emissionen ausgeschlossen werden können. Dadurch wird einerseits sichergestellt, dass festgestellte Veränderungen in den XVOC-Gehalten auf natürliche Emissionen oder Senken zurückgeführt werden können. Andererseits ermöglicht es die Überwachung des atmosphärischen Hintergrunds von langlebigen anthropogenen XVOCs wie FCKW und ergänzt damit bestehende globale Überwachungsnetze wie wie die des Advanced Global Atmospheric Gases Experiment (AGAGE) oder der National Oceanic and Atmospheric Administration (NOAA).

In dieser Dissertation werden XVOCs im Ökosystem des Amazonas-Regenwaldes aus verschiedenen Perspektiven betrachtet. Eine erste Studie untersuchte die stabile Isotopenzusammensetzung (^{2}H, ^{13}C, ^{37}Cl) von Chlormethan, das von Pflanzen gebildet und abgebaut wird. Experimente mit dem Königsfarn (*Osmunda regalis*) lieferten den ersten vollständigen isotopischen Fingerabdruck von Chlormethanemissionen dieser Art. Gleichzeitig zeigte die Isotopenanalyse von Chlormethan-Vorläufern, die für die Bildung durch Pflanzen relevant sind, dass sich die Wasserstoff- und Chlor-Isotopenverhältnisse während der Bildung nur minimal ändern, was künftige Isotopenvorhersagen vereinfacht. Dies ist eine wichtige Erkenntnis, da die Bestimmung der Isotopenzusammensetzung eines XVOC die Möglichkeit bietet, zwischen verschiedenen Quellen und Senken zu unterscheiden und deren jeweilige Stärke zu quantifizieren. Im Fall von Chlormethan gibt es große Unsicherheiten bezüglich des globalen Budgets, wobei die berichteten Senken die Quellen überwiegen, was darauf hindeutet, dass die Entstehungs- und Abbauprozesse noch nicht vollständig verstanden sind. Dies wird durch die Tatsache untermauert, dass bei Abbauexperimenten mit einem Moosfarn (*Selaginella kraussiana*) eine erhebliche Isotopenfraktionierung bei allen drei Elementen festgestellt wurde, was auf einen bisher nicht erkannten biotischen Abbaumechanismus hindeutet. Die Ergebnisse dieser Studie bieten wertvolle Erkenntnisse für isotopenbasierte Modelle zur Verbesserung der Genauigkeit des globalen Chlormethanhaushalts.

Die zweite in dieser Dissertation vorgestellte Studie untersuchte zwei halogenierte sehr kurzlebige Substanzen (VSLS), Chloroform und Bromoform, an der Forschungsstation des Amazon Tall Tower Observatory (ATTO) in Zentralamazonien. Die zugrundeliegende Methode war die Beprobung von Umgebungsluft auf mit Adsorptionsmitteln gefüllten Edelstahlröhrchen und die anschließende Thermodesorption und Analyse mit einem GC-ToF-MS-System. Die Chloroformgehalte der Umgebungsluft innerhalb der Baumkronen zeigten vergleichbare Mittelwerte über drei

verschiedene Jahreszeiten hinweg, wobei in der Übergangs- und Regenzeit kurzzeitige Spitzenwerte beobachtet wurden. Messungen von höheren Ebenen des Turms (80 m und 320 m) ergaben, dass die Emissionen einem tageszeitlichen Muster folgen, mit den höchsten Gehalten gegen Mittag und niedrigeren Gehalten über Nacht, und dass diese Emissionen von Bodennähe ausgehen. Direkte Messungen von Bodenemissionen bestätigten, dass der Boden zu allen Jahreszeiten eine Chloroformquelle ist. Die Bromoformwerte zeigten im Vergleich zu Chloroform schwächere Hinweise auf eine lokale Quelle. Dennoch deuten schwach ausgeprägte Tageszyklen und gelegentliche Spitzenwerte auf mögliche lokale Bromoformquellen hin. Zusammenfassend geht diese Studie davon aus, dass die Chloroformgehalte der Umgebungsluft im Amazonas-Regenwald in erster Linie durch lokale Quellen beeinflusst werden, während die Bromoformgehalte eher durch den Transport von Luftmassen aus größerer Entfernung beeinflusst werden. Die festgestellten saisonalen Schwankungen unterstreichen die Notwendigkeit weiterer Untersuchungen zu den Auswirkungen von Anomalien der El Niño-Southern Oscillation (ENSO) auf lokale Emissionen.

Der dritte Teil dieser Dissertation beschreibt die Methodenentwicklung und den daraus resultierenden Aufbau einer kryogenfreien Luftanreicherungseinheit, die mit einem GC-MS-System an ATTO gekoppelt ist. Dies ist der erste Versuch, eine solche Anlage inmitten eines tropischen Regenwaldes zu implementieren, und sie dient mehreren Zielen. Erstens ermöglicht es die Erfassung langfristiger in situ XVOC-Daten im Amazonas-Regenwald. Zweitens kann die Häufigkeit einer ganzen Reihe von XVOCs in verschiedenen Höhen des ATTO-Turms gemessen werden, vom Boden aus bis in eine Höhe von 320 m über Grund. Dies bietet die Möglichkeit, lokale Quellen und Senken zu identifizieren, die tages- und jahreszeitlichen Schwankungen zu bestimmen und die Nettoflüsse des Ökosystems Amazonas-Regenwald abzuschätzen. Drittens zielt der Aufbau darauf ab, kampagnenbasierte Messungen einzelner XVOC-Quellen und -Senken zu ergänzen. Erste Ergebnisse werden als Machbarkeitsnachweis und zur Validierung der Methode vorgestellt, potenzielle Fehlerquellen werden ausführlich erörtert, und es werden künftige Änderungen und Anwendungen vorgeschlagen.

Contents

Abstract ..... **vii**

Zusammenfassung ..... **ix**

1 Introduction **1**

1.1 General Overview of the Earth's Atmosphere 2

1.2 (Biogenic) Volatile Organic Compounds 3

1.3 Halogenated Volatile Organic Compounds (XVOCs) 4

1.3.1 Sources 5

1.3.2 Sinks and Atmospheric Fate 7

1.3.3 Stratospheric Ozone Depletion 8

1.4 Why We Measure XVOCs in the Heart of the Amazon Rainforest 9

1.5 Research Objectives and Thesis Outline 10

1.6 References 12

2 Triple-Element Stable Isotope Analysis of CH_3Cl Emission and Degradation by Plants 19

2.1 Abstract 20

2.2 Plain Language Summary 20

2.3 Introduction 21

2.4 Materials and Methods 23

2.4.1 Sampling of Rainwater and Conversion of Chloride to CH_3Cl 23

2.4.2 Plant Sampling and Incubation Experiments 23

2.4.3 Quantification of CH_3Cl 24

2.4.4 Stable Hydrogen and Stable Carbon Isotope Analysis of CH_3Cl 25

2.4.5 Stable Chlorine Isotope Analysis of CH_3Cl 25

2.4.6 Stable Carbon and Hydrogen Isotope Analysis of Plant Methoxy Groups 25

2.4.7 Reporting Isotopic Compositions and Isotopic Fractionation 26

2.5 Results and Discussion 27

2.5.1 Emission Rates and Isotopic Composition of CH_3Cl by *Osmunda regalis* 27

2.5.2 Degradation and Isotopic Fractionation of CH_3Cl by *Selaginella Kraussiana* 32

2.6 Implications 35

2.7 Data Availability Statement 36

2.8 Acknowledgements 36

2.9 References 36

3 Investigation of Local Sources of the Halogenated Very Short-Lived Substances Chloroform and Bromoform 41

3.1 Introduction 42

3.2 Sampling and Analysis 43

3.2.1 Sample Collection 43
3.2.2 Analytical Setup 44
3.3 Results and Discussion 45
3.3.1 Volume Mixing Ratios at Canopy Height 45
3.3.2 ATTO Data from January 2023 50
3.3.3 Soil Flux Data 52
3.4 Summary and Conclusions 53
3.5 References 54
4 Establishment of a Setup for Long-Term Online Measurements of Halogenated VOCs in the Amazon Rainforest 61
4.1 Introduction 62
4.2 Motivation for the Method Specifics 63
4.2.1 Benefits of the ATTO Site 63
4.2.2 Comparison: Continuous In Situ Measurements vs. Adsorbent Tubes 63
4.2.3 Comparison of Cryogenic and Cryogen-Free Preconcentration Units 65
4.3 Final Instrumental Setup 67
4.3.1 Inlet System 67
4.3.2 Preconcentration System 68
4.3.3 Gas Chromatography (GC) 71
4.3.4 Mass Spectrometry (MS) 72
4.3.5 Calibration Method 75
4.3.6 Error Assessment 78
4.4 Method Development – from an Idea to Realization 78
4.5 Proof of Concept and First Results 80
4.5.1 Comparison of Chloromethane and CFC-12 Data 80
4.5.2 Potential Sources of Error 81
4.5.3 Correction Method 83
4.5.4 Isoprene Data Validates the Resolution of Potential Diel Fluctuations 85
4.6 Analytical Outlook 86
4.7 Scientific Outlook 86
4.8 References 87
5 Conclusions and Future Perspectives 89
Appendices 93
Supplementary Material 93
S.1 Back-Trajectories 93
S.2 Incubation Experiments with *S. kraussiana* and *O. regalis* 96

S.3 Stable Isotope Blank and Control Experiments 99
List of Figures 100
List of Tables 103
Abbreviations and Acronyms 104
List of Publications: S. C. Hartmann 108

1 Introduction

Halogenated volatile organic compounds (XVOCs) constitute a key category of substances within the atmosphere. As trace constituents, they only make a limited contribution to the bulk atmosphere in terms of mass. However, their presence can significantly impact atmospheric processes across various levels, exerting influences from local to global scales. Comprehending the significance and fate of these XVOCs necessitates a deep understanding of the atmospheric composition and structure and the processes that govern it.

1.1 General Overview of the Earth's Atmosphere

Today's atmosphere is the result of circa 4.5 billion years of Earth's history. Many different geological and biological processes have been involved in its evolution and continue to exert influences today, e.g. volcanism, photosynthesis, biological degradation of organic matter, burning activities, and photochemistry. As the formation of the atmosphere could fill an entire book, only some main processes will be discussed further here. This dissertation aims to give a better understanding of the status quo and prospects of some of the current processes that shape the atmosphere.

The bulk composition of the dry atmosphere is given in **Table 2-1**. The differentiation between dry and wet atmosphere (including water vapor) is important, as the presence of water vapor can vary largely over time and space from almost 0 % in desert regions up to nearly 4 % in the humid tropics (*U.S. Standard Atmosphere*, 1976).

Table 1-1. *Principal gas composition of dry air at sea level*

Gas	Formula	Mixing ratio
Nitrogen	N_2	78.084 %
Oxygen	O_2	20.948 %
Argon	Ar	0.934 %
Carbon Dioxide	CO_2	417 ppmv
Neon	Ne	18.18 ppmv
Helium	He	5.24 ppmv
Methane	CH_4	1.91 ppmv
Krypton	Kr	1.14 ppmv

Note. Data from *U.S. Standard Atmosphere*, 1976. Carbon Dioxide data from Lan et al., 2024a. Methane data from Lan et al., 2024b

The atmosphere can be divided into five principal layers (from high to low): exosphere, thermosphere, mesosphere, stratosphere, and troposphere. This stratification is determined mostly by temperature and pressure. The outer layers (exosphere, thermosphere, mesosphere) are less well studied because of the difficulty of access and because they have less tangible impact on our everyday lives. The layer where most of Earth's weather phenomena take place is the troposphere, as it contains most of the atmospheric water vapor. It begins above the earth's surface and extends on average up to 12 km, with large variations between the poles (7 km) and the tropics (17 km) (Reichle, 2023). The temperature within the troposphere is highest at sea level (average 15 °C; (Andrews, 2010)) and decreases at 6.5 K km^{-1} due to adiabatic cooling of air during convection (Visconti, 2016), resulting in a temperature of about -60 °C in the upper troposphere (Schlesinger and Bernhardt, 2020).

The decrease in temperature with height within the troposphere is in contrast to the layer above: In the stratosphere, temperature rises with height. This is because of high ozone (O_3)

concentrations in this layer. The ozone absorbs energy from the solar UV radiation, which in turn is imparted to the surrounding molecules in the form of heat (Schlesinger and Bernhardt, 2020; Warneck and Williams, 2012). Because the highest parts of the stratosphere absorb most of the UV radiation, the highest temperatures are within the upper stratosphere. This increase in temperature with altitude leads to stable stratification in the stratosphere, which hinders the vertical mixing of air masses. The same temperature gradient impedes a mixing between the troposphere and stratosphere. The resulting stable layer between the troposphere and stratosphere is called the tropopause. Since it acts as a barrier, it marks a transition in the chemical composition of the atmosphere.

1.2 (Biogenic) Volatile Organic Compounds

The troposphere as the lowest layer is the most complex one regarding its chemical composition. This is not so much because of the composition of the principal gases, as those are well mixed within the homosphere (= layer of the atmosphere in which turbulent mixing is the dominant driver of transport; from the surface up to about 100 km, including the troposphere, stratosphere and mesosphere (Warneck and Williams, 2012)) and are chemically fairly inert. It is the trace gases that influence atmospheric chemistry the most.

Trace gases are, as their name suggests, low-concentration gases in the atmosphere. One important class of trace gases is the volatile organic compounds (VOCs). Despite a missing universal definition, VOCs are generally considered organic compounds with a high vapor pressure and consequently a low boiling point at atmospheric pressure. The term organic means a molecule containing carbon and the term compound indicates a stable entity rather than a radical species. There are numerous definitions of VOCs based on various boiling point or vapor pressure ranges and multiple subclass designations. Some common specific terms for these subclasses of VOCs exist, not all of which are relevant to this work but the most common should be mentioned for the sake of completeness, without claiming to be exhaustive:

NMVOC stands for non-methane VOCs and specifies the exclusion of methane from this compound class. Generally, CO_2, CH_4, and CO are not included in the VOCs definition at all as they have much longer lifetimes and are therefore more abundant. These species are investigated individually (Koppmann, 2007). TVOCs is often used in the perspective of indoor quality and stands for total VOCs (in terms of concentration; Molhave et al., 1997). The World Health Organization (WHO) distinguishes VOCs according to their boiling points into very volatile organic compounds (VVOCs), VOCs, and semi-volatile organic compounds (SVOCs) (WHO, 1989). In general, VOCs can include alkanes, alkenes, alkynes, ketones, alcohols, aldehydes, acids, and other oxygenated compounds. If referring only to compounds containing an oxygen atom (as an acid, carbonyl, or alcohol group), the term OVOCs (= oxygenated VOCs) is used.

Some VOC definitions are made from the point of view of their origin. This applies to regions with major problems with air quality like India and China, which focus more on VOCs from various anthropogenic sources (AVOCs), rather than those originating from natural biogenic processes (BVOCs). However, more than 1700 BVOCs were identified in plants (Knudsen et al., 2006). Some researchers estimate the number of measured BVOCs to be much higher, at several tens of thousands, with hundreds of thousands not yet identified (Goldstein and Galbally, 2007). BVOCs dominate global VOC emissions, namely 1019 Tg (VOC) yr^{-1} (Sindelarova et al., 2014) compared to 147 Tg (NMVOC) yr^{-1} of AVOCs (Xiong et al., 2024); although both numbers have large associated uncertainties. Despite the great chemical diversity of BVOCs, only a few of them contribute significantly to global BVOC emissions, and these include isoprene (69.2 % relative contribution to

global emissions), monoterpenes (10.9 %), methanol (6.4 %), acetone (3.0 %) and sesquiterpenes (2.4 %) (Sindelarova et al., 2014).

BVOCs play an important role in plant biology. It has been suggested that plants emit isoprene to improve thermotolerance, i.e., isoprene emissions (C_5H_8) from leaves reduce heat stress and regulate leaf temperature (Loreto and Schnitzler, 2010; Sasaki et al., 2007; Sharkey et al., 2007). Furthermore, isoprene can function as an antioxidant and protect the plant's cells from damage by reactive oxygen species (ROS) (Loreto and Velikova, 2001; Vickers et al., 2009). Isoprene is synthesized de novo, which means that it is emitted right after its synthesis. The so-called monoterpenes ($C_{10}H_{16}$) form the second most important BVOC compound class. They are derived from C_5 isoprene molecules (a hemiterpene) as structural building blocks, following the biogenetic isoprene rule (Ruzicka, 1953), and are classified according to the number of isoprene units they contain: Monoterpenes contain two isoprene units ($C_{10}H_{16}$), sesquiterpenes contain three units ($C_{15}H_{24}$) and diterpenes four units ($C_{20}H_{32}$). This scheme can be continued indefinitely, finally leading to polyisoprene (i.e., natural rubber).

Due to decreasing volatility with increasing mass, the smaller compounds (mono-, sesqui-, and to some extent diterpenes) are more readily released into the gaseous phase. In contrast to isoprene, some volatile terpenes can be stored within the leaf after synthesis and emitted later, although some de-novo emissions of monoterpenes have also been measured (e.g., Byron et al., 2022). It is postulated that isoprene and some terpenes are merely byproducts of a synthetic pathway that leads to the formation of more essential, non-volatile isoprenoids, e.g., plant hormones (Owen and Peñuelas, 2005). However, terpenes serve multifaceted roles within emitting plants. In addition to their protective function against reactive oxygen compounds such as hydroxyl radicals (OH) and ozone, they also serve as signaling substances, being emitted in response to mechanical stress or as a defense mechanism against herbivores or microbes (Dicke and Baldwin, 2010; Rasmann et al., 2005; Scutareanu et al., 1997; Unsicker et al., 2009). In this way, volatile organic compounds (VOCs) function as natural messengers in inter-plant communication (Šimpraga et al., 2019), attracting pollinators (Raguso et al., 2003), and even engaging in allelopathic interactions to suppress competing vegetation (Fischer et al., 1994).

As indicated previously, BVOCs appear in many chemical forms, e.g., alkenes, formic and acetic acid, benzenoid compounds, or oxygenated compounds. Their sources and sinks as well as their emission processes are described in detail elsewhere (Fall, 2003; Guenther, 2013; Kesselmeier and Staudt, 1999; Oikawa and Lerdau, 2013).

1.3 Halogenated Volatile Organic Compounds (XVOCs)

XVOCs are volatile organic compounds that contain at least one halogen atom (Dewulf et al., 2006). There are various ways of classifying them, e.g. according to their halogen content, the way they are formed (natural or anthropogenic), inorganic or organic forms, or their atmospheric lifetimes. Each of these classifications has its merit. This work will mainly use the classifications that depend on their formation processes and lifetime, focusing on naturally occurring XVOCs.

For the sake of completeness, and due to their importance for stratospheric ozone depletion (see 1.3.3 for more details), a brief digression on mainly or exclusively anthropogenic XVOCs at this point: Anthropogenic XVOCs include, among others, prominent compound classes like chlorofluorocarbons (CFCs) and hydrochlorofluorocarbons (HCFCs), which have been extensively used in refrigeration, air conditioning, and as propellants. Among the most abundant are CFC-11 and CFC-12, with mixing ratios of 224 pptv and 497 pptv, respectively (WMO, 2022). Their long total

atmospheric lifetimes (52 and 102 years, respectively (WMO, 2022)) make them highly persistent and allow them time to reach the stratosphere, where they contribute to the depletion of the ozone layer (see 1.3.3). This is why their production and use have been banned under the Montreal Protocol, leading to a gradual, but slow decrease in their atmospheric concentrations over the past few decades.

1.3.1 Sources

To date, around 8000 different natural organohalogen compounds have been described in the literature (Gribble, 2023). This large number of compounds is also accompanied by great diversity, as they can appear as halogenated C_1-Alkanes but also as complex steroids, for example. Of course, not all of these are volatile compounds (see VOC definitions in 1.2). Therefore, the subset of XVOCs includes mostly haloalkanes, halogenated monoterpenes, and some haloaromatics.

XVOCs can be formed in almost every environment there is: from volcanoes (Frische et al., 2006; Schwandner et al., 2013) to plants (Forczek et al., 2015; Yokouchi et al., 2002), from oceans (Stemmler et al., 2015) to soils (Redeker and Kalin, 2012), with formation through biotic and abiotic processes (Huber et al., 2009), emitted by living beings from bacteria (Amachi et al., 2001) to the human body (Keppler et al., 2017).

The complexity of the interplay of sources and sinks for natural XVOCs can be demonstrated using the example of chloromethane (CH_3Cl). Chloromethane is the most abundant natural XVOC with a global average mixing ratio of around 550 pptv and global annual emissions estimated to be around 4.7 Tg, contributing about 17 % to total tropospheric chlorine (WMO, 2022). Only minor anthropogenic sources are known (Li et al., 2017; Mead et al., 2008). The major natural source is tropical plants (Carpenter et al., 2014; Xiao et al., 2010), which are reported to account for emissions of 2200 ± 390 Gg per year (Xiao et al., 2010), even though recent estimates are significantly lower (Bahlmann et al., 2019). Other relevant sources are biomass burning (Lobert et al., 1999; Rudolph et al., 1995), Oceans (Khalil et al., 1999), wood-rotting fungi (Harper, 1985), and salt marshes (Rhew et al., 2000). Further details, references, and information on biochemical processes can be found in Chapter 2.

As shown in **Figure 1-1**, emission and uptake processes can often occur simultaneously in a system such as a soil or a plant. Therefore, it is difficult to identify single processes if only the net flux of an ecosystem is measured. Conversely, one cannot simply derive net fluxes by measuring only individual processes. Even though many sources and sinks are known and extensively investigated, the global chloromethane budget is not balanced, with known sinks outweighing the reported sources (Bahlmann et al., 2019; WMO, 2022). Over the last few years, more and more research has been carried out to tackle this issue using a stable isotope approach (Bahlmann et al., 2019; Keppler et al., 2020; Miller et al., 2004; Nadalig et al., 2013; Ojeda et al., 2020). Isotopes are atoms of the same element that have the same number of protons but different numbers of neutrons. This difference leads to varying atomic masses while the chemical properties remain largely similar. In contrast to radioisotopes that undergo radioactive decay over time, stable isotopes do not emit radiation or change into other elements through decay processes. Carbon, for example, has three isotopes: ^{12}C, ^{13}C (both stable isotopes), and ^{14}C (radioactive). By comparing the isotopic signature of a compound in different samples (i.e., measuring the sample's isotope ratio against a reference), one can therefore conclude on occurring (bio-)chemical reactions that can alter the isotopic signature of a compound in a sample. Here, one can distinguish between different chloromethane formation and

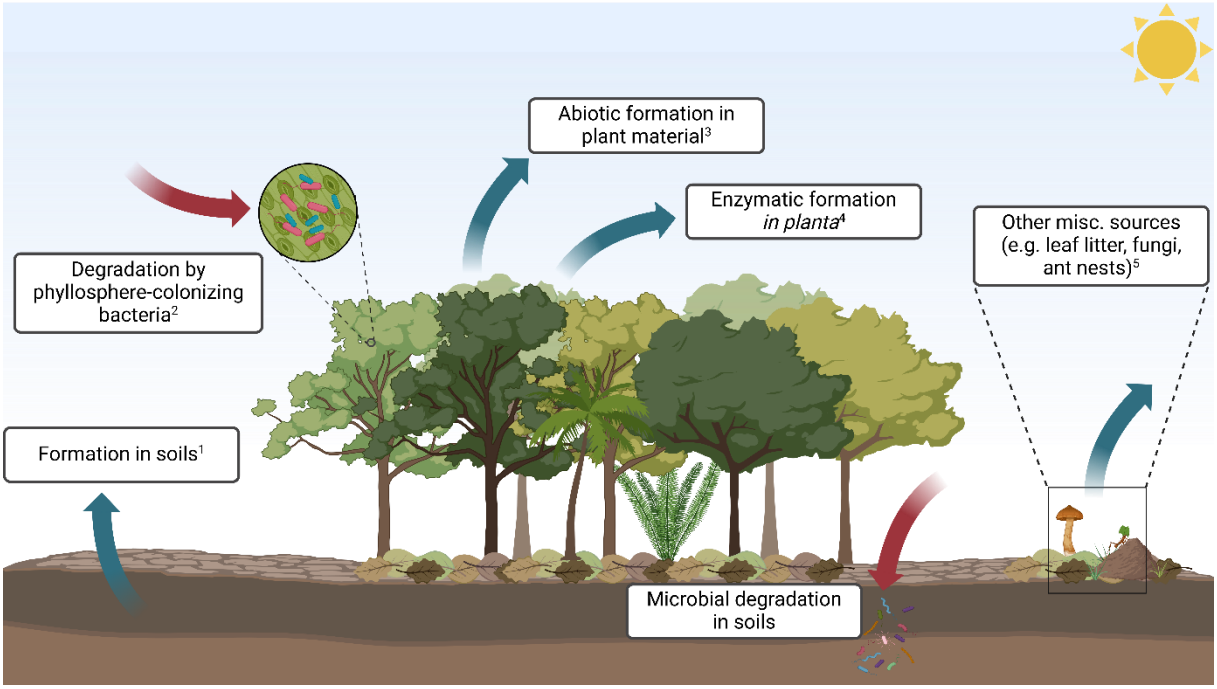

Figure 1-1. *Potential chloromethane sources and sinks in a forest ecosystem (atmosphere-plant-soil). Adapted from Keppler et al., 2020. References: [1]Keppler et al., 2000, [2]Nadalig et al., 2011, [3]Hamilton et al., 2003, [4]Jaeger et al., 2018b, [5]Blei et al., 2010, Anke and Weber, 2006, Berberich et al., 2017, [6]Jaeger et al., 2018a. Figure created in Biorender.com*

degradation processes by analyzing the stable isotope ratios $\delta^{2}H$, $\delta^{13}C$, and $\delta^{37}Cl$ of the resulting chloromethane, as every process produces distinct isotopic patterns. These measurements can help to estimate the total net sources and sinks of chloromethane by comparing the isotopic composition of the atmospheric chloromethane pool with known signatures from various sources and sinks, enabling a better understanding of the global chloromethane budget.

While chloromethane is a compound with mainly terrestrial sources, other natural XVOCs have their dominant sources within marine or coastal environments. This applies in particular, but not exclusively, for XVOCs containing bromine or iodine, as these elements are much less abundant in terrestrial environments compared to chlorine. Chloroform ($CHCl_3$) and bromoform ($CHBr_3$), also very important natural XVOCs and part of the subset of halogenated very short-lived substances (VSLS; atmospheric lifetime of less than 6 months), have predominantly marine sources, for example. See Chapter 3 for more detailed information on their respective sources.

1.3.2 Sinks and Atmospheric Fate

The atmospheric fate of XVOCs depends strongly on their atmospheric lifetimes. This is why one has to distinguish between long-lived XVOCs (atmospheric lifetime >0.5 years) and VSLSs (atmospheric lifetime <0.5 years). The source type (i.e., anthropogenic or natural) does not play a relevant role in this perspective (**Figure 1-2**). The already introduced VSLS example compounds, chloroform and bromoform, have total atmospheric lifetimes of about 180 days (chloroform; WMO, 2022) and tens of days (bromoform; Papanastasiou et al., 2014). This lifetime is, neglecting microbial degradation or uptake by oceans and soils, limited by the photochemical degradation of the compound in the troposphere, the most important factors of which are the reaction with the hydroxyl radical (OH) and photolysis (e.g. Krysztofiak et al., 2012). The chemistry of tropospheric degradation in turn depends on latitude, altitude, and season (Hossaini et al., 2019; Krysztofiak et al., 2012; von Glasow et al., 2004). Therefore, the atmospheric lifetime of VSLSs can vary considerably depending on the emission region. Tropospheric degradation of VSLSs results in different product gases, some of which are phosgene ($COCl_2$) or HCl for chlorinated VSLSs (Ko et al., 2003). A corresponding reaction mechanism is described in McCulloch, 2003.

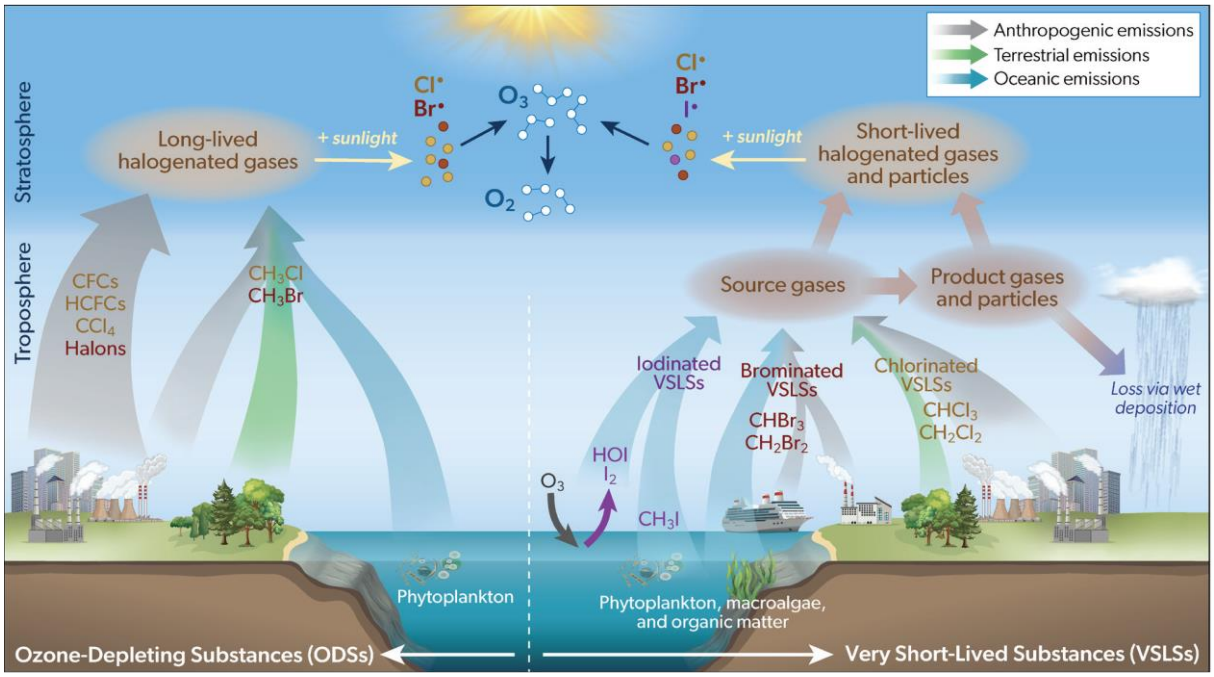

Figure 1-2. *Comparison of long-lived XVOCs and VSLSs concerning their respective sources and atmospheric fate. Taken from WMO, 2022 (Box 1-3 Figure 1).*

Long-lived XVOCs typically have slower degradation rates in the troposphere compared to VSLSs, as they are less susceptible to attack by OH radicals. Due to their lower reactivity, long-lived XVOCs have longer atmospheric lifetimes, ranging from several decades to over a century (WMO, 2022), allowing them to persist in the atmosphere, spread throughout the troposphere, and eventually reach the stratosphere without being significantly degraded in the troposphere. This is especially true for very inert compounds like CFCs. For other long-lived XVOCs, for example, chloromethane, the situation is more complex. Chloromethane does react with OH, which represents its main tropospheric loss process. The reaction with OH and the oxidation by Cl radicals in the marine boundary layer together account for about 70 % of tropospheric chloromethane loss (Keppler et al., 2020). However, this reaction is still much slower compared to VSLSs. Therefore, taking into account other smaller tropospheric loss processes, a small part of the emitted chloromethane is transported into the stratosphere. In the stratosphere, XVOCs eventually undergo photodissociation by UV radiation, which is their primary stratospheric sink (WMO, 2022).

1.3.3 Stratospheric Ozone Depletion

Through UV-induced photodissociation, XVOCs that reach the stratosphere can release halogen atoms such as chlorine and bromine. These halogen atoms then participate in the catalytic depletion of stratospheric ozone (O_3) through a series of reactions (Equations 1, 2, and 3 show this process for chlorine atoms; Molina and Rowland, 1974):

$$Cl + O_3 \rightarrow ClO + O_2 \qquad \textit{Equation 1}$$

$$ClO + O \rightarrow Cl + O_2 \qquad \textit{Equation 2}$$

$$O_3 + O \rightarrow 2O_2 \qquad \textit{Equation 3}$$

This catalytic ozone depletion cycle is terminated by the formation of more stable reservoir species. Halogen reservoir species mean that the reactive halogen atoms are converted into less reactive forms that do not directly participate in the catalytic depletion of ozone. The most important formation reactions for halogen reservoir species are Equations 4 and 5 (Molina and Rowland, 1974; Rowland et al., 1976).

$$Cl + CH_4 \rightarrow HCl + CH_3 \qquad \textit{Equation 4}$$

$$ClO + NO_2 + M \rightarrow ClONO_2 + M \qquad \textit{Equation 5}$$

However, these reservoir species can be also broken down eventually via UV photodissociation, releasing back the reactive halogens and reinitiating the ozone destruction process again. Due to differences in reservoir species formation reactions, bromine atoms are more effective than chlorine in depleting ozone, with bromine being up to 60 times more efficient in catalytic ozone depletion (Sinnhuber et al., 2009; Wayne et al., 1995). Therefore, despite their lower concentrations in the atmosphere, brominated compounds like halons and methyl bromide have a disproportionately large impact on ozone depletion.

The most important classes of compounds with respect to stratospheric ozone depletion are CFCs with their long atmospheric lifetime. As explained above, emitted CFCs reach the stratosphere with almost no losses in the troposphere as they do not react with OH. Their persistence means that these compounds have a long-term impact on stratospheric ozone once emitted to the atmosphere, delaying the recovery of ozone following the Montreal Protocol ban on CFCs (UNEP, 1987). However, VSLS can also contribute to stratospheric ozone depletion despite their shorter lifetime in the atmosphere (e.g., Liang et al., 2014). They can transport halogens into the stratosphere via two main pathways, source gas injection (SGI) and product gas injection (PGI) (Ko and Poulet, 2003): SGI is when VSLSs are directly transported to the stratosphere in their original, unreacted forms. As explained above, the shorter lifetime of VSLSs means they usually undergo degradation in the troposphere but in some cases, they can survive long enough to be carried upwards by strong vertical air currents, particularly during deep convection in the tropics. If emitted there, VSLSs are liable to be rapidly convected to the upper troposphere and then enter the stratosphere through the tropical upward branch of the Brewer-Dobson circulation (Aschmann, 2009; Fueglistaler et al., 2009).

In contrast, PGI involves the transport of the degradation products of VSLSs that have already undergone partial breakdown in the troposphere through photolysis or oxidation by OH. These products, if stable enough, are then transported upward into the stratosphere by atmospheric circulation. Once these halogenated product gases reach the stratosphere, they are further broken down by UV radiation, releasing reactive halogen atoms that take part in the catalytic ozone

depletion described above (Chipperfield and Pyle, 1998; Daniel et al., 1999). The effectiveness of PGI depends on factors like the lifetime of the degradation products, the altitude at which they are formed, and the dynamics of atmospheric transport. The role of PGI becomes particularly important when the VSLSs have short atmospheric lifetimes but produce stable intermediate products that can persist long enough to be transported to the stratosphere.

The discovery of the ozone hole over Antarctica in the 1980s (Farman et al., 1985; Stolarski et al., 1986) highlighted the devastating effects of halogenated compounds on the ozone layer. This depletion allows increased UV radiation to reach the Earth's surface, leading to higher risks of skin cancer, for example, as well as affecting ecosystems (Morgenstern et al., 2008; Newman et al., 2009). Ancient events such as the Siberian Trap volcanism (approx. 250 million years bp) are believed to have released massive amounts of halogenated compounds, leading to significant ozone depletion long ago in Earth's history (Beerling et al., 2007). In response to concerns that anthropogenic emissions of such compounds could similarly devastate the protective ozone layer, the Montreal Protocol was established in 1987, leading to the phase-out of many ozone-depleting substances, e.g., CFCs (UNEP, 1987). The CFCs were replaced with hydrochlorofluorocarbons (HCFCs) and subsequently with hydrofluorocarbons (HFCs), both of which were deliberately engineered to degrade in the troposphere by replacing some of the halogen atoms with hydrogen atoms. However, HCFCs and HFCs are still potent greenhouse gases, even though they pose less or no harm to the stratospheric ozone layer. As many halogenated VOCs have a high global warming potential, their regulation is critical not only for protecting the ozone layer but also for mitigating climate change (WMO, 2022).

1.4 Why We Measure XVOCs in the Heart of the Amazon Rainforest

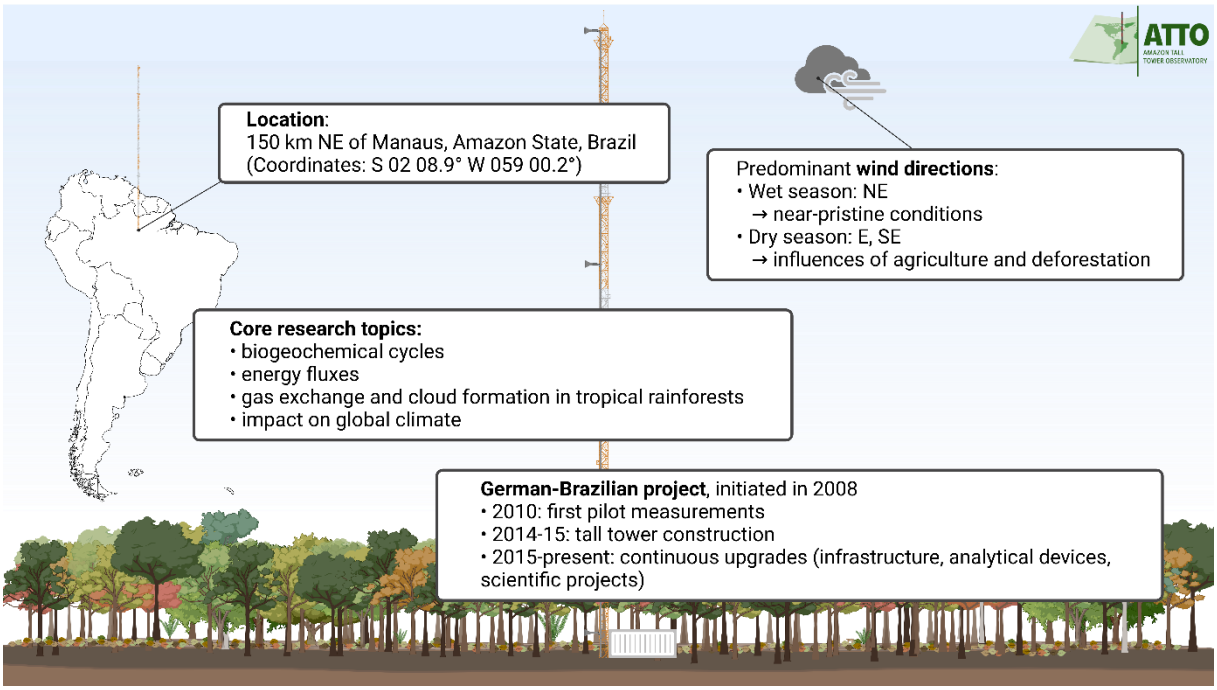

Figure 1-3.*ATTO site overview, including general key information derived from Andreae et al., 2015 and https://www.attoproject.org/. Figure created in Biorender.com*

The underlying main project of this work is the investigation of XVOCs in the Amazon rainforest (see Chapters 2 and 3). As indicated in the previous subchapters, the tropics play a prominent role with regard to XVOCs for various reasons. Chapter 1.3.1 states chloromethane emissions from tropical plants and biomass burning. However, the tropics are not only an interesting region in terms of XVOC sources but, as explained in Chapters 1.3.2 and 1.3.3, deep convection in the tropics

can lead to the rapid ascent of XVOCs and their respective product gases into the stratosphere, where they can deplete ozone.

The Amazon rainforest is the largest of the tropical rainforests, covering about 5.8 million km^2, containing over 10 % of all known species worldwide (Science Panel for the Amazon, 2021) with about 100 Pg carbon bound in biomass (Davidson et al., 2012). The Amazon Tall Tower Observatory (ATTO; see **Figure 1-3** for background information), located in central Amazonia, is a 325 m tall tower built to enable investigations of the interactions between the Amazon rainforest ecosystem and the atmosphere. Its location offers diverse measurements related to atmospheric chemistry with negligible anthropogenic influences (see Chapter 4).

Even though all the factors that make the Amazon rainforest highly relevant in terms of XVOC measurements, there are to date no long-term XVOC measurements carried out by global measurement networks such as AGAGE or NOAA (see **Figure 1-4**) in the whole of continental South America. Future continuous measurements at ATTO could therefore be a valuable complement.

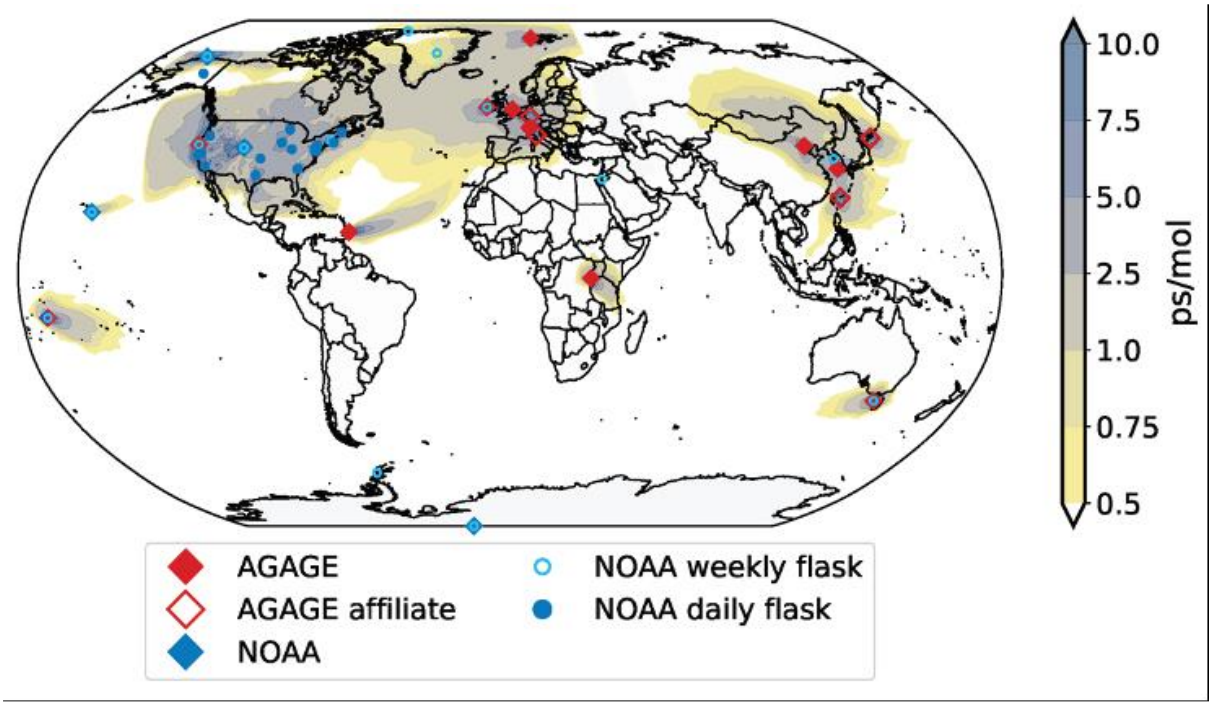

Figure 1-4. *Sampling sites for XVOC source and product gases from the NOAA and AGAGE networks, together with their respective mean footprints. Taken from WMO, 2022*

1.5 Research Objectives and Thesis Outline

The effects on different aspects of atmospheric chemistry, especially on stratospheric ozone depletion, make halogenated volatile organic compounds (XVOCs) an important compound class. The regulation and controlled phase-out of many anthropogenic XVOCs through the Montreal Protocol shifts the focus to natural XVOC sources and increases their relative importance. However, natural XVOC sources and sinks are far from being fully understood, as the example of the unbalanced budget of chloromethane sinks and sources shows (Bahlmann et al., 2019; WMO, 2022). Now that climate change is in full swing, impacting many ecosystems worldwide and potentially affecting XVOC budgets, it is even more important to understand the processes of XVOC formation and degradation to comprehend how climate change affects these processes. Only the use of different methods and instruments can provide insights into the complex interplay of XVOC sources and sinks, taking different perspectives into account. This idea of a holistic approach forms the basis of the present work:

Chapter 2 presents a study that investigates chloromethane formation and degradation pathways in plants as individual sources and sinks, using an approach of triple-element isotopic characterization of chloromethane. It provides the first triple-isotopic (^{2}H, ^{13}C, ^{37}Cl) fingerprint of chloromethane emitted by the royal fern (*Osmunda regalis*) and degraded by a club moss (*Selaginella kraussiana*). Even though the investigated plants are not distributed in the tropics but rather in temperate climates, the study fits within the scope of the present work as its results contribute to the development of isotope-based models that could improve our understanding of chloromethane sources and sinks. It furthermore provides a new approach to estimating the isotopic composition of chloromethane emissions from plants, potentially helping to distinguish between natural and anthropogenic sources.

A study on the abundance of the halogenated very short-lived substances (VSLS) chloroform and bromoform at the ATTO site is presented in Chapter 3. The research involved extensive measurements across three distinct seasons: a dry-to-wet transition (2023), a dry season (2023), and a full-wet season (2024). This approach used an adsorbent tube sampling technique with subsequent analysis with a Gas chromatography-time of flight-mass spectrometer (GC-ToF-MS) setup. Sampling was conducted within the rainforest canopy (23 m), at 80 m and 320 m height from the ATTO tall tower, as well as directly from the soil. The primary objectives were to investigate the presence of local sources of these VSLSs, potential diel cycles, and seasonal variations in their concentrations. The data collection during an El Niño Southern Oscillation (ENSO) event provided an additional layer of insight, particularly in the context of climate change, offering a unique perspective on how such climatic events might influence tropical rainforest emissions and the atmospheric behavior of these substances.

Chapter 4 is primarily a methodology chapter. It summarizes the arguments for the necessity of implementing a campaign-independent setup for on-line and in situ measurements of many different XVOCs directly within the Amazon rainforest. The focus is on the method development and the detailed description of the used instrumental setup in the form of a cryogen-free preconcentration unit coupled to a gas-chromatography mass spectrometer (GC-MS). First results serve as a proof of concept and show the potential of this setup to provide both, XVOC long-term on-line measurements from different heights of the ATTO tower to investigate net emissions of this ecosystem, as well as in situ measurements of individual local sources and sinks, e.g., plants, soils, or insect nests.

In summary, three separate but related projects have been pursued in this work to look at the investigation of halogenated VOCs in the Amazon rainforest from different perspectives. In these three projects, three different methods have been applied: Firstly, isotope ratio mass spectrometry was used to examine chloromethane formation and degradation in plants. This project focused on the investigation of ongoing processes within single sources and sinks. Secondly, the sampling of the halogenated very short-lived substances (VSLSs) chloroform and bromoform on adsorbent-filled cartridges from the ATTO research site and subsequent analysis with GC-ToF-MS gave insights into the regional and seasonal emission patterns of these compounds. Thirdly, the development and validation of a non-cryo preconcentration system coupled to GC-MS (quadrupole) should enable long-term in situ measurement of short- and long-lived XVOCs in the Amazon rainforest. Establishing a reliable, accurate, and long-term measurement system for XVOC in the pristine Amazon rainforest opens the possibility of discovering new sources and sinks and monitoring how ongoing climate change will affect emissions from the rainforest ecosystem. The information contained within this thesis spans many scales from in-plant processes to regional and seasonal emission characteristics of the Amazon rainforest, as well as the technical details of method development and set-up. The underlying objective of all these research approaches is to provide

modelers, the Intergovernmental Panel on Climate Change (IPCC), and policymakers with better knowledge of sources and sinks of XVOCs.

1.6 References

Amachi, S., Kamagata, Y., Kanagawa, T., Muramatsu, Y., 2001. Bacteria Mediate Methylation of Iodine in Marine and Terrestrial Environments. Appl Environ Microbiol 67, 2718–2722. https://doi.org/10.1128/AEM.67.6.2718-2722.2001

Andreae, M. O., Acevedo, O. C., Araùjo, A., Artaxo, P., Barbosa, C. G. G., Barbosa, H. M. J., Brito, J., Carbone, S., Chi, X., Cintra, B. B. L., da Silva, N. F., Dias, N. L., Dias-Júnior, C. Q., Ditas, F., Ditz, R., Godoi, A. F. L., Godoi, R. H. M., Heimann, M., Hoffmann, T., Kesselmeier, J., Könemann, T., Krüger, M. L., Lavric, J. V., Manzi, A. O., Moran-Zuloaga, D., Nölscher, A. C., Santos Nogueira, D., Piedade, M. T. F., Pöhlker, C., Pöschl, U., Rizzo, L. V., Ro, C.-U., Ruckteschler, N., Sá, L. D. A., Sá, M. D. O., Sales, C. B., Santos, R. M. N. D., Saturno, J., Schöngart, J., Sörgel, M., de Souza, C. M., de Souza, R. A. F., Su, H., Targhetta, N., Tóta, J., Trebs, I., Trumbore, S., van Eijck, A., Walter, D., Wang, Z., Weber, B., Williams, J., Winderlich, J., Wittmann, F., Wolff, S., and Yáñez-Serrano, A. M., 2015. The Amazon Tall Tower Observatory (ATTO) in the remote Amazon Basin: overview of first results from ecosystem ecology, meteorology, trace gas, and aerosol measurements, https://doi.org/10.5194/acpd-15-11599-2015

Andrews, D.G., 2010. An Introduction to Atmospheric Physics, Second Edition. Cambridge University Press, New York.

Anke, H. and Weber, R. W. S., 2006. White-rots, chlorine and the environment – a tale of many twists, Mycologist, 20, 83–89, https://doi.org/10.1016/j.mycol.2006.03.011

Aschmann, J., 2009. Modeling the transport of very short-lived substances into the tropical upper troposphere and lower stratosphere. Atmos. Chem. Phys.

ATTO Project Website: https://www.attoproject.org/, last access: 26 September 2024.

Bahlmann, E., Keppler, F., Wittmer, J., Greule, M., Schöler, H.F., Seifert, R., Zetzsch, C., 2019. Evidence for a major missing source in the global chloromethane budget from stable carbon isotopes. Atmos. Chem. Phys. 19, 1703–1719. https://doi.org/10.5194/acp-19-1703-2019

Beerling, D.J., Harfoot, M., Lomax, B., Pyle, J.A., 2007. The stability of the stratospheric ozone layer during the end-Permian eruption of the Siberian Traps. Phil. Trans. R. Soc. A. 365, 1843–1866. https://doi.org/10.1098/rsta.2007.2046

Berberich, G. M., Sattler, T., Klimetzek, D., Benk, S. A., Berberich, M. B., Polag, D., Schöler, H. F., and Atlas, E., 2017. Halogenation processes linked to red wood ant nests (Formica spp.) and tectonics, J Atmos Chem, 74, 261–281, https://doi.org/10.1007/s10874-016-9358-0

Blei, E., Hardacre, C. J., Mills, G. P., Heal, K. V., and Heal, M. R., 2010. Identification and quantification of methyl halide sources in a lowland tropical rainforest, Atmospheric Environment, 44, 1005–1010, https://doi.org/10.1016/j.atmosenv.2009.12.023

Byron, J., Kreuzwieser, J., Purser, G., van Haren, J., Ladd, S.N., Meredith, L.K., Werner, C., Williams, J., 2022. Chiral monoterpenes reveal forest emission mechanisms and drought responses. Nature 609, 307–312. https://doi.org/10.1038/s41586-022-05020-5

Carpenter, L.J., Reimann, S., BURKHOLDER, J.B., Clerbaux, C., Hall, B., Hossaini, R., Laube, J., Yvon-Lewis, S., 2014. Chapter 1: Update on Ozone-Depleting Substances (ODSs) and Other Gases of Interest to the Montreal Protocol, in: Ennis, C.A. (Ed.), Scientific Assessment of Ozone Depletion, Global Ozone Research and Monitoring Project Report. World Meteorological Organization (WMO), Geneva, pp. 21–125.

Chipperfield, M.P., Pyle, J.A., 1998. Model sensitivity studies of Arctic ozone depletion. Journal of Geophysical Research: Atmospheres 103, 28389–28403. https://doi.org/10.1029/98JD01960

Daniel, J.S., Solomon, S., Portmann, R.W., Garcia, R.R., 1999. Stratospheric ozone destruction: The importance of bromine relative to chlorine. Journal of Geophysical Research: Atmospheres 104, 23871–23880. https://doi.org/10.1029/1999JD900381

Davidson, E.A., de Araújo, A.C., Artaxo, P., Balch, J.K., Brown, I.F., C. Bustamante, M.M., Coe, M.T., DeFries, R.S., Keller, M., Longo, M., Munger, J.W., Schroeder, W., Soares-Filho, B.S., Souza, C.M., Wofsy, S.C., 2012. The Amazon basin in transition. Nature 481, 321–328. https://doi.org/10.1038/nature10717

Dewulf, J., Vanlangenhove, H., Huybrechts, T., 2006. Developments in the analysis of volatile halogenated compounds. TrAC Trends in Analytical Chemistry 25, 300–309. https://doi.org/10.1016/j.trac.2005.10.004

Dicke, M., Baldwin, I.T., 2010. The evolutionary context for herbivore-induced plant volatiles: beyond the 'cry for help.' Trends in Plant Science 15, 167–175. https://doi.org/10.1016/j.tplants.2009.12.002

Fall, R., 2003. Abundant Oxygenates in the Atmosphere: A Biochemical Perspective. Chem. Rev. 103, 4941–4952. https://doi.org/10.1021/cr0206521

Farman, J.C., Gardiner, B.G., Shanklin, J.D., 1985. Large losses of total ozone in Antarctica reveal seasonal ClOx/NOx interaction.

Fischer, N.H., Williamson, G.B., Weidenhamer, J.D., Richardson, D.R., 1994. In search of allelopathy in the Florida scrub: The role of terpenoids. J Chem Ecol 20, 1355–1380. https://doi.org/10.1007/BF02059812

Forczek, S.T., Laturnus, F., Doležalová, J., Holík, J., Wimmer, Z., 2015. Emission of climate relevant volatile organochlorines by plants occurring in temperate forests. Plant, Soil and Environment 61, 103–108. https://doi.org/10.17221/900/2014-PSE

Frische, M., Garofalo, K., Hansteen, T.H., Borchers, R., 2006. Fluxes and origin of halogenated organic trace gases from Momotombo volcano (Nicaragua). Geochemistry, Geophysics, Geosystems 7. https://doi.org/10.1029/2005GC001162

Fueglistaler, S., Dessler, A.E., Dunkerton, T.J., Folkins, I., Fu, Q., Mote, P.W., 2009. Tropical tropopause layer. Reviews of Geophysics 47. https://doi.org/10.1029/2008RG000267

Goldstein, A.H., Galbally, I.E., 2007. Known and Unexplored Organic Constituents in the Earth's Atmosphere. Environ. Sci. Technol. 41, 1514–1521. https://doi.org/10.1021/es072476p

Gribble, G.W., 2023. Naturally Occurring Organohalogen Compounds—A Comprehensive Review, in: Kinghorn, A.D., Falk, H., Gibbons, S., Asakawa, Y., Liu, J.-K., Dirsch, V.M. (Eds.), Naturally Occurring Organohalogen Compounds, Progress in the Chemistry of Organic Natural Products. Springer Nature Switzerland, Cham, pp. 1–546. https://doi.org/10.1007/978-3-031-26629-4_1

Guenther, A., 2013. Biological and Chemical Diversity of Biogenic Volatile Organic Emissions into the Atmosphere. ISRN Atmospheric Sciences 2013, 1–27. https://doi.org/10.1155/2013/786290

Hamilton, J. T. G., McRoberts, W. C., Keppler, F., Kalin, R. M., and Harper, D. B., 2003. Chloride Methylation by Plant Pectin: An Efficient Environmentally Significant Process, Science, 301, 206–209. https://doi.org/10.1126/science.1085036

Harper, D.B., 1985. Halomethane from halide ion—a highly efficient fungal conversion of environmental significance. Nature 315, 55–57. https://doi.org/10.1038/315055a0

Hossaini, R., Atlas, E., Dhomse, S.S., Chipperfield, M.P., Bernath, P.F., Fernando, A.M., Mühle, J., Leeson, A.A., Montzka, S.A., Feng, W., Harrison, J.J., Krummel, P., Vollmer, M.K., Reimann, S., O'Doherty, S., Young, D., Maione, M., Arduini, J., Lunder, C.R., 2019. Recent Trends in Stratospheric Chlorine From Very Short-Lived Substances. Journal of Geophysical Research: Atmospheres 124, 2318–2335. https://doi.org/10.1029/2018JD029400

Huber, S.G., Kotte, K., Schöler, H.F., Williams, J., 2009. Natural Abiotic Formation of Trihalomethanes in Soil: Results from Laboratory Studies and Field Samples. Environ. Sci. Technol. 43, 4934–4939. https://doi.org/10.1021/es8032605

Jaeger, N., Besaury, L., Kröber, E., Delort, A.-M., Greule, M., Lenhart, K., Nadalig, T., Vuilleumier, S., Amato, P., Kolb, S., Bringel, F., and Keppler, F., 2018a. Chloromethane Degradation in Soils: A Combined Microbial and Two-Dimensional Stable Isotope Approach, Journal of Environmental Quality, 47, 254–262, https://doi.org/10.2134/jeq2017.09.0358

Jaeger, N., Besaury, L., Röhling, A. N., Koch, F., Delort, A.-M., Gasc, C., Greule, M., Kolb, S., Nadalig, T., Peyret, P., Vuilleumier, S., Amato, P., Bringel, F., and Keppler, F., 2018b. Chloromethane formation and degradation in the fern phyllosphere, Science of The Total Environment, 634, 1278–1287, https://doi.org/10.1016/j.scitotenv.2018.03.316

Keppler, F., Barnes, J.D., Horst, A., Bahlmann, E., Luo, J., Nadalig, T., Greule, M., Hartmann, S.C., Vuilleumier, S., 2020. Chlorine Isotope Fractionation of the Major Chloromethane Degradation Processes in the Environment. Environ. Sci. Technol. 54, 1634–1645. https://doi.org/10.1021/acs.est.9b06139

Keppler, F., Fischer, J., Sattler, T., Polag, D., Jaeger, N., Schöler, H.F., Greule, M., 2017. Chloromethane emissions in human breath. Science of The Total Environment 605–606, 405–410. https://doi.org/10.1016/j.scitotenv.2017.06.202

Keppler, F., Eiden, R., Niedan, V., Pracht, J., and Schöler, H. F., 2000. Halocarbons produced by natural oxidation processes during degradation of organic matter, Nature, 403, 298–301, https://doi.org/10.1038/35002055

Kesselmeier, J., Staudt, M., 1999. Biogenic Volatile Organic Compounds (VOC): An Overview on Emission, Physiology and Ecology. Journal of Atmospheric Chemistry 33, 23–88. https://doi.org/10.1023/A:1006127516791

Khalil, M. a. K., Moore, R.M., Harper, D.B., Lobert, J.M., Erickson, D.J., Koropalov, V., Sturges, W.T., Keene, W.C., 1999. Natural emissions of chlorine-containing gases: Reactive Chlorine Emissions Inventory. Journal of Geophysical Research: Atmospheres 104, 8333–8346. https://doi.org/10.1029/1998JD100079

Knudsen, J.T., Eriksson, R., Gershenzon, J., Ståhl, B., 2006. Diversity and Distribution of Floral Scent. The Botanical Review 72, 1–120. https://doi.org/10.1663/0006-8101(2006)72[1:DADOFS]2.0.CO;2

Ko, M.K.W., Poulet, G., 2003. Very Short-Lived Halogen and Sulfur Substances, in: Scientific Assessment of Ozone Depletion: 2002. World Meteorological Organization, Geneva.

Koppmann, R. (Ed.), 2007. Volatile organic compounds in the atmosphere, 1st ed. ed. Blackwell Pub, Oxford ; Ames, Iowa.

Krysztofiak, G., Catoire, V., Poulet, G., Marécal, V., Pirre, M., Louis, F., Canneaux, S., Josse, B., 2012. Detailed modeling of the atmospheric degradation mechanism of very-short lived brominated species. Atmospheric Environment 59, 514–532. https://doi.org/10.1016/j.atmosenv.2012.05.026

Lan, X., Tans, P., Thoning, K.W., 2024a. Trends in globally-averaged CO2 determined from NOAA Global Monitoring Laboratory measurements. https://doi.org/10.15138/9N0H-ZH07

Lan, X., Thoning, K.W., Dlugokencky, E.J., 2024b. Trends in globally-averaged CH4, N2O, and SF6 determined from NOAA Global Monitoring Laboratory measurements. https://doi.org/10.15138/P8XG-AA10

Li, S., Park, M.-K., Jo, C.O., Park, S., 2017. Emission estimates of methyl chloride from industrial sources in China based on high frequency atmospheric observations. J Atmos Chem 74, 227–243. https://doi.org/10.1007/s10874-016-9354-4

Liang, Q., Atlas, E., Blake, D., Dorf, M., Pfeilsticker, K., Schauffler, S., 2014. Convective transport of very short lived bromocarbons to the stratosphere. Atmos. Chem. Phys. 14, 5781–5792. https://doi.org/10.5194/acp-14-5781-2014

Lobert, J.M., Keene, W.C., Logan, J.A., Yevich, R., 1999. Global chlorine emissions from biomass burning: Reactive Chlorine Emissions Inventory. Journal of Geophysical Research: Atmospheres 104, 8373–8389. https://doi.org/10.1029/1998JD100077

Loreto, F., Schnitzler, J.-P., 2010. Abiotic stresses and induced BVOCs. Trends in Plant Science 15, 154–166. https://doi.org/10.1016/j.tplants.2009.12.006

Loreto, F., Velikova, V., 2001. Isoprene Produced by Leaves Protects the Photosynthetic Apparatus against Ozone Damage, Quenches Ozone Products, and Reduces Lipid Peroxidation of Cellular Membranes. Plant Physiology 127, 1781–1787. https://doi.org/10.1104/pp.010497

McCulloch, A., 2003. Chloroform in the environment: occurrence, sources, sinks and effects. Chemosphere 50, 1291–1308. https://doi.org/10.1016/s0045-6535(02)00697-5

Mead, M.I., Khan, M.A.H., White, I.R., Nickless, G., Shallcross, D.E., 2008. Methyl halide emission estimates from domestic biomass burning in Africa. Atmospheric Environment 42, 5241–5250. https://doi.org/10.1016/j.atmosenv.2008.02.066

Miller, L.G., Warner, K.L., Baesman, S.M., Oremland, R.S., McDonald, I.R., Radajewski, S., Murrell, J.C., 2004. Degradation of methyl bromide and methyl chloride in soil microcosms: Use of stable C isotope fractionation and stable isotope probing to identify reactions and the responsible microorganisms. Geochimica et Cosmochimica Acta 68, 3271–3283. https://doi.org/10.1016/j.gca.2003.11.028

Molhave, L., Clausen, G., Berglund, B., Ceaurriz, J., Kettrup, A., Lindvall, T., Maroni, M., Pickering, A.C., Risse, U., Rothweiler, H., Seifert, B., Younes, M., 1997. Total Volatile Organic

Compounds (TVOC) in Indoor Air Quality Investigations*. Indoor Air 7, 225–240. https://doi.org/10.1111/j.1600-0668.1997.00002.x

Molina, M.J., Rowland, F.S., 1974. Stratospheric sink for chlorofluoromethanes: chlorine atom-catalysed destruction of ozone. Nature 249, 810–812. https://doi.org/10.1038/249810a0

Morgenstern, O., Braesicke, P., Hurwitz, M.M., O'Connor, F.M., Bushell, A.C., Johnson, C.E., Pyle, J.A., 2008. The World Avoided by the Montreal Protocol. Geophysical Research Letters 35. https://doi.org/10.1029/2008GL034590

Nadalig, T., Greule, M., Bringel, F., Vuilleumier, S., Keppler, F., 2013. Hydrogen and carbon isotope fractionation during degradation of chloromethane by methylotrophic bacteria. MicrobiologyOpen 2, 893–900. https://doi.org/10.1002/mbo3.124

Nadalig, T., Farhan Ul Haque, M., Roselli, S., Schaller, H., Bringel, F., and Vuilleumier, S., 2011. Detection and isolation of chloromethane-degrading bacteria from the Arabidopsis thaliana phyllosphere, and characterization of chloromethane utilization genes: Chloromethane-degrading bacteria from A. thaliana, FEMS Microbiology Ecology, 77, 438–448, https://doi.org/10.1111/j.1574-6941.2011.01125.x

Newman, P.A., Oman, L.D., Douglass, A.R., Fleming, E.L., Frith, S.M., Hurwitz, M.M., Kawa, S.R., Jackman, C.H., Krotkov, N.A., Nash, E.R., Nielsen, J.E., Pawson, S., Stolarski, R.S., Velders, G.J.M., 2009. What would have happened to the ozone layer if chlorofluorocarbons (CFCs) had not been regulated? Atmos. Chem. Phys.

Oikawa, P.Y., Lerdau, M.T., 2013. Catabolism of volatile organic compounds influences plant survival. Trends in Plant Science 18, 695–703. https://doi.org/10.1016/j.tplants.2013.08.011

Ojeda, A.S., Phillips, E., Sherwood Lollar, B., 2020. Multi-element (C, H, Cl, Br) stable isotope fractionation as a tool to investigate transformation processes for halogenated hydrocarbons. Environ. Sci.: Processes Impacts 22, 567–582. https://doi.org/10.1039/C9EM00498J

Owen, S.M., Peñuelas, J., 2005. Opportunistic emissions of volatile isoprenoids. Trends in Plant Science 10, 420–426. https://doi.org/10.1016/j.tplants.2005.07.010

Raguso, R.A., Levin, R.A., Foose, S.E., Holmberg, M.W., McDade, L.A., 2003. Fragrance chemistry, nocturnal rhythms and pollination "syndromes" in *Nicotiana*. Phytochemistry 63, 265–284. https://doi.org/10.1016/S0031-9422(03)00113-4

Rasmann, S., Köllner, T.G., Degenhardt, J., Hiltpold, I., Toepfer, S., Kuhlmann, U., Gershenzon, J., Turlings, T.C.J., 2005. Recruitment of entomopathogenic nematodes by insect-damaged maize roots. Nature 434, 732–737. https://doi.org/10.1038/nature03451

Redeker, K.R., Kalin, R.M., 2012. Methyl chloride isotopic signatures from I rish forest soils and a comparison between abiotic and biogenic methyl halide soil fluxes. Global Change Biology 18, 1453–1467. https://doi.org/10.1111/j.1365-2486.2011.02600.x

Reichle, D.E., 2023. Chapter 10 - The global carbon cycle and the biosphere, in: Reichle, D.E. (Ed.), The Global Carbon Cycle and Climate Change (Second Edition). Elsevier, pp. 235–283. https://doi.org/10.1016/B978-0-443-18775-9.00014-0

Rhew, R.C., Miller, B.R., Weiss, R.F., 2000. Natural methyl bromide and methyl chloride emissions from coastal salt marshes. Nature 403, 292–295. https://doi.org/10.1038/35002043

Rowland, F.S., Spencer, J.E., Molina, M.J., 1976. Stratospheric formation and photolysis of chlorine nitrate. J. Phys. Chem. 80, 2711–2713. https://doi.org/10.1021/j100565a019

Rudolph, J., Khedim, A., Koppmann, R., Bonsang, B., 1995. Field study of the emissions of methyl chloride and other halocarbons from biomass burning in Western Africa. J Atmos Chem 22, 67–80. https://doi.org/10.1007/BF00708182

Ruzicka, L., 1953. The isoprene rule and the biogenesis of terpenic compounds. Experientia 9, 357–367. https://doi.org/10.1007/BF02167631

Sasaki, K., Saito, T., Lämsä, M., Oksman-Caldentey, K.-M., Suzuki, M., Ohyama, K., Muranaka, T., Ohara, K., Yazaki, K., 2007. Plants Utilize Isoprene Emission as a Thermotolerance Mechanism. Plant and Cell Physiology 48, 1254–1262. https://doi.org/10.1093/pcp/pcm104

Schlesinger, W.H., Bernhardt, E.S., 2020. The Atmosphere, in: Biogeochemistry. Elsevier, pp. 51–97. https://doi.org/10.1016/B978-0-12-814608-8.00003-7

Schwandner, F.M., Seward, T.M., Giże, A.P., Hall, K., Dietrich, V.J., 2013. Halocarbons and other trace heteroatomic organic compounds in volcanic gases from Vulcano (Aeolian Islands, Italy). Geochimica et Cosmochimica Acta 101, 191–221. https://doi.org/10.1016/j.gca.2012.10.004

Science Panel for the Amazon, 2021. Amazon Assessment Report 2021, 1st ed. UN Sustainable Development Solutions Network (SDSN). https://doi.org/10.55161/RWSX6527

Scutareanu, P., Drukker, B., Bruin, J., Posthumus, M.A., Sabelis, M.W., 1997. Volatiles from Psylla-Infested Pear Trees and Their Possible Involvement in Attraction of Anthocorid Predators. J Chem Ecol 23, 2241–2260. https://doi.org/10.1023/B:JOEC.0000006671.53045.16

Sharkey, T.D., Wiberley, A.E., Donohue, A.R., 2007. Isoprene Emission from Plants: Why and How. Annals of Botany 101, 5–18. https://doi.org/10.1093/aob/mcm240

Šimpraga, M., Ghimire, R.P., Van Der Straeten, D., Blande, J.D., Kasurinen, A., Sorvari, J., Holopainen, T., Adriaenssens, S., Holopainen, J.K., Kivimäenpää, M., 2019. Unravelling the functions of biogenic volatiles in boreal and temperate forest ecosystems. Eur J Forest Res 138, 763–787. https://doi.org/10.1007/s10342-019-01213-2

Sindelarova, K., Granier, C., Bouarar, I., Guenther, A., Tilmes, S., Stavrakou, T., Müller, J.-F., Kuhn, U., Stefani, P., Knorr, W., 2014. Global data set of biogenic VOC emissions calculated by the MEGAN model over the last 30 years. Atmos. Chem. Phys. 14, 9317–9341. https://doi.org/10.5194/acp-14-9317-2014

Sinnhuber, B.-M., Sheode, N., Sinnhuber, M., Chipperfield, M.P., Feng, W., 2009. The contribution of anthropogenic bromine emissions to past stratospheric ozone trends: a modelling study. Atmospheric Chemistry and Physics 9, 2863–2871. https://doi.org/10.5194/acp-9-2863-2009

Stemmler, I., Hense, I., Quack, B., 2015. Marine sources of bromoform in the global open ocean – global patterns and emissions. Biogeosciences 12, 1967–1981. https://doi.org/10.5194/bg-12-1967-2015

Stolarski, R.S., Krueger, A.J., Schoeberl, M.R., McPeters, R.D., Newman, P.A., Alpert, J.C., 1986. Nimbus 7 satellite measurements of the springtime Antarctic ozone decrease. Nature 322, 808–811. https://doi.org/10.1038/322808a0

United Nations Environment Programme (UNEP), 1987. Montreal Protocol on substances that deplete the ozone layer.

Unsicker, S.B., Kunert, G., Gershenzon, J., 2009. Protective perfumes: the role of vegetative volatiles in plant defense against herbivores. Current Opinion in Plant Biology 12, 479–485. https://doi.org/10.1016/j.pbi.2009.04.001

U.S. Standard Atmosphere, 1976. . U.S. Government Printing Office, Washington, D.C.

Vickers, C.E., Gershenzon, J., Lerdau, M.T., Loreto, F., 2009. A unified mechanism of action for volatile isoprenoids in plant abiotic stress. Nat Chem Biol 5, 283–291. https://doi.org/10.1038/nchembio.158

Visconti, G., 2016. Fundamentals of Physics and Chemistry of the Atmosphere. Springer International Publishing, Cham. https://doi.org/10.1007/978-3-319-29449-0

von Glasow, R., von Kuhlmann, R., Lawrence, M.G., Platt, U., Crutzen, P.J., 2004. Impact of reactive bromine chemistry in the troposphere. Atmospheric Chemistry and Physics 4, 2481–2497. https://doi.org/10.5194/acp-4-2481-2004

Warneck, P., Williams, J., 2012. The Atmospheric Chemist's Companion: Numerical Data for Use in the Atmospheric Sciences. Springer Netherlands, Dordrecht. https://doi.org/10.1007/978-94-007-2275-0

Wayne, R.P., Poulet, G., Biggs, P., Burrows, J.P., Cox, R.A., Crutzen, P.J., Hayman, G.D., Jenkin, M.E., Bras, G.L., Moortgat, G.K., Platt, U., Schindler, R.N., 1995. Halogen oxides: Radicals, sources and reservoirs in the laboratory and in the atmosphere. Atmospheric Environment 29, 2677–2881. https://doi.org/10.1016/1352-2310(95)98124-Q

WHO, 1989. Indoor air quality: organic pollutants. Report on a WHO meeting. EURO Rep Stud 1–70.

World Meteorological Organization (WMO) (Ed.), 2022. Scientific Assessment of Ozone Depletion: 2022. Geneva.

Xiao, X., Prinn, R.G., Fraser, P.J., Simmonds, P.G., Weiss, R.F., O'Doherty, S., Miller, B.R., Salameh, P.K., Harth, C.M., Krummel, P.B., Porter, L.W., Mühle, J., Greally, B.R., Cunnold, D., Wang, R., Montzka, S.A., Elkins, J.W., Dutton, G.S., Thompson, T.M., Butler, J.H., Hall, B.D., Reimann, S., Vollmer, M.K., Stordal, F., Lunder, C., Maione, M., Arduini, J., Yokouchi, Y., 2010. Optimal estimation of the surface fluxes of methyl chloride using a 3-D global chemical transport model. Atmos. Chem. Phys. 10, 5515–5533. https://doi.org/10.5194/acp-10-5515-2010

Xiong, Y., Du, K., Huang, Y., 2024. One-third of global population at cancer risk due to elevated volatile organic compounds levels. npj Clim Atmos Sci 7, 54. https://doi.org/10.1038/s41612-024-00598-1

Yokouchi, Y., Ikeda, M., Inuzuka, Y., Yukawa, T., 2002. Strong emission of methyl chloride from tropical plants. Nature 416, 163–165. https://doi.org/10.1038/416163a

2 Triple-Element Stable Isotope Analysis of CH_3Cl Emission and Degradation by Plants

This chapter has been published as: Hartmann, S. C., Keppler, F., Greule, M., Lauer, R., & Horst, A. (2023). Triple-element stable isotope analysis of chloromethane emitted by royal fern and degraded by club moss. In: *Journal of Geophysical Research: Biogeosciences*, 128, e2022JG007256. https://doi.org/10.1029/2022JG007256

Contribution to this paper by S. Christoph Hartmann: Contributed to the experiment design, conducted the sampling, performed the measurements, analyzed the data, and drafted parts of the manuscript.

Triple-Element Stable Isotope Analysis of Chloromethane Emitted by Royal Fern and Degraded by Club Moss

S. Christoph Hartmann[1,2], Frank Keppler[1,3], Markus Greule[1], Rebekka Lauer[1], and Axel Horst[4]

[1]Institute of Earth Sciences, University of Heidelberg, Heidelberg, Germany, [2]Now at Max Planck Institute for Chemistry, Mainz, Germany, [3]Heidelberg Center for the Environment (HCE), Heidelberg University, Heidelberg, Germany, [4]Helmholtz Centre for Environmental Research—UFZ, Leipzig, Germany

2.1 Abstract

Chloromethane (CH_3Cl) is the most abundant natural chlorinated organic compound in the atmosphere playing an important role in catalyzing stratospheric ozone loss. Vegetation emits the largest amounts of CH_3Cl to the atmosphere but its source strength is highly uncertain leading also to large uncertainties in the global budget of CH_3Cl. Triple-element stable isotope analysis may help to reduce uncertainties because it provides additional process-level information compared to conventional quantification methods. In this study we performed experiments to obtain a first triple-elemental isotopic fingerprint (^2H, ^{13}C, ^{37}Cl) of CH_3Cl emitted by a relevant plant species (royal fern, *Osmunda regalis*). Isotopic values of all three elements showed considerable differences compared to isotopic values of industrially manufactured CH_3Cl which bodes well for future applications to distinguish individual sources. Isotopic analysis of potential precursors (rain, methoxy groups) of CH_3Cl in plants revealed no measurable change of hydrogen and chlorine isotopic ratios during formation which may provide a simpler route to estimate the isotopic composition of CH_3Cl emissions. Plant degradation experiments of CH_3Cl were carried out with club moss (*Selaginella kraussiana*) revealing significant isotopic fractionation for all three elements. The fractionation pattern characterized by epsilon and lambda is inconsistent with known biotic dechlorination reactions indicating a yet unreported biotic degradation mechanism for CH_3Cl. Overall, this study provides first insights into the triple-elemental isotopic fingerprint of plant emissions and degradation. The results may represent important input data for future isotope-based models to improve global budget estimates of CH_3Cl and to explore the yet unknown degradation pathways.

2.2 Plain Language Summary

Chloromethane is the most abundant chlorinated organic compound in the atmosphere. It contributes to the destruction of the ozone layer that protects us from skin cancer and genetic damage. Currently, we do not have a good understanding of the sources and removal processes of chloromethane in the atmosphere. In this paper, we use a technique that takes advantage of the different varieties of a chemical element. These so-called isotopes behave differently during chemical reactions that lead to individual isotopic fingerprints depending on the source or removal process. We used isotopic fingerprints of all three chemical elements in chloromethane and showed that chloromethane produced by a plant (royal fern) differs substantially from chloromethane manufactured by industry. Other plant species such as club moss are able to remove chloromethane from the atmosphere but it is often not clear how this occurs. Isotopic analysis revealed that the studied club moss uses a unique, thus far unknown, way to break down chloromethane. This study demonstrates how information extracted from isotopic fingerprints will help to improve our

understanding of sources and removal processes of chloromethane in the atmosphere. It can help to better predict how ozone destruction in the stratosphere affects us in the future.

2.3 Introduction

Chloromethane (CH_3Cl, methyl chloride) represents the largest natural source of chlorine in the atmosphere currently contributing about 17% of total chlorine (Engel et al., 2018). Chlorine together with other halogens and nitrogen compounds cause the depletion of the stratospheric ozone layer that absorbs most of the sun's ultraviolet radiation known to cause adverse effects in plants and animals (Ravishankara et al., 2009). The sources of CH_3Cl mostly are of natural origin (Carpenter et al., 2014) even though previously unrecognized minor anthropogenic sources have recently been reported (Keppler et al., 2017; Li et al., 2017; Thornton et al., 2016). Despite the large uncertainties in the global budget of CH_3Cl, plants have been suggested to be the major source of CH_3Cl (Carpenter et al., 2014). In this context, large emissions have been reported not only for tropical plants (Blei et al., 2010; Gebhardt et al., 2008; Saito & Yokouchi, 2008; Xiao et al., 2010) but also for halophytic plants (Bill et al., 2002; Deventer et al., 2018; Harper et al., 2001; Rhew et al., 2003), fern species (Yokouchi et al., 2015), and crops (Harper et al., 1999) also occurring in temperate climate regions. Apart from producing and emitting CH_3Cl, plants are also known to degrade CH_3Cl with the help of bacteria colonizing the leaves (Bringel et al., 2019; Jaeger et al., 2018a; Krober et al., 2021; Nadalig et al., 2011; Saito et al., 2013) which often hampers a more precise quantification of sources and sinks because the net flux is influenced by both (Keppler et al., 2020a). The largest sinks of CH_3Cl are OH radical reaction in the troposphere as well as degradation in soils and oceans (Carpenter et al., 2014). Thus, large gaps in the budget of CH_3Cl persist because the magnitude of emissions from vegetation includes large uncertainties (Bahlmann et al., 2019), and the sink strength by plants is largely unknown.

The formation processes of CH_3Cl in living terrestrial plants have been investigated in a variety of previous studies (Bayer et al., 2009; Nagatoshi & Nakamura, 2007; Rhew et al., 2003; Schmidberger et al., 2010; Wuosmaa & Hager, 1990). Accordingly, biosynthesis of CH_3Cl and other halomethanes not only in plants but also in fungi, algae, and bacteria is primarily related to the so-called HOL genes (harmless to ozone layer), which generate production of halide methyltransferases. These enzymes catalyze production of halomethanes by combining a methyl group from the ubiquitous S-adenosyl methionine (SAM) with a halide ion in a nucleophilic substitution reaction. Even though the exact mechanisms of halomethane biosynthesis by methyltransferases are not fully understood yet their significance for contributing ozone-depleting compounds is undisputed.

Biotic degradation by living plants is, similarly as production, driven by enzymatic processes. Bacteria colonizing the phyllosphere but also other habitats such as the rhizosphere are able to use CH_3Cl as an energy source. A number of different bacterial strains utilizing CH_3Cl as an energy and carbon source have been identified in soils; for example, *Methylobacterium*, *Hyphomicrobium*, and *Aminobacter* (Doronina et al., 1996; McAnulla et al., 2001; McDonald et al., 2005). The metabolic pathway was discovered by Vanelli and colleagues (Vannelli et al., 1999) and first described for *Methylobacterium sp.* CM4 (now *Methylorubrum extorquens* CM4). Accordingly, CH_3Cl is dehalogenated by a methyltransferase/corrinoid-binding protein (CmuA), and the methyl group is transferred to a corrinoid cofactor. This corrinoid-bound methyl group is then further transferred by another methyltransferase (CmuB) to tetrahydrofolate (H_4F). Methyl-H_4F is oxidized to methylene-H_4F and subsequently to formate and CO_2 (Nadalig et al., 2014; Schäfer et al., 2007). In addition to the Cmu pathway, other yet uncharacterized metabolic pathways were identified in bacteria in the phyllosphere of fern trees such as *Friedmanniella* (Krober et al., 2021) or in bacteria from aquatic habitats such as *Leisingera methylohalidivorans* MB2 (Nadalig et al., 2014).

Stable isotope analysis may be beneficial to further elucidate those enzymatic production and consumption processes of CH_3Cl, and they have been applied in various studies (Jaeger et al., 2018b; Keppler et al., 2020b; Miller et al., 2004; Nadalig et al., 2014). Isotopic approaches also aimed at quantifying the contribution of emission and consumption of CH_3Cl by plants in the atmosphere (Rhew, 2011; Saito & Yokouchi, 2008; Saito et al., 2013; Weinberg et al., 2013) and in relation to the other sources and sinks (Bahlmann et al., 2019; Keppler et al., 2005; Keppler et al., 2020a). Isotopic analysis in CH_3Cl was shown to be particularly useful when the stable isotopes of all three available elements were investigated because different biotic and abiotic degradation processes showed distinct isotopic patterns which may help to identify or even quantify different processes (Horst et al., 2019; Keppler et al., 2020a). Particularly hydrogen and chlorine provided important information because, other than carbon, they were not involved in each reaction and hence did not undergo changes in their isotopic composition during such reactions. For instance, chemical decomposition via hydroxyl (OH) radical reactions showed large isotopic shifts for hydrogen (Keppler et al., 2018) but negligible shifts for chlorine whereas microbial degradation showed the opposite: small shifts for hydrogen isotopes but large shifts for chlorine isotopes (Keppler et al., 2020a). This could be explained by the underlying reaction mechanisms which either cleave the H-C bond (OH-radical reaction) or the Cl-C bond (microbial dechlorination). Keppler and co-authors (Keppler et al., 2020a) also used isotopic constraints to confirm that the two metabolic pathways of CH_3Cl dechlorination by *Methylorubrum extorquens* CM4 and *Leisingera methylohalidivorans* MB2 are actually different. This may have further implications because CM4 and MB2 might be representative for terrestrial and marine organisms, respectively. It was argued that, if the metabolic pathways are actually representative for each respective environment, this would provide a strong isotopic tool for the distinction of terrestrial and marine CH_3Cl degradation pathways.

Triple-element isotopic studies of CH_3Cl are, however, very scarce and have only been carried out for abiotic degradation pathways such as OH and Cl radical reactions (Keppler et al., 2020a) and hydrolysis and transhalogenation reactions (Horst et al., 2019). One study investigated microbial dechlorination pathways using cell extracts (Keppler et al., 2020a). Till now, there are no triple-element isotopic studies of emissions or degradation of CH_3Cl by living plants. Several studies applied dual element isotope analysis (stable isotopes of H and C) to disentangle degradation processes (Jaeger et al., 2018a; Nadalig et al., 2014) and to isotopically characterize emissions of CH_3Cl (Jaeger et al., 2018b) but stable chlorine isotope analysis has not been applied yet in this context.

Hence, the current study aimed at exploring the benefits of triple-element stable isotope analysis for the characterization of CH_3Cl emitted and consumed by vegetation. *Osmunda regalis* (royal fern) was used to isotopically characterize CH_3Cl production. *O. regalis* is a common fern species growing in temperate and subtropical regions. This fern species was chosen because it is known to produce large amounts of CH_3Cl (Jaeger, Besaury, Rohling, et al., 2018; Yokouchi et al., 2007, 2015). In addition, experiments with a club moss (*Selaginella kraussiana*) were carried out to investigate degradation of CH_3Cl and associated isotopic fractionation. Results are discussed in comparison to known fractionation patterns obtained in previous experiments with bacterial cell cultures. *S. kraussiana* has been used in this current study as it was observed in preliminary investigations at the Botanical Garden of Heidelberg University for its potential to strongly degrade CH_3Cl.

2.4 Materials and Methods

2.4.1 Sampling of Rainwater and Conversion of Chloride to CH_3Cl

Rainwater samples were collected at three different sites between April and June 2021 in order to determine the stable chlorine isotopic composition of the primary chlorine source for plants in terrestrial environments which are not located at the coast or close to halite deposits. Three sampling sites were chosen representing urban (Heidelberg, Leipzig) and rural (Rastenberg) environments that stretch along a transect of about 400 km in North-Western direction following the main wind direction in Germany. Two replicate samples were collected directly in the botanical garden of the city of Heidelberg from the roof of a greenhouse. Two replicate samples were taken at a rural site in central Germany (Rastenberg, Thuringia). Two more individual samples were collected in Leipzig, Saxony. All samples (1–2.5 L) were concentrated down to 30 mL by boiling. Containing Cl ions were precipitated as AgCl by adding $AgNO_3$. Next, AgCl was filtered off under safelight conditions and filters and iodomethane (CH_3I, 10 times excess concentration) sealed in borosilicate glass tubes. The tubes were placed in a furnace held at 80°C for 48 hr to react AgCl and CH_3I to CH_3Cl. The whole procedure followed established protocols (Eggenkamp, 2014; Gilevska et al., 2015).

2.4.2 Plant Sampling and Incubation Experiments

In preliminary field experiments using larger teflon-foil chambers (~11 l volume), we monitored several plants in the Botanical Garden of Heidelberg University for their potential to degrade CH_3Cl at ambient CH_3Cl concentrations (at around 500 to 600 pptv). The plants were not physically damaged before and during enclosure. We found several CH_3Cl degraders such as *Polystichum setiferum*, *Selaginella kraussiana*, and *Dryopterix filix-mas* that reduced the atmospheric concentration inside the chamber by up to 30% within 15–30 min yielding CH_3Cl degradation rates in the range of 1–5 ng g_{dw}^{-1} h^{-1}. For the current study, we chose *S. kraussiana* for investigation of degradation mechanisms with isotopic methods.

Fresh samples of *S. kraussiana* were collected in July and September 2019 and April 2021, respectively, at a greenhouse of the Heidelberg Botanical Garden. The greenhouse is characterized by high relative humidity (RH >90%). The whole stem of the living plant including attached leaves was cut and the sampled plant material was subsequently incubated in the lab to explore biotic degradation of CH_3Cl by plant-associated microbes. We did not expect any additional abiotic reactions to disturb the results because reactions such as hydrolysis previously showed rate constants of about 0.002 d^{-1} (Horst et al., 2019) which is several orders of magnitude slower than observed in previous microbial degradation experiments (Jaeger et al., 2018b). For incubation, the plant material was evenly distributed over nine vessels (~7–9 g wet weight plant material in each 170 ml custom-made glass cylinder). All vessels were sealed gas-tight at the same time under the fume hood to ensure all of them contain the same (lab-) air and therefore have the same initial CH_3Cl mixing ratio and isotopic ratios. After sealing, we artificially increased the CH_3Cl mixing ratio of the vessels by injecting 2 ml of a diluted CH_3Cl reference (~1000 parts per million by volume (ppmv) CH_3Cl in N_2) into each of these vessels and waited for equilibrium to be established before measuring the initial CH_3Cl concentration t = 0 in each vessel. Concentrations were checked frequently and samples for isotope analysis were collected at selected time intervals (**Figure 0-10** and **Figure 0-11** in the Supplementary Material S.2).

Emission experiments were carried out with plant material of *O. regalis*. The samples of this plant were collected in July and September 2019. In contrast to *S. kraussiana*, the collected samples of *O.*

regalis grew in the outside area of the Heidelberg Botanical Garden under the local climatic conditions. Whole fern fronds were cut off and brought to the lab for subsequent incubation. As for *S. kraussiana*, 7–9 g wet weight of *O. regalis* were put into the same 170 ml custom-made glass cylinders used for the degradation experiments and all vessels were sealed at the same time under the fume hood. The temperature in the lab (23.5 ± 1°C) was constant throughout the whole incubation period. Seven and eight experiments were run in parallel during the two experimental campaigns, respectively. Concentrations were checked frequently and samples for isotopic analysis were collected after the last concentration measurement (**Figure 0-12** and **Figure 0-13** in Supplementary Material S.2).

Microcosm experiments as those described above represent very different environmental conditions for a plant compared to its natural habitat. It might be questioned whether the data collected in the laboratory is representative for field conditions. Isotopic data, however, seems to be quite robust in this context. For example, in a laboratory study Harper et al. (2001) measured a $\delta^{13}C$ of –65.7 ± 3.4 ‰ VPDB for CH_3Cl emitted by saltwort (*Batis maritima*) which is consistent with the values of –62 ‰ VPDB reported for emissions by this plant in the field (Bill et al., 2002) indicating a good agreement between emission data collected in the laboratory and in the field.

Blank measurements with reaction vessels only containing CH_3Cl without plant material in the vessels were carried out in order to evaluate whether any losses of CH_3Cl occurred, and if so, whether they caused isotopic fractionation. For this purpose, a CH_3Cl/N_2 gas mixture was filled into the vessels creating a final mixing ratio of 9.5 ± 0.5 ppmv. Samples were taken at t = 0 and after 25 hr (t = 1) which was the longest incubation period. Both the concentration in the reaction vessels and the stable carbon and chlorine isotope values of the blank samples were measured. Whereas the mixing ratio and the stable carbon isotopes only varied within analytical uncertainty, stable chlorine isotopes showed a slightly larger shift over time and a linear correction was applied as described more in detail in Supplementary Material S.3. Control measurements were also carried out with dried plant material to evaluate abiotic reactions that might occur alongside biotic reactions. In these experiments, we only observed a very small concentration decrease, which may not change the isotopic composition (Supplementary Material S.3).

2.4.3 Quantification of CH_3Cl

The CH_3Cl mixing ratio in each incubation vessel was determined at different times throughout the experiments. For quantification, gas chromatography-mass spectrometry (GC-MS) was used (HP 5973 mass selective detector; Hewlett-Packard/Agilent Technologies, Palo Alto, CA, USA). We extracted 100 µL headspace directly from the incubation vessel and injected it with a 100 µL gas-tight Luer lock syringe (SGE Analytical Science, Australia) onto the GC column (GS Gaspro 60 m × 0.32 mm; 1 mL min^{-1} constant flow, 150°C isothermal) using a split ratio of 5:1. Mass spectrometry was carried out in SIM mode using the masses m/z = 50, m/z = 51, m/z = 52, and m/z = 53.

The GC/MS system was calibrated by measuring a diluted reference (99.8% CH_3Cl in N_2, AirLiquide, France) at different mixing ratios with n = 3. For the samples obtained from the incubation of *S. kraussiana*, a four-point calibration in the range from 0 to 10 ppmv CH_3Cl was applied. Due to high CH_3Cl emission rates observed during incubation of *O. regalis*, we conducted a nine-point calibration in the range from 0 to 75 ppmv CH_3Cl for quantification of mixing ratios in the incubation vessels. At selected time intervals, samples for stable isotope analysis were taken. For this purpose, 25–30 ml of gas was removed from the incubation vessels, passed through an Ascarite® trap to remove CO_2, and subsequently transferred to 12 ml pre-evacuated exetainers to be analyzed at a later time for measurements of stable hydrogen, carbon, and chlorine isotope values of CH_3Cl. Furthermore,

15 mL of the CH_3Cl reference gas that was supplemented to the *S. kraussiana* incubation vessels was filled in exetainers for measuring the isotopic composition before changes due to degradation occurred.

2.4.4 Stable Hydrogen and Stable Carbon Isotope Analysis of CH_3Cl

Stable hydrogen and stable carbon isotopic ratios of CH_3Cl (expressed as δ_2H-CH_3Cl and $\delta^{13}C$-CH_3Cl) were measured by an in-house cryogenic pre-concentration unit coupled to gas chromatography (HP 6890, Agilent Technologies, Palo Alto, CA) and isotope ratio mass spectrometry (IRMS) (Isoprime, Manchester, UK), as previously described (Greule et al., 2012; Keppler et al., 2020a; Nadalig et al., 2013). Deviating from the cited methods, an in-house modified interface was used which is based on the GC Combustion III Interface from ThermoQuest Finnigan (Bremen, Germany). For stable hydrogen isotope analysis of CH_3Cl, a ceramic tube reactor (length 320 mm, 0.5 mm i.d.) heated to 1,450°C was used for high-temperature conversion. For stable carbon isotope analysis the oxidation reactor (length 320 mm, 0.5 mm i.d.) contained Cu/Ni/Pt wires inside (activated by oxygen) and was operated at 960°C. The CH_3Cl working standard was calibrated against the IAEA standards NBS 22, LVSEC (carbon), VSMOW and SLAP (hydrogen) using TC/EA-IRMS (elemental analyzer-isotopic ratio mass spectrometry, IsoLab, Max Planck Institute for Biogeochemistry, Jena, Germany), yielding the following values: $\delta^{13}C$: −32.84 ± 0.06 ‰ VPDB (n = 11, 1σ) and δ_2H: −140.1 ± 1.0 ‰ VSMOW (n = 10, 1σ). The H_{3+} factor, determined daily during this investigation (~2-month period), was in the range 5.22–5.35 ppm/nA.

2.4.5 Stable Chlorine Isotope Analysis of CH_3Cl

Stable chlorine isotope analysis was carried out by applying gas chromatography coupled via a heated transfer line to multiple-collector inductively coupled plasma mass spectrometry (GC-MC-ICPMS, Neptune, Thermo Fisher Scientific, Germany) according to previously published protocols (Horst et al., 2017; Renpenning et al., 2018). Up to 6 mL of gas collected during plant experiments were extracted from the vials using a 10 mL gas-tight syringe equipped with a valve (VICI precision sampling). In order to inject such large amounts of gas the GC was operated in splitless mode and equipped with a cryotrap as described in Keppler et al. (2020a). This cryotrap was cooled with liquid nitrogen to assure loss-less collection of the injected sample gas. After cryofocussing was complete, the trap was immersed in warm water (40°C) in order to release the analytes onto the chromatographic column (ZB1 Phenomenex, 60m, 0.32 ID, 2 mL min^{-1} constant flow, 30°C isothermal). For analysis of CH_3Cl obtained from conversion of Cl^- in rainwater samples, sealed borosilicate tubes were inserted into 120 mL serum bottles, flushed with nitrogen, and capped with gray PTFE-coated stoppers (Wheaton®). Before analysis these bottles were shaken to break the tube in the bottle. Several aliquots were injected in split mode (1:10) keeping the GC column at 120°C, which was sufficient to separate CH_3Cl and CH_3I. Two analyses of a reference-CH_3Cl were injected before each sample to determine the raw-$\delta^{37}Cl$ of each sample relative to this reference (see Equation 6). Raw-$\delta^{37}Cl$ values were then linked to SMOC and normalized to the currently used scale by applying a linear two-point calibration approach using organic in-house reference material (trichlorethylene TCE2 and TCE6, as well as CH_3Cl) (Horst et al., 2017).

2.4.6 Stable Carbon and Hydrogen Isotope Analysis of Plant Methoxy Groups

Stable hydrogen and carbon isotope values of methoxy groups (δ_2H-OCH_3 and $\delta^{13}C$-OCH_3 values) were measured using the "HI method" described in previous investigations (Greule et al., 2012; Keppler et al., 2020b; Nadalig et al., 2013). Briefly, hydriodic acid (250 µL) was added to dried and milled *O. regalis* (30 and 100 mg for carbon and hydrogen isotopes, respectively) and *S. kraussiana*

(25 and 65 mg for carbon and hydrogen isotopes, respectively) samples in crimp-top glass vials (1.5 ml). The vials were sealed with crimp caps containing PTFE-lined butyl rubber septa (thickness 0.9 mm) and incubated for 30 min at 130°C. After equilibration at room temperature, aliquots of the generated CH_3I in the headspace (carbon: 70 µL; hydrogen: 90 µL) were directly injected into a Hewlett Packard HP 6890N gas chromatography system (Agilent Technologies, Palo Alto, CA) coupled to a Delta^{PLUS} XL isotope ratio mass spectrometry system (ThermoQuest Finnigan, Bremen, Germany).

All δ_2H-OCH_3 and δ^{13}C-OCH_3 values were normalized by applying a two-point linear calibration approach using stable isotope values of the three working standards HUBG1, HUBG2 and HUBG3 which all were calibrated against international reference substances at the IsoLab of the Max Planck Institute for Biogeochemistry in Jena (Germany). The calibrated δ_2H values versus VSMOW were –102.0 ± 1.3 ‰ (n = 32, 1σ) for HUBG2 and –272.9 ‰ ± 1.5 ‰ (n = 11, 1σ) for HUBG3. The calibrated δ^{13}C values versus VPDB were –50.31 ± 0.16 ‰ (n = 14, 1σ) for HUBG1 and +1.60 ‰ ± 0.12 ‰ (n = 16, 1σ) for HUBG2. Details of the calibration procedure are provided in the studies by Greule and co-authors (Greule et al., 2019, 2020).

2.4.7 Reporting Isotopic Compositions and Isotopic Fractionation

Isotopic values are expressed in the delta notation according to the following equation:

$$\delta^i E\ (‰, Ur) = \frac{(R)sample}{(R)standard} - 1 \qquad \textit{Equation 6}$$

where ^{i}E indicates ^{2}H, ^{13}C, ^{37}Cl and R is the isotopic ratio ^{2}H/^{1}H, ^{13}C/^{12}C, and ^{37}Cl/^{35}Cl. Delta values are expressed in per mil (‰) or Urey (Ur) relative to the international standards VSMOW (Vienna Standard Mean Ocean Water) for hydrogen (δ_2H_{VSMOW}), VPDB (Vienna Pee Dee Belemnite) for carbon ($\delta^{13}C_{VPDB}$), and SMOC (Standard Mean Ocean Chloride) for chlorine ($\delta^{37}Cl_{SMOC}$) (Brand et al., 2014). In this paper, isotopic values are reported in per mil notation.

Isotopic fractionation (ε) is usually calculated by using the Rayleigh equation which characterizes the constant change of the isotopic composition of the substrate reservoir due to a preferential loss of heavy or light isotopes caused by a reaction or process (Mariotti et al., 1981):

$$ln\left(\frac{\delta^i E+1}{\delta^i E_0+1}\right) \approx ln\ (f)\varepsilon_x \qquad \textit{Equation 7}$$

where δ^iE is the isotopic value (δ_2H, δ^{13}C, δ^{37}Cl) of a compound after partial degradation, $\delta^i E_0$ is the initial delta value (δ_2H_0, $\delta^{13}C_0$, $\delta^{37}Cl_0$), and f is the fraction of compound remaining after partial degradation. The Rayleigh equation derives the isotopic fractionation for first-order or pseudo-first-order reactions (van Breukelen, 2007).

Λ-values (lambda) describe the ratio of the isotopic fractionation of two different isotopic systems (van Breukelen, 2007). Λ values should be determined graphically by plotting isotopic data of one element versus the isotopic data of another element determined from samples of the same experiment (Ojeda et al., 2019). When isotopic data was obtained in separate experiments, Λ-values may also be estimated according to the following relationship (van Breukelen, 2007):

$$\Lambda_{x/y} \approx \frac{\varepsilon_x}{\varepsilon_y} \qquad \textit{Equation 8}$$

where ε_x and ε_y are the isotopic fractionations of two different elements x and y determined for the same mechanism in a certain compound.

2.5 Results and Discussion

2.5.1 Emission Rates and Isotopic Composition of CH_3Cl by *Osmunda regalis*

2.5.1.1 Emission Rates of CH_3Cl by Osmunda regalis

Emission rates obtained during the experiments ranged from 0.8 to 22 µg g_{dw}^{-1} d^{-1} and were thus comparable to those reported in the literature for O. regalis (Jaeger et al., 2018b) and other species of the Osmunda family (Yokouchi et al., 2007, 2015) but were higher than median emissions reported for a tropical rainforest (0.72 µg g_{dw}^{-1} d^{-1} (Saito et al., 2008)). The relatively large range of emission rates may result from plant material of different growth stages and sampling time (July and September) which, despite this variability, provide a more realistic picture of emission of CH_3Cl from *O. regalis*. Due to our incubation method we also cannot completely exclude additional variation of emission rates due to wounding and stress. Chloride availability might also be considered a limiting factor because cutting the branches theoretically interrupts water and thus chloride supply. In our experiments we could not detect any signs of decreasing chloride supply. The CH_3Cl concentration in the reaction vessels was constantly increasing which indicates that chloride was available throughout our experiments (**Figure 0-12** and **Figure 0-13** in Supplementary Material S.2). Overall, *O. regalis* was well suited for the planned experiments because it provided the high amounts of CH_3Cl necessary for isotopic analysis. Information regarding determination of emission rates is provided in Supplementary Material S.2.

2.5.1.2 Isotopic Composition of CH_3Cl Emitted by Osmunda regalis

Chloromethane emissions collected from *O. regalis* were also measured for their isotopic composition. Average δ^2H-CH_3Cl, δ^{13}C-CH3Cl, and δ^{37}Cl-CH_3Cl values were −242 ± 39 ‰ VSMOW, −83.9 ± 4.2 ‰ VPDB, and −0.91 ± 0.84 ‰ SMOC, respectively (**Figure 2-1**). All data showed relatively small variations over the entire incubation period (up to 16 hr) and thus may be considered representative for CH_3Cl emissions by *O. regalis* (**Figure 2-1**). This consistency may also be an indicator that, in contrast to emission rates, stress, and wounding are not affecting the isotopic results. Measured δ^{37}Cl represent the first chlorine isotopic characterization of a natural source of CH_3Cl and hence these values provide a first estimate for the magnitude of δ^{37}Cl values of CH_3Cl emitted by plants. Stable hydrogen and stable carbon isotopic values largely agree with those obtained in a former study for the same fern species (**Table 2-3**): δ^2H = −202 ± 10 ‰ VSMOW and δ^{13}C = −97 ± 8 ‰ VPDB (Jaeger et al., 2018b). Other comparable experiments have, thus far, only been conducted in studies measuring stable carbon isotopes for a variety of higher living plants which showed a range of −56 ‰ to −114 ‰ VPDB (Saito & Yokouchi, 2008; Saito et al., 2008). In general, δ^{13}C-CH_3Cl emitted by plants seem to be more depleted than in CH_3Cl emitted by other natural sources such as biomass burning, wood rotting fungi, and salt marshes (Bahlmann et al., 2019; Keppler et al., 2005; Saito & Yokouchi, 2008). Overall, isotopic values for all elements are slightly (δ^{37}Cl) to more considerably (δ^2H, δ^{13}C) depleted compared to their respective standards (SMOC, VSMOW, VPDB).

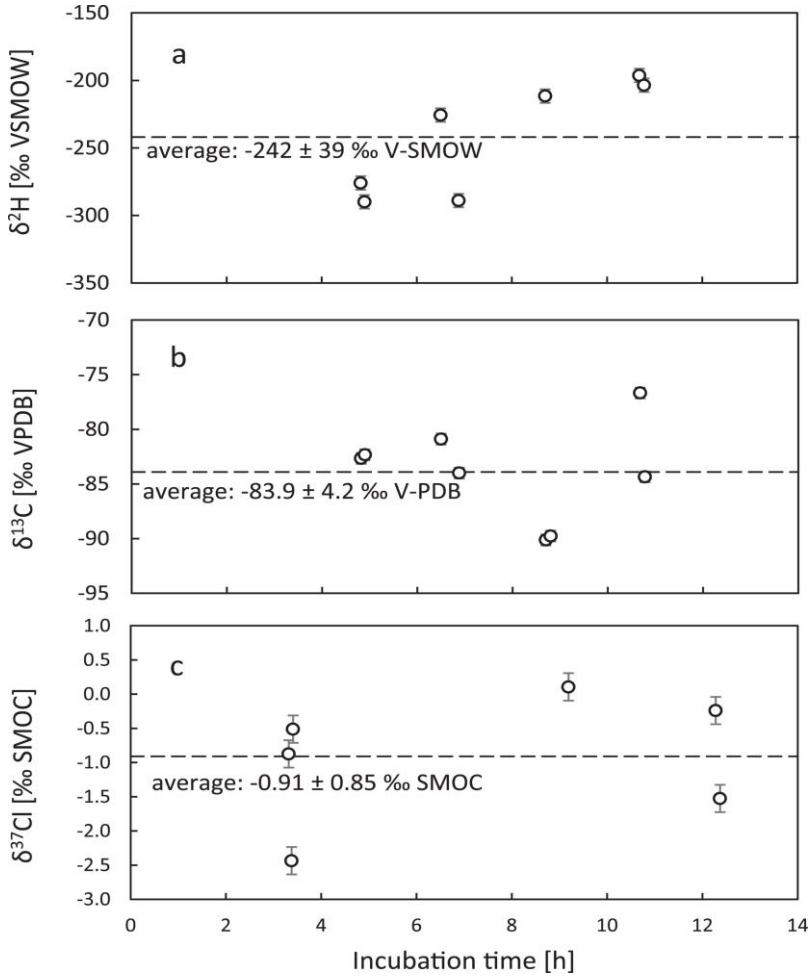

Figure 2-1. *Isotopic values of hydrogen (a), carbon (b), and chlorine (c) of CH_3Cl emitted by O. regalis. Error bars indicate the overall uncertainty of the corresponding method which is usually 5 ‰ (δ^2H), 0.5 ‰ ($\delta^{13}C$), and 0.2 ‰ ($\delta^{37}Cl$) for a single analysis.*

The measured isotopic values for hydrogen, carbon, and chlorine may serve as an isotopic fingerprint of CH_3Cl emitted by *O. regalis* and possibly also for other plants if isotopic values show comparable ranges. The strongly depleted δ_2H and $\delta^{13}C$ values of CH_3Cl emitted by *O. regalis* are clearly different from two available industrially manufactured CH_3Cl (δ_2H −127 ± 20 ‰ VSMOW and $\delta^{13}C$ = −45 ± 15 ‰ VPDB, working reference compounds used in the stable isotope labs at Heidelberg University and UFZ in Leipzig) or CH_3Cl emitted from salt marshes (δ_2H −185 ± 18 ‰ VSMOW and $\delta^{13}C$ = −49.1 ± 3 ‰ VPDB (Keppler et al., 2020b)). For stable chlorine isotopes no previous emission data is available but the slightly depleted values ($\delta^{37}Cl$ = −0.91 ± 0.89 ‰ SMOC) compared to seawater differ substantially from reported values of two industrially manufactured CH_3Cl samples ($\delta^{37}Cl$-CH_3Cl = +6.0 ± 0.1‰ SMOC (Keppler et al., 2020a)). These results suggest that all, thus far, isotopically characterized sources of CH_3Cl may indeed be distinguishable when the isotopes of three different elements are measured and compared. Published studies investigating stable carbon isotopes in CH_3Cl provided first evidence that some major sources may be distinguishable based on their carbon isotopic composition alone. For instance, CH_3Cl from biomass burning showed a $\delta^{13}C$-CH_3Cl value of −47 ‰ VPDB (weighted mean of C3 and C4 plants, range of −38 to −68 ‰ VPDB) (Czapiewski et al., 2002; Thompson et al., 2002) which is, on average, more enriched in ^{13}C compared to CH_3Cl emissions from living plants (−56‰ to −114‰ VPDB (Saito & Yokouchi, 2008; Saito et al., 2008)). Even higher $\delta^{13}C$-CH_3Cl; that is, CH_3Cl was more enriched in the heavy isotope, were reported for emissions from

oceans which covered a range of –12 to –43 ‰ VPDB and an estimated isotopic source signature of –36 ‰ VPDB (Bahlmann et al., 2019). Adding hydrogen and chlorine isotope analysis may provide additional isotopic tools to also identify and quantify those sources that are currently not distinguishable with stable carbon isotope analysis alone.

Table 2-1. *$\delta^{37}Cl$ Values of Chloride in Rainwater Samples Taken at Three Different Sites in Germany Between April and June 2021*

	Sampling date	Volume (L)	Concentration (Cl^- mg/L)	$\delta^{37}Cl$ of Cl^-‰ SMOC	Σ ‰	*n*
Heidelberg 1a	27 April 2021	1.2	0.80	–0.28	0.04	3
Heidelberg 1b	27 April 2021	1.2	0.56	–0.21	0.03	3
Rastenberg 1a	5 June 2021	2.5	n.d.	–0.89	0.07	3
Rastenberg 1b	5 June 2021	2.5	n.d.	–0.94	0.02	3
Leipzig 1	7 June 2021 (2 mm)	1.2	n.d.	–0.52	0.09	3
Leipzig 2	20 June 2021 (14.8 mm)	2.5	n.d.	–0.09	0.08	3

Note. The uncertainty indicates the standard deviation for triplicate measurements of the corresponding sample.

2.5.1.3 Isotopic Fractionation During Formation of CH_3Cl From Precursors

Isotopic fractionation during formation of CH_3Cl from their potential precursors was also investigated during this study by additionally determining the $\delta^{37}Cl$ of chloride in rainwater samples and the $\delta^{13}C$ and δ_2H of the plant methoxy pool which may be representative for the isotopic composition of the entire methyl pool in plants (Jaeger et al., 2018b). The $\delta^{37}Cl$ of chloride in rainwater samples varied between –0.94 ‰ and –0.09 ‰ SMOC which is consistent with the $\delta^{37}Cl$ of rainwater sampled in North America (Koehler & Wassenaar, 2010). There seems to be a tendency toward more depleted values for the rural site Rastenberg compared to the urban sites Heidelberg and Leipzig. Also, the rain event with higher precipitation (Leipzig 2, 14.8 mm) produced a more ^{37}Cl enriched isotopic value than the short precipitation event at Leipzig 1 (2 mm). The reason for this variation is unclear but it might be associated with additional heterogeneous reactions of chloride in the atmosphere such as the formation of HCl from primary sea salt aerosols. HCl is formed by acidification of the salt-containing aerosol by atmospheric sulfuric and nitric acid which is an isotope fractionating mechanism (Volpe & Spivack, 1994). Chloride in marine aerosols is produced by bubble bursting and wave-crest tearing mechanisms (Erickson & Duce, 1988) but most of this chloride is quickly removed from the atmosphere by wet or dry deposition (Koehler & Wassenaar, 2010). Hence HCl might be the largest source of chloride in the study area which is situated several hundred kilometers from the coast. The variability of $\delta^{37}Cl$ of chloride in rain in the studied region is small. The average of –0.49 ± 0.33 ‰ SMOC and the range of 0.85 ‰ may be considered as a first best estimate of $\delta^{37}Cl$ values in rainwater for South and Central Germany (**Table 2-1**).

Methoxy groups of plants have been shown to be direct precursors of methyl halides in abiotic as well as biotic reactions with abiotic reactions depending largely on temperature (Derendorp et al., 2012; Hamilton et al., 2003; Keppler et al., 2004; Wishkerman et al., 2008). The isotopic composition of plant methoxy groups might be considered representative for the entire methyl (CH_3) pool in plants. Although this assumption is a large simplification requiring further validation, as a first approximation it might be applied to indirectly characterize the stable hydrogen and stable carbon isotope composition of the methyl group in SAM, the precursor for enzymatic forma- tion of CH_3Cl (Jaeger et al., 2018b; Keppler et al., 2004). *S. kraussiana* showed $\delta^{13}C$-OCH_3 and δ_2H-OCH_3 values of –47.1 ‰ VPDB and –313 ‰ VSMOW, respectively (**Table 2-2**). For *O. regalis*, which was investigated for its CH_3Cl emissions in the current study, $\delta^{13}C$-OCH_3 and δ_2H-OCH_3 values were found to be –60.8

Table 2-2. *$\delta^{13}C$ and $\delta^{2}H$ Values of Methoxy Groups of the two Selected Plant Species*

	$\delta^{13}C$ [‰ VPDB]	σ (n = 5)	$\delta^{2}H$ [‰ VSMOW]	σ (n = 5)
S. kraussiana EW1	−46.76	0.19	−314.0	2.2
S. kraussiana EW2	−47.46	0.19	−312.5	2.1
O. regalis EW1	−60.84	0.20	−260.1	2.5
O. regalis EW2	−60.75	0.19	−257.5	2.4

Note. The uncertainty indicates the propagated error including the analytical uncertainty of measurements (90% Student factor) and the weighted analytical uncertainty of the scaling standards.

‰ VPDB and −259 ‰ VSMOW, respectively (**Table 2-2**). The δ_2H of *O. regalis* matches a previously published value of −259 ‰ VSMOW (Jaeger et al., 2018b). Generally, δ_2H of the two plants are within or close to the range of −200 to −296 ‰ reported for different plant material by Greule et al. (2012), while $\delta^{13}C$-OCH_3 are within the range of −40.5 to −77.2 ‰ published for different plant material by Keppler et al. (2004). However, the relatively negative isotopic values for carbon and hydrogen in methoxy groups suggest a large fractionation during plant growth. Rainwater and atmospheric CO_2 are the assumed sources of hydrogen and carbon in plants with approximate source values of δ_2H = −55 ‰ (annual longterm average of the GNIP station Karlsruhe nearby Heidelberg (IAEA/WMO, 2021)) and $\delta^{13}C$ = −8.5 ‰ (Schaeffer et al., 2008). Hence, the isotopic composition of methoxy groups and presumably the entire methyl pool of *O. regalis* indicates a shift of about −200 ‰ for δ_2H-OCH_3 and about −50 ‰ for $\delta^{13}C$-OCH_3 values compared to the primary sources of hydrogen and carbon. For *S. kraussiana* this shift is about −260 ‰ for δ_2H-OCH_3 and −40 ‰ for $\delta^{13}C$-OCH_3 values. The systematics of 2H patterns of methoxy groups in plants are controlled by the plants source water (usually precipitation) and are related to the C1 metabolism including the transfer of the methyl group of SAM as it was recently proposed by Greule et al. (2021). As for carbon, both carbon fixation in photosynthesis and C1 biosynthesis; that is, the transfer of the methyl group of SAM and/or methionine, may largely contribute to carbon isotope fractionation.

These additional measurements (**Table 2-1** and **Table 2-2**) indicated that the δ_2H-CH_3Cl values of *O. regalis* are, within analytical uncertainty, indistinguishable from the δ_2H-OCH_3 values in *O. regalis* whereas $\delta^{13}C$-CH_3Cl values of CH_3Cl released by *O. regalis* are about 23 ‰ depleted in 13C compared to the methoxy pool in the investigated fern samples. Similarly to hydrogen isotopes, the $\delta^{37}Cl$ values of CH_3Cl emissions by *O. regalis* are indistinguishable from the potential precursor-$\delta^{37}Cl$; the chloride in the collected rainwater. These results suggest that formation of CH_3Cl in plants cause rather small and negligible isotopic fractionation for hydrogen and chlorine. This might be explained with none of the three hydrogen atoms of the methyl group (stemming from SAM) exchanging or reacting during formation of CH_3Cl and presumably only negligible secondary isotope effects occur. For chlorine, the insignificant isotopic fractionation may be rationalized with the absence of any reaction of Cl ions until formation of CH_3Cl takes place. Apparently, uptake and transport of chlorine ions within *O. regalis* only cause small and insignificant isotopic fractionation. In contrast, results for carbon isotopes in CH_3Cl emitted by *O. regalis* indicate substantial isotopic fractionation of about −23 ‰, which is likely caused by a primary isotope effect due to bond cleavage of the methyl group from SAM or methoxy groups (Keppler et al., 2020b). It is conceivable that these observed isotopic fractionation pattern may also be found for other important plant species since formation of CH_3Cl is mainly linked to SAM as precursor and hence the formation mechanism and associated isotope effects might be similar.

Table 2-3. *Overview of Isotopic Data of CH_3Cl Obtained from Previous Emission and Degradation Experiments*

Species	δ^2H ‰ VSMOW	$\delta^{13}C$ ‰ VPDB	$\delta^{37}Cl$ ‰ SMOC	ε_H	ε_C	ε_{Cl}	$\lambda_{H/C}$	$\lambda_{C/Cl}$	Comment	Reference
Emission experiments										
Tropical plants		−87.4 ± 12.3							average 12 tropical plants	Saito and Yokouchi, 2008
Fern trees		−61.9 ± 9.7							average 3 fern trees	Yokouchi et al., 2007
Osmunda regalis	−202 ± 10	−97 ± 8								Jaeger et al., 2018a, 2018b
Osmunda regalis	−242 ± 39	−83.9 ± 4.2	−0.91 ± 0.84							this study
Batis maritima (saltwort)		−65.7 ± 3.4								Harper et al., 2001
Solanum tuberosum (potato)		−62.7 ± 1.3								Harper et al., 2001
Phellinus pomaceus (mycelium of fungus)		−42.3 ± 0.7								Harper et al., 2001
Degradation experiments										
Microbial degradation in soils	−29 to −54	−37 to −59								Keppler et al., 2020a, 2020b Jaegeret al., 2018a Miller et al., 2004
Marine bacteria	0 to −20	−76 to −92							unknown pathway	Keppler et al., 2020a, 2020b Nadalig et al., 2014
Cyathea cooperi, *Dryopteris filix-mas* (ferns)	−8 ± 19‰	−39 ± 13‰					≈0.2			Jaeger et al., 2018b
Methylorubrum extorquens CM4	−35 ± 5	−42 ± 1					≈0.8			Nadalig et al., 2013 Nadalig et al., 2014
Hyphomicrobium sp. MC1	−27	−38								Nadalig et al., 2013
Methylorubrum extorquens CM4	−54 ± 8	−59 ± 6	−10.9 ± 0.7				0.6 ± 0.1	5.1 ± 0.1	Cmu pathway, terrestrial origin	Keppler et al., 2020a, 2020b
Leisingera methylohalidovorans MB2	−20 ± 5	−92 ± 16	−9.4 ± 0.6				0.9 ± 0.1	9.1 ± 0.1	unknown pathway, marine origin	Keppler et al., 2020a, 2020b
Selaginella kraussiana (club moss)	−77 ± 12	−10.8 ± 2.5	−5.7 ± 0.5				≈7.1	≈1.9		this study

Note. Rounded lambda values were calculated according to Equation 8 when experiments were conducted under similar experimental conditions.

2.5.2 Degradation and Isotopic Fractionation of CH_3Cl by *Selaginella Kraussiana*

2.5.2.1 Degradation Rates of CH_3Cl

The main objective of this part of the study was to explore triple-element isotopic analysis as a tool to identify potential reaction mechanisms. Current state of the art methods are not able to measure the δ_2H-CH_3Cl, δ^{13}C-CH_3Cl, and δ^{37}Cl-CH_3Cl values of ambient mixing ratios of CH_3Cl of 500–600 parts per trillion (pptv) and below. Therefore, degradation experiments were carried out by spiking reaction vessels containing *S. kraussiana* with CH_3Cl to produce a mixing ratio of 10 ppmv in the incubation vial. During incubation, absolute CH_3Cl mixing ratios in the flasks approximately halved within 24 hrs resulting in degradation rates between 0.6 and 1.5 μg g_{dw}^{-1} d^{-1}. To the best of our knowledge, there are no CH_3Cl degradation rates published yet for *S. kraussiana* but several preliminary and unpublished experiments with this plant showed rates in the same order of magnitude. CH_3Cl degradation by *S. kraussiana* is in the same order of magnitude as those rates previously observed for several fern species (0.3–17 μg g_{dw}^{-1} d^{-1}; Jaeger et al., 2018b) when spiked with 5 ppmv CH_3Cl. Observed rates are considerably higher than those observed for tropical trees (~0.1 ± 0.07 μg g_{dw}^{-1} d^{-1}; Saito et al., 2013) at ambient mixing ratios. Transformation of CH_3Cl by *S. kraussiana* followed pseudo first-order kinetics with rate constants of 17.5–19.9 d^{-1} (**Figure 0-14** in Supplementary Material S.2) which is a prerequisite for the application of the Rayleigh equation (Equation 7). It should be mentioned at this point that the incubation in microcosms using a higher mixing ratio might cause changes in the reaction kinetics. Rate constants shown here might therefore not be extrapolatable to much higher or much lower mixing ratios and also degradation rates should be interpreted with caution. Isotopic fractionation, however, is less sensitive to such changes; that is, data reported for laboratory experiments carried out at higher concentrations agrees reasonably well with field data and hence this approach is widely used in the field of contaminant science and recommended by the EPA (Hunkeler et al., 2008).

2.5.2.2 Isotopic Fractionation in CH_3Cl Caused by Degradation by S. kraussiana

Isotope analysis of CH_3Cl in the subsamples revealed considerable isotopic fractionation for all three elements (**Figure 2-2**). Isotopic hydrogen, carbon, and chlorine fractionation expressed as ε_H, ε_C, and ε_{Cl} was −77 ± 12 ‰, −10.8 ± 2.5 ‰, and −5.7 ± 0.5 ‰, respectively. Comparable triple-element isotopic data has not been published yet. One former dual-element isotope study investigated stable hydrogen and stable carbon isotopic fractionation in CH_3Cl degraded by various fern species (Jaeger et al., 2018b) when spiked with 5 ppmv CH_3Cl. Compared to our study, isotopic fractionation was negligible for hydrogen (-8 ± 19 ‰) but considerably larger for carbon reporting an ε_C of −39 ± 19 ‰. Metagenomic investigations by Jaeger et al. (2018b) did not detect any genes associated to the only known chloromethane utilization pathway (Cmu) and suggested an unknown pathway for CH_3Cl breakdown in the fern phyllosphere. Jaeger et al., 2018a, 2018b also used lambda values (dual element isotopic ratios) to corroborate these findings. The $\Lambda_{H/C}$ of 0.2 was considerably smaller than the $\Lambda_{H/C}$ associated to the Cmu pathway (Methylorubrum extorquens, $\Lambda_{H/C}$ = 0.6 to 0.8) (Keppler et al., 2020a; Nadalig et al., 2013, 2014). The assumption of a new mechanism was also supported by another CH_3Cl degradation study with plants (Kröber et al., 2021).

The largely differing $\Lambda_{H/C}$ of 7.1 obtained in the current study for degradation of CH_3Cl by *S. kraussiana* suggests that yet another pathway may be responsible for consumption of CH_3Cl. Degradation by the Cmu pathway supposedly starts with dehalogenation by nucleophilic attack (S_N2-type) which explains the relatively large ε_{Cl} of −10.9 ‰ reported for consumption of CH_3Cl by M. extorquens (Keppler et al., 2020a). The ε_{Cl} measured for CH_3Cl degradation by *S. kraussiana* in the current study is smaller (−5.7 ‰) but still within the range of ε_{Cl} for abiotic and biotic S_N2 reactions

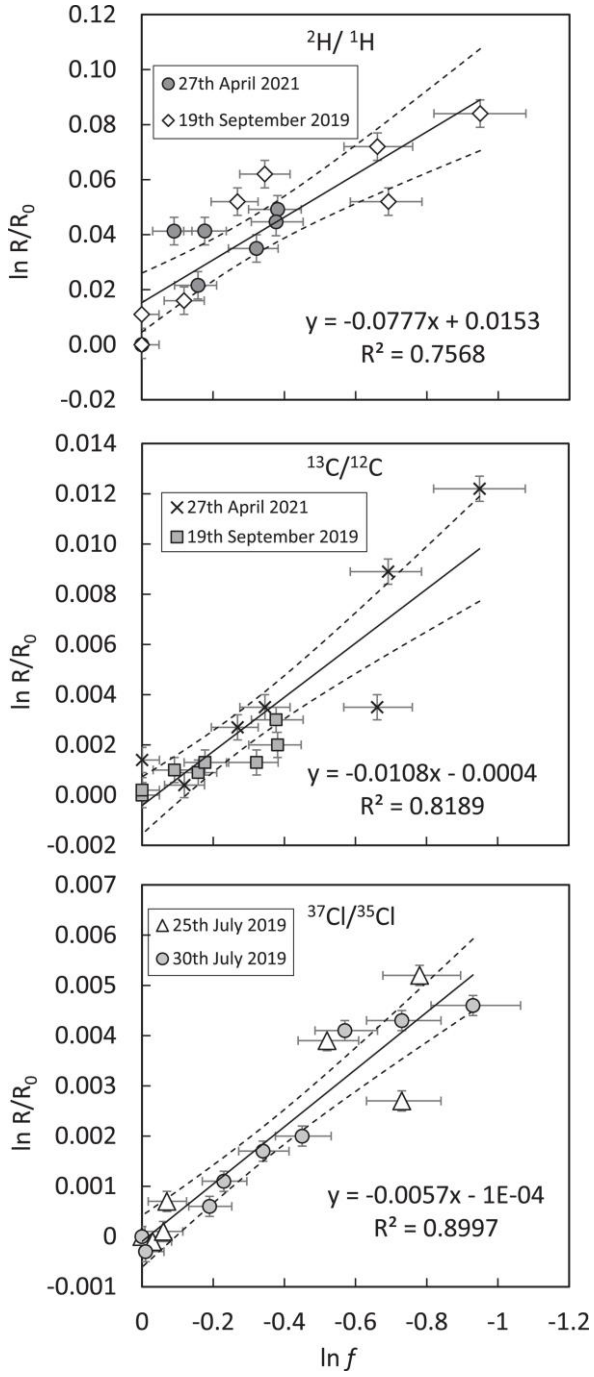

Figure 2-2. *Rayleigh plots for stable hydrogen, stable carbon and stable chlorine isotopic fractionation in CH3Cl during degradation by club moss (S. kraussiana). The linear regressions result from the combination of two separate experiments for which the slopes were indistinguishable based on the standard error. Error bars indicate the analytical uncertainty and the dashed lines show the 95% confidence intervals.*

reported thus far (Horst et al., 2019; Keppler et al., 2020a; Westaway, 2007). In contrast to chlorine isotopes, parameters for fractionation of hydrogen and carbon isotopes (ε_H, ε_C, $\Lambda_{H/C}$, $\Lambda_{C/Cl}$) indicate a different reaction mechanism. For hydrogen the secondary isotope effect of −77 ‰ is the largest so far reported for CH_3Cl degradation in biological samples contrasting the small or even negligible ε_H for secondary hydrogen isotope effects found in other experiments (**Table 2-3**). Carbon, in contrast, yielded a rather small ε_C of −10.8 ‰ which is outside the range of −37 ‰ to −92 ‰ reported for degradation by other plants or microbes (**Table 2-3**). Hence the isotopic data does not support the hypothesis that dehalogenation in the current experiments follows a S_N2-type nucleophilic substitution reaction.

The magnitude of isotopic fractionation of all three elements resembles, however, a S_N1-type nucleophilic substitution mechanism even though, from a chemical point of view, such a reaction is rather unlikely for CH_3Cl (Schwarzenbach et al., 2003). Elsner et al. (2005), and references therein, give a range of about 0 to −30 ‰ for stable carbon isotopic fractionation and about −100 to −200 ‰ for stable hydrogen isotopic fractionation which fit quite well with our experimental data. These values differ substantially from those reported for a S_N2-type reaction (ε_C = −30 to −90 and −50 < ε_H < +50). Hence, these clearly different carbon and hydrogen isotope fractionation values may be considered indicative for S_N1 and S_N2 mechanisms, respectively, and those differences are closely linked to the transition state of the reacting molecule (Westaway, 2007). During a S_N1 type reaction a carbenium ion is formed before nucleophilic attack occurs whereas in a S_N2 type reaction nucleophilic attack and dehalogenation occur in a concerted reaction; that is, simultaneously. Halogenated methanes usually do not react via S_N1 in chemical reactions because a stable carbenium ion, other than in compounds with secondary or tertiary carbon-halogen bonds, may not be formed (Melander and Saunders, 1980; Schwarzenbach et al., 2003). Biochemical reactions, however, involve large proteins (enzymes) with charged active sites which stabilize ionic transition states such as the carbenium ion (Nelson & Cox, 2005; Warshel et al., 2006). Hence it may be conceivable that the methyl cation reaches a reasonably stable transition state in the enzyme-substrate complex and thus the reaction might indeed proceed via a S_N1 reaction as indicated by the isotopic data. Further evidence to prove this hypothesis is currently not available due to the rather exploratory nature of this study. In general, microorganisms and associated microbial key enzymes responsible for halogen cycling in the environment are still largely unknown. Future studies involving a much larger set of CH_3Cl degrading plants in combination with isotopic and metagenomics studies are required to further investigate the largely unknown degradation mechanisms of CH_3Cl by plants.

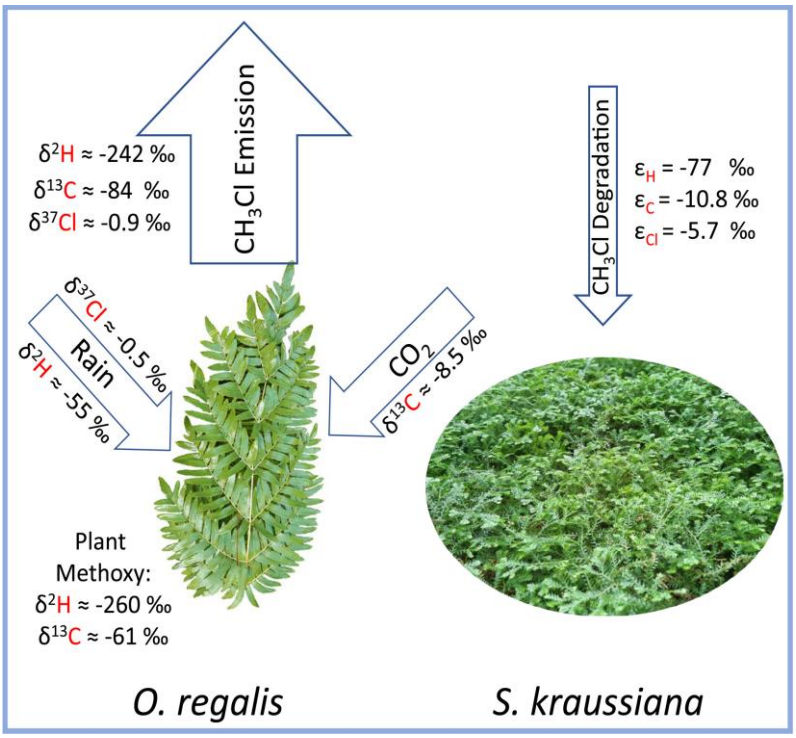

Figure 2-3. *Emission and degradation of CH_3Cl by the two plant species O. regalis and S. kraussiana and associated isotopic fingerprints and isotopic fractionation, respectively. δ_2H and $\delta_{13}C$ values for primary precursors (rain, CO_2) were estimated for the location (Heidelberg) or taken from the literature, respectively. The sizes of the blue arrows (emission, degradation) indicate the approximate relative importance of plant emissions in general.*

2.6 Implications

In this study, we presented the first triple-element isotopic characterization of a natural source of CH_3Cl. Formation and emission of CH_3Cl by plants contributes more than 50% of this important ozone-depleting gas to the atmosphere (Carpenter et al., 2014). Quantifying emissions of CH_3Cl from plants, however, is associated with large uncertainties (1,430–2,650 Gg a^{-1} (Carpenter et al., 2014)). A balanced budget has not been achieved yet and a recent study argues against tropical plants being the major source of CH_3Cl to the atmosphere (Bahlmann et al., 2019). The isotopic data collected in this study represents an important step toward creating a triple-element isotopic database of sources and sinks of CH_3Cl which is a prerequisite for future isotope based global models to improve unbalanced budget estimates. The isotopic patterns of CH_3Cl formation and degradation of the two studied plant species are graphically summarized in **Figure 2-3**.

Whether the isotopic composition of CH_3Cl emitted by *O. regalis* is representative for other plant species remains speculative but in principle it may serve as a first best estimate for other CH_3Cl producing plants. CH_3Cl is, according to current knowledge, formed by similar precursors (rainwater, SAM) in all plants and hence the isotopic composition of CH_3Cl produced by other important plants might show similar isotopic patterns as those observed for *O. regalis*. If this hypothesis turns out to be true, the isotopic signatures of plant-produced CH_3Cl should fall within a similar isotopic range for all plants. Similar source ranges in combination with strongly depleted isotopic values, in this case for carbon and hydrogen, bode well for future studies attempting to distinguish plant emissions from, for example, anthropogenic emissions and to quantify the amounts of produced CH_3Cl by the different sources (e.g., plants, soils, and fungi) and the fraction that is released to the atmosphere.

In this study we also investigated isotope effects caused during formation of CH_3Cl from potential precursors. The isotopic composition of direct precursors (SAM, rain) and emitted CH_3Cl revealed, within analytical uncertainty, no difference for hydrogen and chlorine isotope ratios and a measurable offset of about 20 ‰ for carbon isotopes. This absence of isotopic fractionation for chlorine also means that soil processes as well as uptake, transport, and conversion of dissolved Cl^- to CH_3Cl in the plant did not cause measurable isotopic fractionation throughout our experiments. Should emissions of other relevant plant species show similarly small or negligible isotopic differences between precursors and CH_3Cl, this might open up a much simpler way to isotopically characterize CH_3Cl produced by plants. This alternative approach would only require the collection of rainwater and plant samples of relevant species to estimate the isotopic composition of plant-emitted CH_3Cl without the need for laborious large-volume air sampling and preconcentration methods.

In comparison to CH_3Cl emission, the importance of CH_3Cl degradation by plants for the atmospheric budget is even more uncertain. For tropical forests some former studies reported degradation rates being at least one order of magnitude smaller than production rates with overall strong net emissions (Gebhardt et al., 2008; Saito et al., 2013). In addition, our results from degradation experiments and previous studies suggest that several transformation pathways exist causing distinct isotopic patterns (ε, λ). This fact may complicate the inclusion of degradation by plants in isotopic models because different isotope fractionation patterns may have to be considered for a variety of plants. These different isotopic patterns, however, will be clearly an asset in future microbial studies aiming at identifying different enzymatic pathways and CH_3Cl transformation processes.

2.7 Data Availability Statement

The data of this article is available via the data management portal of the UFZ (https://doi.org/10.48758/ufz.13388). The data of the manuscript was calculated and diagrams created with Microsoft Excel. Figures were created with Microsoft PowerPoint. The manuscript was prepared with Microsoft Word.

2.8 Acknowledgements

This study was part of the CHLORO-FILTER project (German Research Foundation/DFG KE 884/10-1) and supported by DFG KE 884/8-2. Furthermore, this work was supported by the Max Planck Graduate Center with the Johannes Gutenberg-Universität Mainz (MPGC). A. Horst was funded by an HGF recognition award (ERC-RA-0039) which was financed by the Initiative and Network Fund (IVF) of the Helmholtz Association, Germany. We further thank A. Zinck for collecting the rainwater samples in Leipzig, the Biogeochemistry group at Heidelberg University for analytical and technical support, and the Botanic Garden of Heidelberg University for providing the plant samples. The two anonymous reviewers are acknowledged for their valuable comments which helped to further improve the manuscript. Open Access funding enabled and organized by Projekt DEAL.

2.9 References

Bahlmann, E., Keppler, F., Wittmer, J., Greule, M., Schöler, H. F., Seifert, R., & Zetzsch, C. (2019). Evidence for a major missing source in the global chloromethane budget from stable carbon isotopes. *Atmospheric Chemistry and Physics*, *19*(3), 1703–1719. https://doi.org/10.5194/ acp-19-1703-2019

Bayer, T. S., Widmaier, D. M., Temme, K., Mirsky, E. A., Santi, D. V., & Voigt, C. A. (2009). Synthesis of methyl halides from biomass using engineered microbes. *Journal of the American Chemical Society*, *131*(18), 6508–6515. https://doi.org/10.1021/ja809461u

Bill, M., Rhew, R. C., Weiss, R. F., & Goldstein, A. H. (2002). Carbon isotope ratios of methyl bromide and methyl chloride emitted from a coastal salt marsh. *Geophysical Research Letters*, *29*(4), 1045. https://doi.org/10.1029/2001gl012946

Blei, E., Hardacre, C. J., Mills, G. P., Heal, K. V., & Heal, M. R. (2010). Identification and quantification of methyl halide sources in a lowland tropical rainforest. *Atmospheric Environment*, *44*(8), 1005–1010. https://doi.org/10.1016/j.atmosenv.2009.12.023

Brand, W. A., Coplen, T. B., Vogl, J., Rosner, M., & Prohaska, T. (2014). Assessment of international reference materials for isotope-ratio analysis (IUPAC Technical Report). *Pure and Applied Chemistry*, *86*(3), 425–467. https://doi.org/10.1515/pac-2013-1023

Bringel, F., Besaury, L., Amato, P., Krober, E., Kolb, S., Keppler, F., et al. (2019). Methylotrophs and methylotroph populations for chloromethane degradation. *Current Issues in Molecular Biology*, *33*, 149–172. https://doi.org/10.21775/cimb.033.149

Carpenter, L. J., Reimann, S., Burkholder, J. B., Clerbaux, C., Hall, B. D., Hossaini, R., et al. (2014). Ozone-depleting substances (ODSs) and other gases of interest to the Montreal protocol. Global Ozone Research and Monitoring Project – Report No. 55. In *Chapter 1 in Scientific Assessment of Ozone Depletion*. World Meteorological Organization.

Czapiewski, K. V., Czuba, E., Huang, L., Ernst, D., Norman, A. L., Koppmann, R., & Rudolph, J. (2002). Isotopic composition of non-methane hydrocarbons in emissions from biomass burning. *Journal of Atmospheric Chemistry*, *43*(1), 45–60. https://doi.org/10.1023/a:1016105030624

Derendorp, L., Wishkerman, A., Keppler, F., McRoberts, C., Holzinger, R., & Rockmann, T. (2012). Methyl chloride emissions from halophyte leaf litter: Dependence on temperature and chloride content. *Chemosphere*, *87*(5), 483–489. https://doi.org/10.1016/j.chemosphere.2011.12.035

Deventer, M. J., Jiao, Y., Knox, S. H., Anderson, F., Ferner, M. C., Lewis, J. A., & Rhew, R. C. (2018). Ecosystem-scale measurements of methyl halide fluxes from a brackish tidal marsh invaded with perennial pepperweed (*Lepidium latifolium*). *Journal of Geophysical Research: Biogeosciences*, *123*(7), 2104–2120. https://doi.org/10.1029/2018jg004536

Doronina, N. V., Sokolov, A. P., & Trotsenko, Y. A. (1996). Isolation and initial characterization of aerobic chloromethane-utilizing bacteria. *FEMS Microbiology Letters*, *142*(2–3), 179–183. https://doi.org/10.1111/j.1574-6968.1996.tb08427.x

Eggenkamp, H. G. M. (2014). The geochemistry of stable chlorine and bromine isotopes.

Elsner, M., Zwank, L., Hunkeler, D., & Schwarzenbach, R. P. (2005). A new concept linking observable stable isotope fractionation to transfor- mation pathways of organic pollutants. *Environmental Science & Technology*, *39*(18), 6896–6916. https://doi.org/10.1021/es0504587

Engel, A., Rigby, M. L. A., Burkholder, J. B., Fernandez, R. P., Froidevaux, L., Hall, B. D., et al. (2019). Update on ozone-depleting substances (ODSs) and other gases of interest to the montreal protocol. Global Ozone Research and Monitoring Project — Report No. 58. In *Chapter 1 in Scientific Assessment of Ozone Depletion*. World Meteorological Organization.

Erickson, D. J., & Duce, R. A. (1988). On the global flux of atmospheric sea salt. *Journal of Geophysical Research*, *93*(C11), 14079. https://doi. org/10.1029/jc093ic11p14079

Gebhardt, S., Colomb, A., Hofmann, R., Williams, J., & Lelieveld, J. (2008). Halogenated organic species over the tropical South American rainforest. *Atmospheric Chemistry and Physics*, *8*(12), 3185–3197. https://doi.org/10.5194/acp-8-3185-2008

Gilevska, T., Ivdra, N., Bonifacie, M., & Richnow, H. H. (2015). Improvement of analytical method for chlorine dual-inlet isotope ratio mass spectrometry of organochlorines. *Rapid Communications in Mass Spectrometry*, *29*(14), 1343–1350. https://doi.org/10.1002/rcm.7220

Greule, M., Huber, S. G., & Keppler, F. (2012). Stable hydrogen-isotope analysis of methyl chloride emitted from heated halophytic plants. *Atmospheric Environment*, *62*, 584–592. https://doi.org/10.1016/j.atmosenv.2012.09.007

Greule, M., Moossen, H., Geilmann, H., Brand, W. A., & Keppler, F. (2019). Methyl sulfates as methoxy isotopic reference materials for delta(13) C and delta(2) H measurements. *Rapid Communications in Mass Spectrometry*, *33*(4), 343–350. https://doi.org/10.1002/rcm.8355

Greule, M., Moossen, H., Lloyd, M. K., Geilmann, H., Brand, W. A., Eiler, J. M., et al. (2020). Three wood isotopic reference materials for δ2H and δ13C measurements of plant methoxy groups. *Chemical Geology*, *533*, 533. https://doi.org/10.1016/j.chemgeo.2019.119428

Greule, M., Wieland, A., & Keppler, F. (2021). Measurements and applications of δ2H values of wood lignin methoxy groups for palaeoclimatic studies. *Quaternary Science Reviews*, *268*, 107107. https://doi.org/10.1016/j.quascirev.2021.107107

Hamilton, J. T., McRoberts, W. C., Keppler, F., Kalin, R. M., & Harper, D. B. (2003). Chloride methylation by plant pectin: An efficient environ- mentally significant process. *Science*, *301*(5630), 206–209. https://doi.org/10.1126/science.1085036

Harper, D. B., Harvey, B. M. R., Jeffers, M. R., & Kennedy, J. T. (1999). Emissions, biogenesis and metabolic utilization of chloromethane by tubers of the potato (Solanum tuberosum). *New Phytologist*, *142*(1), 5–17. https://doi.org/10.1046/j.1469-8137.1999.00382.x

Harper, D. B., Kalin, R. M., Hamilton, J. T., & Lamb, C. (2001). Carbon isotope ratios for chloromethane of biological origin: Potential tool in determining biological emissions. *Environmental Science & Technology*, *35*(18), 3616–3619. https://doi.org/10.1021/es0106467

Horst, A., Bonifacie, M., Bardoux, G., & Richnow, H. H. (2019). Isotopic characterization ((2)H, (13)C, (37)Cl, (81)Br) of abiotic degradation of methyl bromide and methyl chloride in water and implications for future studies. *Environmental Science & Technology*, *53*(15), 8813–8822. https://doi.org/10.1021/acs.est.9b02165

Horst, A., Renpenning, J., Richnow, H. H., & Gehre, M. (2017). Compound specific stable chlorine isotopic analysis of volatile aliphatic compounds using gas chromatography hyphenated with multiple collector inductively coupled plasma mass spectrometry. *Analytical Chemistry*, *89*(17), 9131–9138. https://doi.org/10.1021/acs.analchem.7b01875

Hunkeler, D., Meckenstock, R. U., Sherwood Lollar, B., Schmidt, T. C., & Wilson, J. T. (2008). *A guide for assessing biodegradation and source identification of organic ground water contaminants using*

compound specific isotope analysis (CSIA). U.S. Environmental Protection Agency. EPA/600/R-08/148.

IAEA/WMO. (2021). *Global Network of isotopes in precipitation*. The GNIP Database. Retrieved from http://www.iaea.org/water

Jaeger, N., Besaury, L., Krober, E., Delort, A. M., Greule, M., Lenhart, K., et al. (2018a). Chloromethane degradation in soils: A combined micro- bial and two-dimensional stable isotope approach. *Journal of Environmental Quality*, *47*(2), 254–262. https://doi.org/10.2134/jeq2017.09.0358

Jaeger, N., Besaury, L., Rohling, A. N., Koch, F., Delort, A. M., Gasc, C., et al. (2018b). Chloromethane formation and degradation in the fern phyllosphere. *Science of The Total Environment*, *634*, 1278–1287. https://doi.org/10.1016/j.scitotenv.2018.03.316

Keppler, F., Bahlmann, E., Greule, M., Schöler, H. F., Wittmer, J., & Zetzsch, C. (2018). Mass spectrometric measurement of hydrogen isotope fractionation for the reactions of chloromethane with OH and Cl. *Atmospheric Chemistry and Physics*, *18*(9), 6625–6635. https://doi. org/10.5194/acp-18-6625-2018

Keppler, F., Barnes, J. D., Horst, A., Bahlmann, E., Luo, J., Nadalig, T., et al. (2020a). Chlorine isotope fractionation of the major chloromethane degradation processes in the environment. *Environmental Science & Technology*, *54*(3), 1634–1645. https://doi.org/10.1021/acs.est.9b06139

Keppler, F., Fischer, J., Sattler, T., Polag, D., Jaeger, N., Scholer, H. F., & Greule, M. (2017). Chloromethane emissions in human breath. *Science of The Total Environment*, *605–606*, 405–410. https://doi.org/10.1016/j.scitotenv.2017.06.202

Keppler, F., Harper, D. B., Rockmann, T., Moore, R. M., & Hamilton, J. T. G. (2005). New insight into the atmospheric chloromethane budget gained using stable carbon isotope ratios. *Atmospheric Chemistry and Physics*, *5*(9), 2403–2411. https://doi.org/10.5194/acp-5-2403-2005

Keppler, F., Kalin, R. M., Harper, D. B., McRoberts, W. C., & Hamilton, J. T. G. (2004). Carbon isotope anomaly in the major plant C-1 pool and its global biogeochemical implications. *Biogeosciences*, *1*(2), 123–131. https://doi.org/10.5194/bg-1-123-2004

Keppler, F., Rohling, A. N., Jaeger, N., Schroll, M., Hartmann, S. C., & Greule, M. (2020b). Sources and sinks of chloromethane in a salt marsh ecosystem: Constraints from concentration and stable isotope measurements of laboratory incubation experiments. *Environmental Science: Processes & Impacts Journal*, *22*(3), 627–641. https://doi.org/10.1039/c9em00540d

Koehler, G., & Wassenaar, L. I. (2010). The stable isotopic composition (37Cl/35Cl) of dissolved chloride in rainwater. *Applied Geochemistry*, *25*(1), 91–96. https://doi.org/10.1016/j.apgeochem.2009.10.004

Krober, E., Wende, S., Kanukollu, S., Buchen-Tschiskale, C., Besaury, L., Keppler, F., et al. (2021). 13C-chloromethane incubations provide evidence for novel bacterial chloromethane degraders in a living tree fern. *Environmental Microbiology*, *23*(8), 4450–4465. https://doi. org/10.1111/1462-2920.15638

Li, S., Park, M.-K., Jo, C. O., & Park, S. (2017). Emission estimates of methyl chloride from industrial sources in China based on high frequency atmospheric observations. *Journal of Atmospheric Chemistry*, *74*(2), 227–243. https://doi.org/10.1007/s10874-016-9354-4

Mariotti, A., Germon, J. C., Hubert, P., Kaiser, P., Letolle, R., Tardieux, A., & Tardieux, P. (1981). Experimental-determination of nitrogen kinetic isotope fractionation - some principles - illustration for the denitrification and nitrification processes. *Plant and Soil*, *62*(3), 413–430. https:// doi.org/10.1007/bf02374138

McAnulla, C., McDonald, I. R., & Murrell, J. C. (2001). Methyl chloride utilising bacteria are ubiquitous in the natural environment. *FEMS Microbiology Letters*, *201*(2), 151–155. https://doi.org/10.1111/j.1574-6968.2001.tb10749.x

McDonald, I. R., Kampfer, P., Topp, E., Warner, K. L., Cox, M. J., Hancock, T. L. C., et al. (2005). Aminobacter ciceronei sp. nov. and Amino- bacter lissarensis sp. nov., isolated from various terrestrial environments. *International Journal of Systematic and Evolutionary Microbiology*, *55*(5), 1827–1832. https://doi.org/10.1099/ijs.0.63716-0

Melander, L., & Saunders, W. H. (1980). *Reaction rates of isotopic molecules* (2nd ed.). John Wiley.

Miller, L. G., Warner, K. L., Baesman, S. M., Oremland, R. S., McDonald, I. R., Radajewski, S., &

Murrell, J. (2004). Degradation of methyl bromide and methyl chloride in soil microcosms: Use of stable C isotope fractionation and stable isotope probing to identify reactions and the responsible microorganisms. *Geochimica et Cosmochimica Acta*, *68*(15), 3271–3283. https://doi.org/10.1016/j.gca.2003.11.028

Nadalig, T., Farhan Ul Haque, M., Roselli, S., Schaller, H., Bringel, F., & Vuilleumier, S. (2011). Detection and isolation of chloromethane-degrading bacteria from the Arabidopsis thaliana phyllosphere, and characterization of chloromethane utilization genes. *FEMS Microbiology Ecology*, *77*(2), 438–448. https://doi.org/10.1111/j.1574-6941.2011.01125.x

Nadalig, T., Greule, M., Bringel, F., Keppler, F., & Vuilleumier, S. (2014). Probing the diversity of chloromethane-degrading bacteria by compar- ative genomics and isotopic fractionation. *Frontiers in Microbiology*, *5*, 523. https://doi.org/10.3389/fmicb.2014.00523

Nadalig, T., Greule, M., Bringel, F., Vuilleumier, S., & Keppler, F. (2013). Hydrogen and carbon isotope fractionation during degradation of chloromethane by methylotrophic bacteria. *Microbiologyopen*, *2*(6), 893–900. https://doi.org/10.1002/mbo3.124

Nagatoshi, Y., & Nakamura, T. (2007). Characterization of three halide methyltransferases in *Arabidopsis thaliana*. *Plant Biotechnology*, *24*(5), 503–506. https://doi.org/10.5511/plantbiotechnology.24.503

Nelson, D. L., & Cox, M. M. (2005). *Lehninger principles of biochemistry*. W.H. Freeman and Company.

Ojeda, A. S., Phillips, E., Mancini, S. A., & Lollar, B. S. (2019). Sources of uncertainty in biotransformation mechanistic interpretations and remediation studies using CSIA. *Analytical Chemistry*, *91*(14), 9147–9153. https://doi.org/10.1021/acs.analchem.9b01756

Ravishankara, A. R., Daniel, J. S., & Portmann, R. W. (2009). Nitrous oxide (N_2O): The dominant ozone-depleting substance emitted in the 21st century. *Science*, *326*(5949), 123–125. https://doi.org/10.1126/science.1176985

Renpenning, J., Horst, A., Schmidt, M., & Gehre, M. (2018). Online isotope analysis of 37Cl/35Cl universally applied for semi-volatile organic compounds using GC-MC-ICPMS. *Journal of Analytical Atomic Spectrometry*, *33*(2), 314–321. https://doi.org/10.1039/c7ja00404d

Rhew, R. C. (2011). Sources and sinks of methyl bromide and methyl chloride in the tallgrass prairie: Applying a stable isotope tracer technique over highly variable gross fluxes. *Journal of Geophysical Research*, *116*(G3), 116. https://doi.org/10.1029/2011jg001704

Rhew, R. C., Ostergaard, L., Saltzman, E. S., & Yanofsky, M. F. (2003). Genetic control of methyl halide production in Arabidopsis. *Current Biology*, *13*(20), 1809–1813. https://doi.org/10.1016/j.cub.2003.09.055

Saito, T., & Yokouchi, Y. (2008). Stable carbon isotope ratio of methyl chloride emitted from glasshouse-grown tropical plants and its implication for the global methyl chloride budget. *Geophysical Research Letters*, *35*(8), L08807. https://doi.org/10.1029/2007gl032736

Saito, T., Yokouchi, Y., Kosugi, Y., Tani, M., Philip, E., & Okuda, T. (2008). Methyl chloride and isoprene emissions from tropical rain forest in Southeast Asia. *Geophysical Research Letters*, *35*(19), L19812. https://doi.org/10.1029/2008gl035241

Saito, T., Yokouchi, Y., Phillip, E., & Okuda, T. (2013). Bidirectional exchange of methyl halides between tropical plants and the atmosphere. *Geophysical Research Letters*, *40*(19), 5300–5304. https://doi.org/10.1002/grl.50997

Schaeffer, S. M., Miller, J. B., Vaughn, B. H., White, J. W. C., & Bowling, D. R. (2008). Long-term field performance of a tunable diode laser absorption spectrometer for analysis of carbon isotopes of CO_2 in forest air. *Atmospheric Chemistry and Physics*, *8*(17), 5263–5277. https://doi.org/10.5194/acp-8-5263-2008

Schäfer, H., Miller, L. G., Oremland, R. S., & Murrell, J. C. (2007). Bacterial cycling of methyl halides. *Advances in Applied Microbiology*, *61*, 307–346.

Schmidberger, J. W., James, A. B., Edwards, R., Naismith, J. H., & O'Hagan, D. (2010). Halomethane biosynthesis: Structure of a SAM-dependent halide methyltransferase from *Arabidopsis thaliana*. *Angewandte Chemie International Edition in English*, *49*(21), 3646–3648. https://doi.org/10.1002/anie.201000119

Schwarzenbach, R. P., Gschwent, P. M., & Imboden, D. M. (2003). *Environmental Organic Chemistry*. John Wiley & Sons.

Thompson, A. E., Anderson, R. S., Rudolph, J., & Huang, L. (2002). Stable carbon isotope signatures of background tropospheric chloromethane and CFC113. *Biogeochemistry*, *60*(2), 191–211.

https://doi.org/10.1023/a:1019820208377
Thornton, B. F., Horst, A., Carrizo, D., & Holmstrand, H. (2016). Methyl chloride and methyl bromide emissions from baking: An unrecognized anthropogenic source. *Science of the Total Environment*, *551–552*, 327–333. https://doi.org/10.1016/j.scitotenv.2016.01.213
van Breukelen, B. M. (2007). Extending the Rayleigh equation to allow competing isotope fractionating pathways to improve quantification of biodegradation. *Environmental Science & Technology*, *41*(11), 4004–4010. https://doi.org/10.1021/es0628452
Vannelli, T., Messmer, M., Studer, A., Vuilleumier, S., & Leisinger, T. (1999). A corrinoid-dependent catabolic pathway for growth of a Methy- lobacterium strain with chloromethane. *Proceedings of the National Academy of Sciences of the United States of America*, *96*(8), 4615–4620. https://doi.org/10.1073/pnas.96.8.4615
Volpe, C., & Spivack, A. J. (1994). Stable chlorine isotopic composition of marine aerosol-particles in the Western Atlantic-Ocean. *Geophysical Research Letters*, *21*(12), 1161–1164. https://doi.org/10.1029/94gl01164
Warshel, A., Sharma, P. K., Kato, M., Xiang, Y., Liu, H., & Olsson, M. H. (2006). Electrostatic basis for enzyme catalysis. *Chemical Reviews*, *106*(42), 3210–3235. https://doi.org/10.1002/chin.200642255
Weinberg, I., Bahlmann, E., Michaelis, W., & Seifert, R. (2013). Determination of fluxes and isotopic composition of halocarbons from seagrass meadows using a dynamic flux chamber. *Atmospheric Environment*, *73*, 34–40. https://doi.org/10.1016/j.atmosenv.2013.03.006
Westaway, K. C. (2007). Determining transition state structure using kinetic isotope effects. *Journal of Labelled Compounds and Radiopharma- ceuticals*, *50*(11–12), 989–1005. https://doi.org/10.1002/jlcr.1434
Wishkerman, A., Gebhardt, S., McRoberts, C. W., Hamilton, J. T., Williams, J., & Keppler, F. (2008). Abiotic methyl bromide formation from vegetation, and its strong dependence on temperature. *Environmental Science and Technology*, *42*(18), 6837–6842. https://doi.org/10.1021/ es800411j
Wuosmaa, A. M., & Hager, L. P. (1990). Methyl chloride transferase: A carbocation route for biosynthesis of halometabolites. *Science*, *249*(4965), 160–162. https://doi.org/10.1126/science.2371563
Xiao, X., Prinn, R. G., Fraser, P. J., Simmonds, P. G., Weiss, R. F., O'Doherty, S., et al. (2010). Optimal estimation of the surface fluxes of methyl chloride using a 3-D global chemical transport model. *Atmospheric Chemistry and Physics*, *10*(12), 5515–5533. https://doi.org/10.5194/ acp-10-5515-2010
Yokouchi, Y., Saito, T., Ishigaki, C., & Aramoto, M. (2007). Identification of methyl chloride-emitting plants and atmospheric measurements on a subtropical island. *Chemosphere*, *69*(4), 549–553. https://doi.org/10.1016/j.chemosphere.2007.03.028
Yokouchi, Y., Takenaka, A., Miyazaki, Y., Kawamura, K., & Hiura, T. (2015). Emission of methyl chloride from a fern growing in subtrop- ical, temperate, and cool-temperate climate zones. *Journal of Geophysical Research: Biogeosciences*, *120*(6), 1142–1149. https://doi.org/10.1002/2015jg002994

3 Investigation of Local Sources of the Halogenated Very Short-Lived Substances Chloroform and Bromoform

3.1 Introduction

As ozone-depleting substances (ODSs) with significant global warming potentials (GWPs), chloroform ($CHCl_3$) and bromoform ($CHBr_3$) play important roles in the chemistry and physics of the atmosphere. Both compounds are triple-halogenated and possess a hydrogen atom that is susceptible to oxidation by OH radicals. Their atmospheric lifetimes are estimated as ~0.5 years and 13 days, respectively (WMO, 2022), making them very short-lived substances (VSLSs) that are not regulated by the Montreal Protocol, despite their contribution to stratospheric ozone loss (WMO, 2022). Natural VSLSs emissions are expected to increase due to increasing sea-to-air fluxes (Butler et al., 2007; Hepach et al., 2014; Leedham et al., 2013).

Chloroform is the second most abundant VSLS known, ranging between 5 and 15 pptv in the lower troposphere (Hossaini et al., 2019; Prinn et al., 2018) and with estimated global net emissions of 339 (±70) Gg yr^{-1} (for 2020; WMO, 2022). There are both anthropogenic and natural chloroform sources. Chloroform is widely used as a solvent and for the production of HCFC-22, which has been used as a refrigerant and is still used as a precursor for the production of polytetrafluoroethylene (PTFE). Another significant source of chloroform in the atmosphere is the pulp and paper manufacturing industry (Aucott et al., 1999), and it is also known to arise as a by-product of water disinfection by chlorination. The anthropogenic contribution to the total global emission is estimated at between 10 and 29 % (McCulloch, 2003; Worton et al., 2006). Natural sources are diverse and less well understood, although both marine and terrestrial areas have been established (McCulloch, 2003). Individual marine and littoral zone sources are micro- and macroalgae, accounting for about half of the total emissions (Bahlmann et al., 2015; Lim et al., 2018; Mtolera et al., 1996; Nightingale et al., 1995; Orlikowska et al., 2015). Terrestrial emissions have been reported from the (Ant-)Arctic (Johnsen et al., 2016; Rhew et al., 2008b; Zhang et al., 2021), temperate (Forczek et al., 2015) and tropical ecosystems (Gebhardt et al., 2008; Scheeren et al., 2003). The main terrestrial source of chloroform is thought to be soil, where both biotic and abiotic formation have been reported (Albers et al., 2011; Grøn et al., 2012; Hoekstra et al., 1998a, 2001). Miscellaneous other chloroform sources have been documented including volcanoes (Frische et al., 2006; Jordan et al., 2000), fungi (Hoekstra et al., 1998b), rice paddies (Khalil et al., 1990a), peatlands (Dimmer et al., 2001), biomass burning (Lobert et al., 1999), as well as termites (Khalil et al., 1990b) and ant nests (Berberich et al., 2017). Besides its ozone depletion potential, chloroform has a global warming potential (GWP) of 20 for the 100-year time scale and an even higher GWP of 72 for the 20-year time horizon (WMO, 2022).

Bromoform is much less abundant than chloroform, with mixing ratios between 0.4-4 pptv in the marine boundary layer (MBL) and 0.3-1.11 pptv in the tropical tropopause layer (WMO, 2018). The atmospheric lifetime of bromoform is reported to be in the range of tens of days, largely depending on the region, altitude, and season (Papanastasiou et al., 2014). Bromoform is considered to be a mostly naturally emitted compound. However, there are minor anthropogenic sources (e.g., coastal nuclear power plants (Allonier et al., 1999)), but these specific sources do not play a significant role globally (Quack and Wallace, 2003). Major natural sources are emissions from macroalgae (Bondu et al., 2008; Laturnus, 2001; Leedham et al., 2013) and phytoplankton (Lim et al., 2017; Lin and Manley, 2012; Moore et al., 1996). Quack and Wallace (2003) described the main drivers of emission, biological production pathways of marine bromoform, and its subsequent atmospheric fate in detail. Even though bromoform sources are almost exclusively associated with the marine environment, some studies have shown that soils can be potential bromoform emitters (Huber et al., 2009; Weigold et al., 2016). To the best of our knowledge, so far only Macdonald et al. (2019) have been able to show in-situ bromoform emissions from soils.

Chloroform and bromoform share similar atmospheric degradation processes, i.e., the reaction with OH radicals in the troposphere, and photolysis and reaction with ozone in the stratosphere. The atmospheric lifetime of these VSLSs is too short relative to hemispheric and interhemispheric mixing times to enable an equal global distribution. The transport of Cl_y and Br_y (total inorganic chlorine and bromine, respectively) into the stratosphere is possible via two processes: source gas injection (direct transport of CHX_3 into the stratosphere; SGI) and product gas injection (transport of products of CHX_3 degradation into the stratosphere; PGI) (Ko and Poulet, 2003). This applies especially if CHX_3 are emitted in the tropics where vertical transport through deep convection is faster and more common (Aschmann, 2009; Fueglistaler et al., 2009; Liang et al., 2014; Sinnhuber and Folkins, 2006). It has been suggested that VSLSs make up about 25 % of the ozone loss observed between 1998 and 2018 in the tropical lower stratosphere (Villamayor et al., 2023). The catalytic ozone loss cycles in the stratosphere for chlorine and bromine have been described in detail elsewhere (Chipperfield and Pyle, 1998; Daniel et al., 1999). Despite Cl_y being more abundant in the stratosphere, bromine is about 60 times more potent regarding stratospheric ozone depletion than chlorine on a per-atom basis (Crutzen, 1995; Sinnhuber et al., 2009).

Not only do CHX_3 exert an influence on stratospheric chemistry, but such compounds are also highly relevant in the free troposphere as well by influencing HO_x, NO_x, and DMS speciations and abundancies (e.g., von Glasow et al., 2004). The degradation pathways of CHX_3 within the troposphere depend on oxidant abundance, temperature, pressure, and UV radiation, but they are almost exclusively initiated by the reaction with OH or by UV photodissociation (Krysztofiak et al., 2012; WMO, 2022). Degradation with Cl atoms and with nitrate radicals only play a minor role, as well as biodegradation (Cappelletti et al., 2012).

In this study we present atmospheric measurements of chloroform and bromoform taken over one dry-to-wet transition (January 2023), one full-wet (April-May 2024), and one dry season (October 2023) in the pristine Amazonian rainforest canopy (23 m), taken at the ATTO field site (Andreae et al. 2015). Additional measurements were taken at greater heights above the canopy up to 325 m to show how the concentration of these compounds changes with altitude, as well as soil flux measurements. These data are used to investigate potential local sources and their seasonal dependency.

3.2 Sampling and Analysis

3.2.1 Sample Collection

All sampling took place at the Amazon Tall Tower Observatory site (ATTO), located in the pristine Amazon rainforest approx. 150 km NE of Manaus, Brazil. The site's core is the 325 m tall tower, which is accompanied by the 80 m "instant tower". The average canopy height is 35-40 m. For a detailed site description, we refer the reader to Andreae et al., 2015.

All data shown in this work was collected using adsorbent tube sampling. Sampling on the instant tower was performed using inert-coated stainless steel tubes 89 × 5.33 mm I.D (SilcoNert 2000 (SilcoTek™, Germany)) filled with 150 mg Tenax® TA (Buchem BV, Apeldoorn, The Netherlands) and 150 mg Carbograph™ 5 TD (560 m2 /g) (L.A.R.A s.r.l, Rome, Italy)) for the 23 m instant tower samples. The sorbent tubes used at 80 m and 320 m on the ATTO tower were filled with 130 mg of Carbograph™ 1 followed by 130 mg of Carbograph™ 5 (L.A.R.A s.r.l, Rome, Italy). The size of the Carbograph™ particles was in the range of 20-40 mesh. A quartz filter impregnated with 10% w/w sodium thiosulfate was used at the inlet of the sampling line to scrub ozone (Ernle et al., 2023). Several autosamplers, described in detail elsewhere (Kuhn et al., 2005), have been installed on both

the tall tower (80 m and 320 m), as well as on the instant tower (23 m). Sorbent tubes were placed into the autosamplers and sampled at the respective starting times for 30 min each with a flow between 44 and 200 sccm, resulting in a sample volume ranging between 1 and 6 l. The mass flow controllers installed in the autosamplers were calibrated with a Gilibrator. Soil samples were collected from chambers placed on the ground close to the ATTO tower. A collar was gently placed on the soil at least 24 hours before sampling. No litter was removed from the sampled soil spots. It was placed on ground with a high organic content and high respiration. The lid was placed on the collar 15 minutes prior to sampling with a handheld pump (Gilian GilAir Plus). Cartridges were sampled from inside the chamber and from the outside air next to the chambers for 30 minutes with a 200 mL min^{-1} flow rate. Soil flux sampling was done 5-6 times a day for 4 days in dry-to-wet transition season in January 2023, 7 days in the dry season in October 2023, and for 8 days in the wet season 2024. Collected samples have been stored on-site in a fridge at -20 °C and room temperature and shipped to MPIC in Mainz, Germany, where the sample analysis was carried out.

3.2.2 Analytical Setup

The analysis of the sorbent tubes sampled was carried out using a two-stage automated thermal desorber (TD100-xr, MARKES International, U.K.), with helium 5.0 carrier gas. The sample was desorbed at a temperature of 250 °C and a flow of 50 ml min^{-1} of helium for 5 minutes and was pre-concentrated onto a cold trap (materials emissions, MARKES International, U.K.) at 30 °C. The cold trap was purged with carrier gas for 1 minute with a flow of 50 ml min^{-1} then rapidly heated to 250 °C. The sample was swept from the cold trap with a flow of 3 ml min^{-1} and injected into the column. The separation of the sampled compounds was achieved using a 60 m β-DEX™ 120 column (Sigma-Aldrich Chemie GmbH, Germany) with a 0.25 mm internal diameter and a film thickness of 0.25 µm. The temperature program used was as follows, 50 °C for 5 minutes then 50 °C to 110 °C at 1.5 °C min^{-1} and 110 °C to 220 °C at 10 °C min^{-1}, and then held at 220 °C for 10 minutes. The column flow was set to 1 ml min^{-1}. Detection was achieved using a time-of-flight mass spectrometer (Bench TOF-Select, MARKES International, U.K.). A standard gas calibration mixture (Apel-Riemer 2019) containing alpha-pinene was used to make the first calibration and then a second gas calibration mixture containing chloroform and bromoform was used to make a later calibration in tandem with a second alpha-pinene calibration to perform a back calibration for all data.

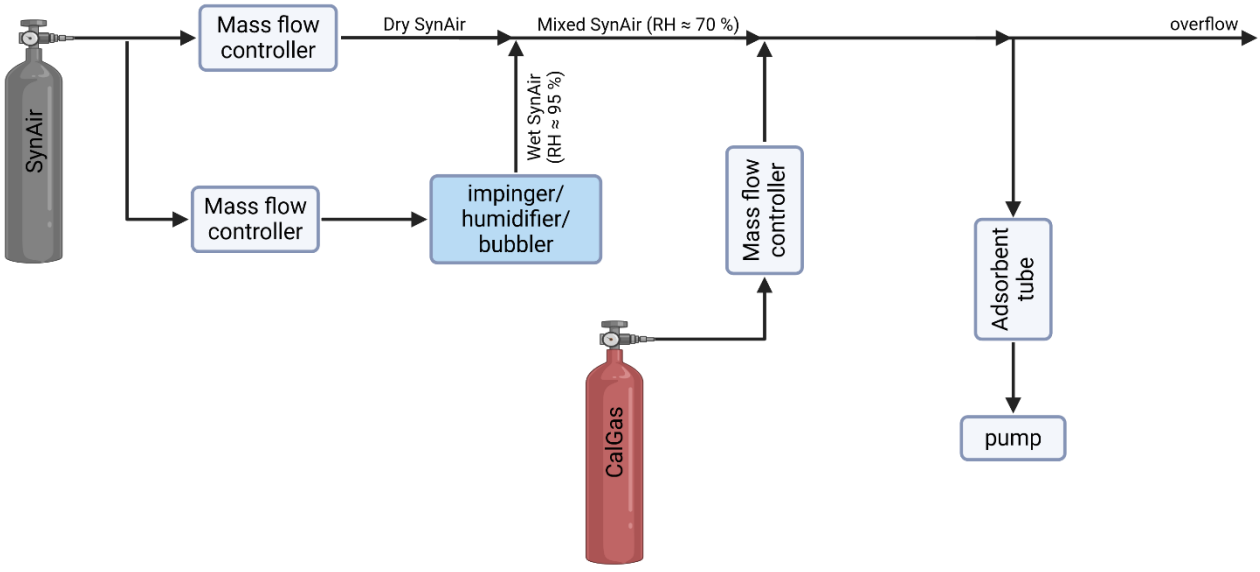

Figure 3-1. *Flow path used for filling of calibration sorbent tubes. Figure created in Biorender.com*

For the soil samples, the trap low temperature for preconcentration was set to 10°C instead of 30°C. The GC method was extended to 50 °C for 5 minutes then 50 °C to 120 °C at 1.5 °C min^{-1} and 110 °C to 220 °C at 5 °C min^{-1} and then held at 220 °C for 10 minutes. The column flow was set to 1.2 ml min^{-1}.

We carried out a 5-point calibration for chloroform and bromoform. As shown in **Figure 3-1**, synthetic air and a multi-compound calibration gas were mixed to gain the respective diluted mixing ratios. To improve the comparability with the ambient air in the tropical rainforest, we increased the relative humidity of the initially dry diluted calibration gas mixture to 70 %.

As the samples from the presented experiments were intended to be used solely for terpenoid emission data, the initially used calibration gas did not include halogenated VOCs. To be able to quantify the chloroform and bromoform data, we later used another calibration gas which included halocarbons (**Table 4-3**) to perform a back-calibration with relative response factors. We derived a correction factor for each halocarbon compound by the intercomparison with the alpha-pinene signal of the respective calibration steps of the first calibration gas (CalGas).

3.3 Results and Discussion

3.3.1 Volume Mixing Ratios at Canopy Height

3.3.1.1 Chloroform

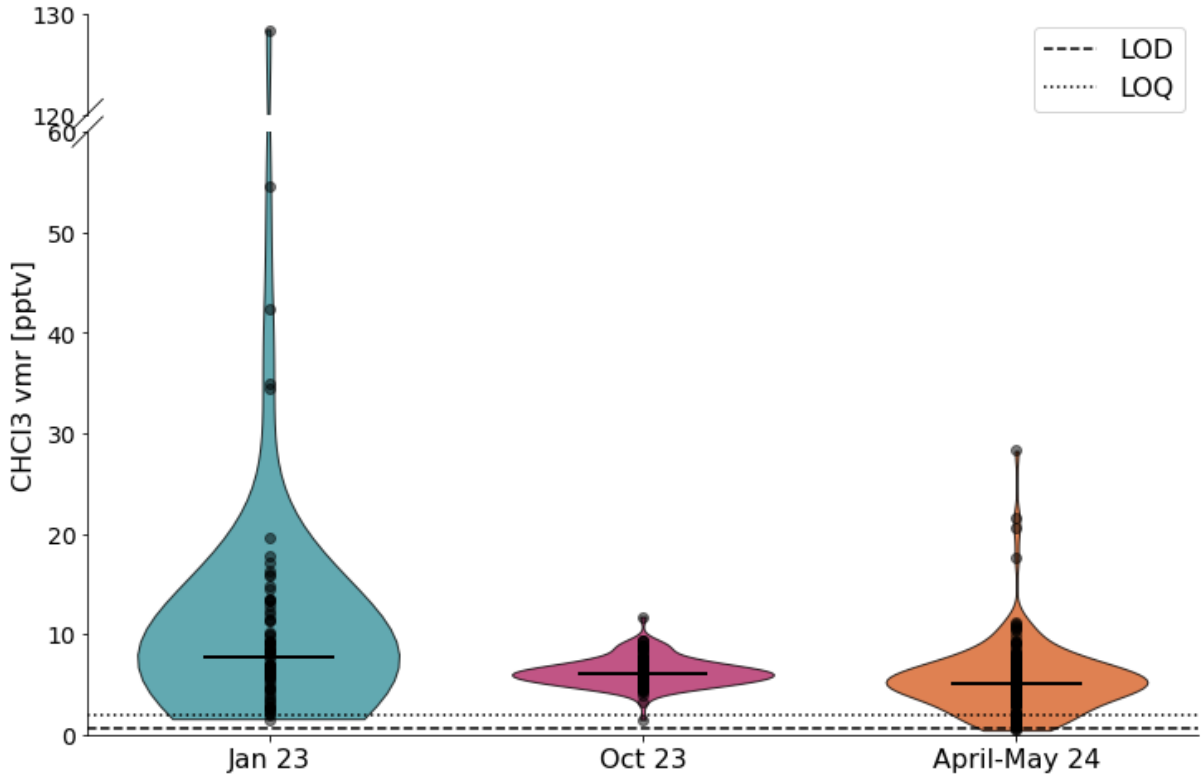

Figure 3-2. *Violin plots of chloroform volume mixing ratios (VMR) from dry-to-wet transition season 2023 (Jan 23; n=80), dry season 2023 (Oct 23; n=112), and full-wet season 2024 (April-May 24; n=158). Samples taken from Instant Tower (23 m sampling height). Black horizontal bars represent the median values of the respective dataset. Limit of detection (LOD) and limit of quantification (LOQ) are displayed in dashed and dotted lines, respectively.*

Chloroform volume mixing ratios (VMR) from three different seasons, sampled at 23 m above ground level, are shown in **Figure 3-2**. Strikingly, the medians were rather similar throughout all seasons, however, a slight decrease in the median was seen from January 2023 (dry-to-wet

transition season) to April-May 2024 (wet season) from 7.8 pptv to 5.2 pptv. This could be interpreted as representing the site's local atmospheric background value, as the medians are within the range of chloroform values reported by the AGAGE network whose sites are selected to monitor the atmospheric background (Hossaini et al., 2019; Prinn et al., 2018). During dry season 2023, there was only a negligible natural variability in the chloroform data equal to 1.4 pptv. VMRs measured during the dry-to-wet transition season 2023 and wet season 2024 showed much larger variabilities than dry season 2023, equal to 15.7 pptv and 3.6 pptv, respectively. In January 2023, these occasional chloroform spikes reached almost 130 pptv, corresponding to an increase of about 1400 % compared to the local atmospheric background. Wet season 2024 showed single spikes up to ~30 pptv. These sharp VMR increases were only of short duration, indicating local, rather short-term emission events. Long-term effects with widespread elevated chloroform emissions would increase the median value of the respective season, which was not the case here.

The chloroform spikes do not obviously correlate with rain events or soil moisture (see Chapter 3.3.1.3). Since the dynamics of the local Chloroform have not been obtained yet at high time resolution, it's still a possibility that rain events – and the associated elevated soil moisture – have an indirect or delayed impact on high-emission events (see Chapter 3.3.3). It is worth noting that rainfall events can occur a short distance from the tower and trigger emission without registering as rain at the site. Furthermore, the cause for the elevated chloroform VMRs might be an interplay of heterogenic emission processes occurring at the same time. This needs to be further investigated with the measurement of direct emissions from e.g., fungi, insect colonies, or even plants. Data obtained from a past study on cryptogamic covers were investigated for emissions of chloroform and bromoform but no peak belonging to either compound was found (Edtbauer et al., 2021).

Another factor potentially influencing the seasonal variation in the VMRs of chloroform was the effect of the El Niño-Southern Oscillation (ENSO). According to the Oceanic Niño Index (ONI), there was an ENSO anomaly from (boreal) spring 2023 to spring 2024 (NOAA's Climate Prediction Center, 2024) indicating strong El Nino conditions. ENSO could affect the chloroform emissions over the sea by indirectly affecting a significant source of chloroform, i.e., micro- and macroalgae. Relevant parameters influenced by ENSO in this regard could be potential changes in sea surface temperature, light availability/cloud cover changes, or frequency of tropical storms. However, El Nino conditions are known to raise temperatures and lower precipitation in Amazonia (Pfannerstill et al., 2018), so local sources should also be taken into account. To what extent and for how long these effects influenced the chloroform formation processes must be the subject of further research.

3.3.1.2 Bromoform

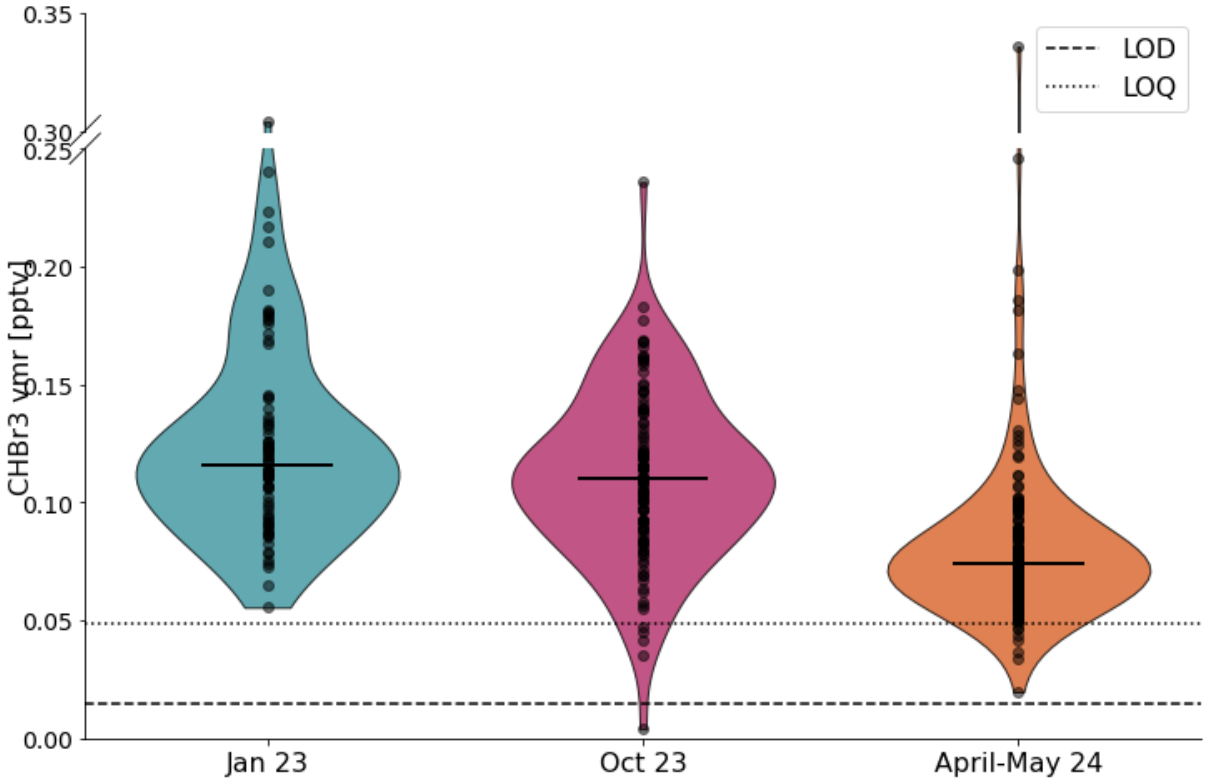

Figure 3-3. *Violin plots of bromoform volume mixing ratios (VMR) from dry-to-wet transition season 2023 (Jan 23; n=80), dry season 2023 (Oct 23; n=112), and full-wet season 2024 (April-May 24; n=158). Samples taken from Instant Tower (23 m sampling height). Black horizontal bars represent the median values of the respective dataset. Limit of detection (LOD) and limit of quantification (LOQ) are displayed in dashed and dotted lines, respectively.*

The measured VMRs of bromoform were overall one or two orders of magnitude lower compared to chloroform (see **Figure 3-3**) which is consistent with chloroform's higher global atmospheric abundance compared to bromoform (WMO, 2022). Moreover, bromoform is known to have mainly marine sources, which is why low VMRs at a continental site far away from the coast, such as ATTO, can be expected. The large distance to the assumed source regions makes the obtained measurements more difficult to interpret. Just as for chloroform, three factors must be taken into account when considering the presented results of bromoform: local sources, the origin of the measured air masses, and potential El Nino effects.

The median values for January and October 2023 are nearly identical, 0.12 pptv and 0.11 pptv, respectively. Although wet season 2024 shows a lower median than the two previous seasons with only 0.07 pptv, it also has the highest maximum values with spikes up to 0.35 pptv. These spikes might indicate a local source, even if not yet identified. As there are some reports on bromoform emissions by soils (Huber et al., 2009; Macdonald et al., 2019; Weigold et al., 2016), this and other potential sources need to be further investigated, even though no bromoform emissions from soil flux measurements were detected in this work (Chapter 3.3.3).

Next to local sources, the hemispheric influence, or, more precisely, the history of the measured air masses is relevant to the overall seasonal atmospheric bromoform background in the Amazon rainforest. The hemispheric influence of the sampled air is important because there are regions with higher Bromoform emissions, largely depending on the current season as well as anthropogenic sources in the respective footprint region. The footprint region, in turn, depends on the seasonal shift of the Inter-Tropical Convergence Zone (ITCZ): In the wet season, the ITCZ is located south of the ATTO site, leading to the northern hemisphere being the predominant origin

of most of the air arriving at the ATTO site (Pöhlker et al., 2019). When the ITCZ shifts and is located north of the ATTO site during the dry season, the sampled air at ATTO has its origin predominantly in the southern hemisphere. Clusters of 14-day backward trajectories have been calculated for the time frames discussed in this article using the HYSPLIT model (Draxler, 1999; Draxler and Hess, 1997, 1998; Stein et al., 2015), confirming the assumed footprint regions (S.1).

Bromoform is considered to be mostly emitted by biogenic sources with dominant marine sources (Quack and Wallace, 2003). Consequently, its seasonal and spatial distribution is strongly coupled to the occurrence of phytoplankton and macroalgae emissions. As a result, bromoform concentrations are highest during summer in the respective hemisphere, i.e., peaking in December-January-February in the southern hemisphere and June-July-August in the northern hemisphere (Booge et al., 2024; Stemmler et al., 2015). Since the southern hemisphere is covered to a greater extent by oceans than the northern hemisphere, the global annual bromoform concentrations show the highest values during boreal winter (Stemmler et al., 2015). Bringing these aspects together, along with published global models the measured air shown in this study was influenced by relatively low concentrations from the northern hemisphere in January and April as well as relatively low concentrations from the southern hemisphere in October (Booge et al., 2024; Stemmler et al., 2015). However, there might be extraordinary bromoform sources in the respective footprint regions, e.g., regional algae blooms, influencing the sampled air at ATTO, even though it wasn't possible to link the respective backward trajectories to such events with this data.

Both factors influencing bromoform mixing ratios, long-range transport ways and potential local sources, could be affected by the ENSO anomalies, as was discussed above for chloroform. Since bromoform VMRs at ATTO seem to be more influenced by the footprint regions and only to a smaller amount influenced by local sources, it is the marine ENSO effects (e.g., altered abundance and intensity of algal blooms or sea surface temperature) that need to be considered here rather than terrestrial ENSO effects like drought at the ATTO site. In the future, this work's data needs to be compared to seasons without ENSO effects to evaluate its consequences.

3.3.1.3 Correlations of Chloroform and Bromoform Emissions with Other Parameters

Table 3-1. *Pearson correlation coefficients for chloroform and bromoform VMRs and other environmental parameters.*

	Chloroform			**Bromoform**		
	Jan	Oct	Apr	Jan	Oct	Apr
VMR_{CHBr3}/VMR_{CHCl3}	0.50	0.15	0.22	0.50	0.15	0.22
Soil Temperature (10 cm depth)	0.04	0.08	-0.04	0.16	-0.11	0.06
Soil Temperature (20 cm depth)	0.18	0.12	-0.16	0.09	0.06	0.10
Soil Humidity (10 cm depth)	0.03	0.02	-0.03	-0.07	-0.11	0.09
Soil Humidity (20 cm depth)	-0.03	0.07	0.11	-0.05	-0.18	-0.03
Precipitation	-0.08	-0.08	-0.03	-0.12	-0.04	-0.02
Evapotranspiration	0.16	-0.21	0.03	0.17	0.15	0.01
Ambient Air Temperature (26 m height)	-0.02	-0.13	0.12	-0.09	-0.04	-0.02
Photosynthetically Active Radiation (25 m height)	0.09	-0.18	0.13	0.03	0.08	0.04

In January 2023, there was a positive correlation between elevated chloroform and bromoform VMR values (**Table 3-1**). This suggests that both compounds may follow similar formation processes at the investigated site or at least that their local formation processes are somewhat linked. However, in the other two seasons studied, this correlation is weaker. This difference could be because, in January, we consider the predominant factor influencing the measured VMRs – especially for chloroform – to be primarily local formation, as previously mentioned. In contrast, in October, the main sources of the compounds are distant, such as the oceans. These distant sources result in the compounds being diluted by various air masses as they travel, leading to a weaker correlation.

The correlation coefficients for the other environmental parameters are difficult to interpret, as there are no clear patterns. Soil temperature and humidity don't show a strong or consistent correlation, even though we expect formation processes to occur in the soil. Possibly, soil temperature and humidity impact the formation processes but only with some latency that could blur an existing correlation, or those formation processes are driven or limited by other soil parameters.

We also did not find a correlation between elevated chloroform and bromoform VMRs and precipitation, evapotranspiration, air temperature, or photosynthetically active radiation (PAR). However, we have not yet identified or localized specific processes of local chloroform and bromoform formation or the soil parameters driving this formation. Once these sources and parameters are identified, potential correlations with other environmental factors might become clearer and be put into a better perspective. It is important to note that we did not expect to find correlation coefficients close to 1 or -1 for this data. This is because our dataset reflects the net VMRs at this site. Without identifying individual sources and conducting measurements close to them, we are measuring air that has been influenced by various factors, resulting in potentially weakened correlations.

3.3.2 ATTO Data from January 2023

3.3.2.1 Chloroform

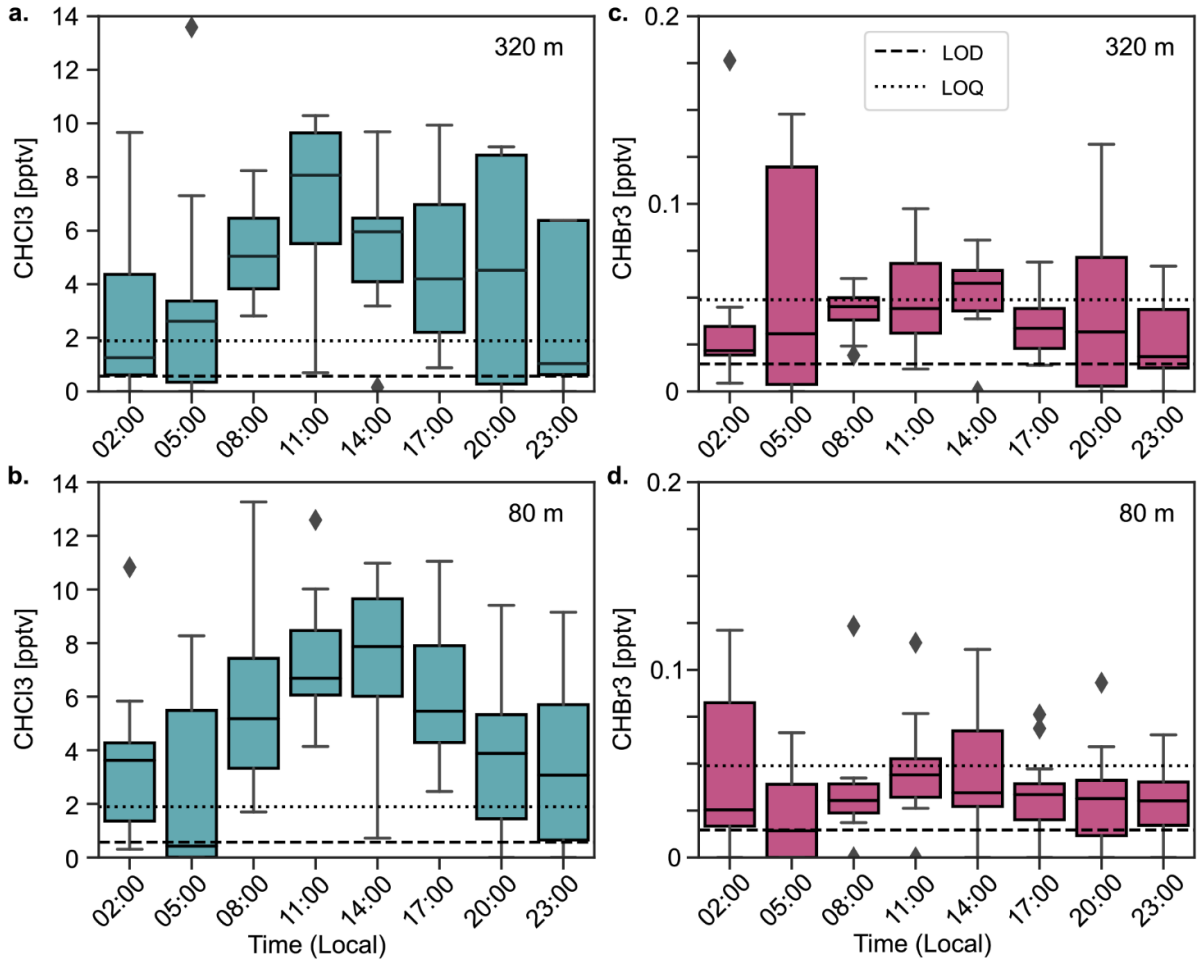

Figure 3-4. *Volume mixing ratios (VMR) of chloroform (left) and bromoform (right) throughout the day at 320 m (a, c) and 80 m (b, d) sampling height, respectively. Black horizontal bars: median (n=12 per box for 80 m; n=10 per box for 320 m); boxes: interquartile range (25 to 75 percentiles); whiskers: extend to 1.5 times the IQR from the quartiles; black diamonds: outliers. Limit of detection (LOD) and limit of quantification (LOQ) are displayed in dashed and dotted lines, respectively. Outliers exceeding the y-axis range are included in the data but not shown in the plot.*

Unexpected diel cycles of chloroform at 80 m and 320 m (**Figure 3-4** a and b) were obtained from samples measured during January 2023 on the ATTO tower. Chloroform mixing ratios built up in the early morning, starting from around 2-3 pptv at night, peaking between 11 am and 2 pm at 8 pptv, and decreased in the evening into the night-time.

The overall chloroform mixing ratios were slightly higher at 80 m than at 320 m, suggesting a source at the ground and dilution with increasing height. This indication was supported by the canopy data (see Chapter 3.3.1.1), where even higher values were measured within the canopy at 23 m height than at 80 m and 320 m on the ATTO tower. The data of **Figure 3-4** shows that whatever the source of the chloroform is, it follows a diel pattern. One explanation could be that physical atmospheric effects like the development of the nocturnal boundary layer or other processes linked to thermal convection could lead to such a pattern. However, if chloroform was emitted constantly from the soil, it would accumulate below the canopy or at least within the nocturnal boundary layer during the night, peaking around sunrise and dropping at midday to afternoon, when thermal convection and therefore turbulent mixing is highest. Since the opposite was the case here, this means that the emission process must follow a diel characteristic itself and is either directly

dependent on sunlight or temperature if being of an abiotic nature, or, if it is a biological process, indirectly coupled to these parameters over a living organism which emits chloroform and relying on a diel metabolism itself. In the plots shown, the 320 m data peaked at 11 am while the 80 m data peaked at 2 pm. However, as we expect an emission process in any way coupled to light or temperature, we expect the actual VMR peaks for both heights around noon, even if this can't be shown here due to the limited temporal resolution of our dataset.

There are rare reports of higher plants to emit chloroform (Forczek et al., 2015). Within the soil, microorganisms can follow a circadian rhythm (Staley et al., 2017), and there are fungi in soils that follow a diel cycle when it comes to their metabolism (Gusareva et al., 2019; Hernandez and Allen, 2013). As fungi are reported to be able to emit chloroform (Hoekstra et al., 1998b), these organisms come into question to be as well a source of the investigated ecosystem. To prove this, future research needs to be done with the isolated fungal communities of local soils and their potential to release chloroform.

3.3.2.2 Bromoform

Bromoform showed mixing ratios about one order of magnitude lower than chloroform VMRs. The 80 m mixing ratio of bromoform didn't show elevated mixing ratios for the respective times when compared to 320 m mixing ratios (**Figure 3-4** c and d), which supports the argument that bromoform presented in this study was rather dominated by the long-range transport from its coastal and marine sources than by local sources.

There are, however, two indications for local bromoform sources in the ecosystem around the ATTO site which can be derived from the 80 m and 320 m data: First, the bromoform mixing ratios at these heights were significantly lower compared to the values measured at 23 m during the same time. Secondly, a diel pattern is visible in the plot which is less pronounced, yet similar to that for chloroform. At night, the lowest observed median mixing ratio at 80 m was ~0.01 pptv, rising in the morning and peaking at 11 am with 0.04 pptv before decreasing again in the evening. We must take into account that for bromoform, many values are below the statistical limit of quantification and therefore need to be interpreted with caution.

One could argue that, given an assumed local bromoform source at ground level, there would need to be a decrease as well between 80 m and 320 m visible in the data, similar to chloroform. But while for chloroform, this suspected ground source would lead to the constant decrease of mixing ratios from 23 m to 80 m to 320 m, for bromoform, a similar source could plausibly lead to the decrease being only detectable from 23 m to 80 m, as the overall lower atmospheric bromoform mixing ratios could lead to faster dilution during vertical transport. For chloroform, this process would take longer due to the stronger local source (and additionally the lower reactivity compared to bromoform, see Chapter 3.1), leading to greater differences between the sampled heights. Furthermore, since bromoform is known to have coastal/marine sources, long-range transport from these regions could affect measurements at elevated heights, potentially evening out height effects from dilution of local ground sources. Overall, the data shown in **Figure 3-4** covers only 19 days, including single days without sampling. With data covering a longer period, diel patterns will be better defined. Additionally, data from flight measurements covering different altitudes may be better suited to uncovering these effects.

3.3.3 Soil Flux Data

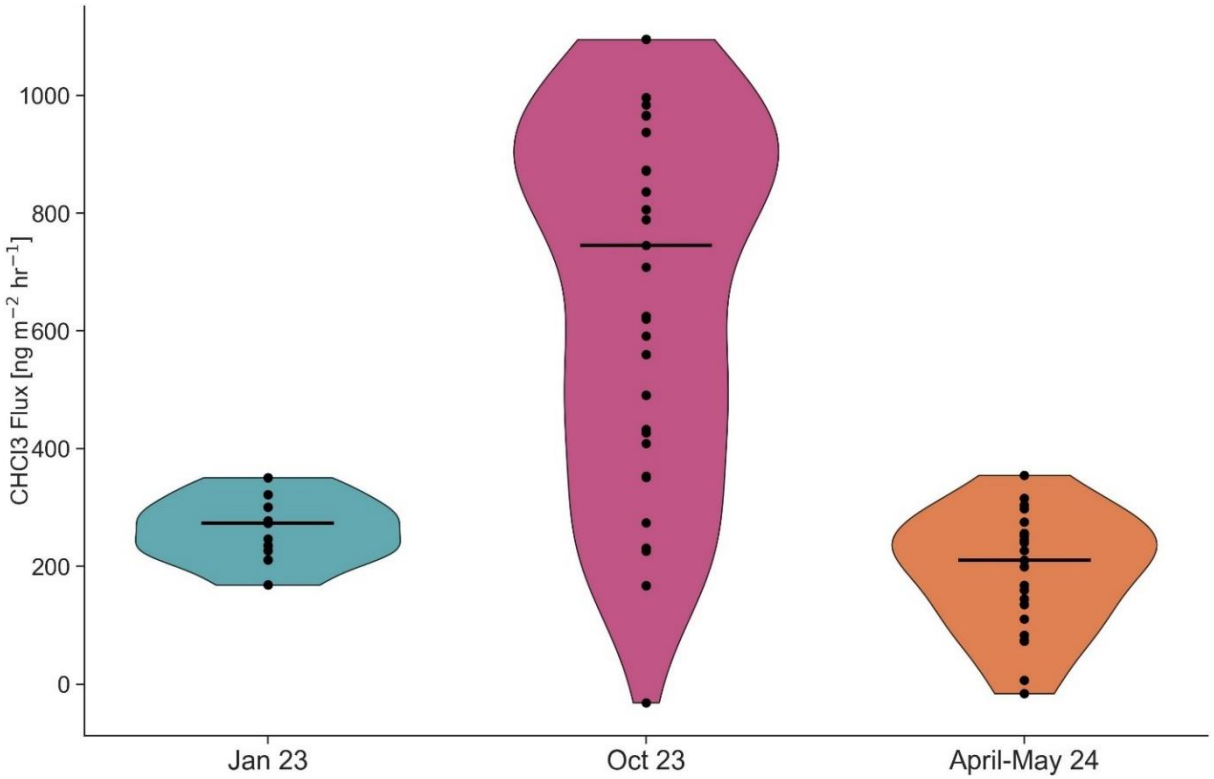

Figure 3-5. *Violin plots of chloroform soil fluxes from dry-to-wet transition season 2023 (Jan 23; n=10), dry season 2023 (Oct 23; n=28), and full-wet season 2024 (April-May 24; n=23). Black horizontal bars represent the median values of the respective dataset.*

Figure 3-5 shows chloroform flux data from a soil chamber as described in 3.2.1. The medians of the measured fluxes are 260 ng h^{-1} m^{-2} and 211 ng h^{-1} m^{-2} for the dry-to-wet transition season 2023 and the wet season 2024, respectively. The fluxes measured in the 2023 dry season were considerably higher, with a median of 575 ng h^{-1} m^{-2}. Bromoform fluxes can not be presented here, as they were below the limit of detection. The data shows that the soil was a clear local chloroform source in all sampled seasons. The presented chloroform fluxes were in a comparable range as reported for direct soil flux measurements in other ecosystems (Albers et al., 2011, 2017; Rhew et al., 2008b, a; Zhang et al., 2021) and in the same order of magnitude as total net flux estimations in tropical ecosystems (Gebhardt et al., 2008; Scheeren et al., 2003). However, there are large spatial variations reported for chloroform fluxes from soils (Albers et al., 2011), making it necessary to put the significance of the spatially limited measurements presented in this work into the right perspective.

Interestingly, soil fluxes, with the highest values in the dry season, showed an inverse pattern compared to the seasonal chloroform VMR data from within the canopy (see Chapter 3.3.1), where no strong differences in median VMRs were detected, but the described VMR spikes only occurred in the wet and dry-to-wet transition seasons, not in the dry season (see **Figure 3-2**). An explanation for this could be that, provided that the measured fluxes indeed directly reflect the chloroform formation within the soil, too much water within the soil leads to some kind of containment of the relevant metabolic pathways, which in turn restricts chloroform formation. For example, limited soil respiration due to excessive soil moisture could lead to reduced or altered microbial activity, affecting the biotic part of chloroform formation pathways suggested by Hoekstra et al., 1998a. On the other hand, it might be that not the chloroform sources in the soil are limited in the wetter seasons, but microbial degradation in the soil, as reported by (Cappelletti et al., 2012), could be

limited during the dry season. During dry seasons, the abundance and diversity of the soil's microbiome are strongly restricted by low soil moisture (Finck et al., 2024). If chloroform-degrading microorganisms are less affected by this than chloroform-forming microorganisms, their relative increase could result in a higher chloroform net flux from the soil.

A simpler explanation for the lower chloroform fluxes in wet and dry-to-wet transition seasons could be due to physicochemical effects: chloroform is very mobile in aquifers (Ciavarelli et al., 2012) and could be either washed out by rain from the soil pores or affected by transpiration or guttation, i.e., water with dissolved chloroform would be absorbed by plants in the rhizosphere, transported to the leaves via the xylem system, and subsequently excreted as water droplets via the leaf surfaces (guttation) or evaporated through the stomata (transpiration) (McCulloch, 2003; Scheffer et al., 1965). This process could explain both, lower chloroform fluxes from soils in the wetter seasons, as well as higher VMRs within the canopy in these seasons. This hypothesis cannot be confirmed due to the lack of strong correlations between chloroform emissions and soil moisture or precipitation (**Table 3-1**). However, as discussed in Chapter 3.3.1.3, one has to question these correlations carefully because of the low temporal resolution of the data. To identify a single or an interplay of the previously hypothesized processes, more research needs to be done in the form of experiments with better temporal and spatial resolution, a comparison of different soils, and the investigation of the microbial communities present in the soil. Measuring the isotopic fingerprint of the chloroform emitted by the soil could provide further insights into the formation processes (Breider and Hunkeler, 2014).

3.4 Summary and Conclusions

Our measurements of chloroform showed overall comparable medians across dry-to-wet transition season 2023, dry season 2023, and wet season 2024. We observed significant spikes during the wet and dry-to-wet transition seasons, indicating local emission events, with the optimal conditions for these emissions occurring during transitional seasons when dry and wetting cycles are most prevalent. Tower measurements taken at elevated heights (80 m and 320 m) suggest that these emissions originate at ground level and follow a diel cycle, peaking at midday and decreasing overnight.

Bromoform values measured at the ATTO site were lower than those typically reported for the marine boundary layer, as expected for continental measurements far from the sea. Potential local sources of bromoform are less pronounced compared to chloroform. Nonetheless, there are indications of local bromoform sources, such as altitude gradients, a slightly pronounced diel cycle, and occasional spikes that could not be linked to emission events via back trajectories (Supplementary Material S.1).

Soil flux measurements detected the soil to be a chloroform source throughout all seasons, with the highest fluxes in the dry season. As these measurements were limited in temporal and spatial resolution, they can only serve as a first-best estimate, while the underlying processes need to be further investigated.

Overall, our findings suggest that in the central Amazon rainforest, local sources play a more significant role in the chloroform mixing ratios than marine source regions, while the origin of the sampled air masses is more important than local sources for bromoform. Future investigations should focus on potential single-source emissions relevant to the Amazon rainforest ecosystems, reasons for and characteristics of seasonal variances, and the effects of ENSO anomalies compared to regular conditions. Understanding these factors could provide valuable insights for evaluating

future emissions, especially regarding predicted ecosystem changes in the Amazon basin and more frequent El Niño events.

3.5 References

Albers, C. N., Jacobsen, O. S., Flores, É. M. M., Pereira, J. S. F., and Laier, T.: Spatial variation in natural formation of chloroform in the soils of four coniferous forests, Biogeochemistry, 103, 317–334, https://doi.org/10.1007/s10533-010-9467-9, 2011.

Albers, C. N., Jacobsen, O. S., Flores, E. M. M., and Johnsen, A. R.: Arctic and Subarctic Natural Soils Emit Chloroform and Brominated Analogues by Alkaline Hydrolysis of Trihaloacetyl Compounds, Environ. Sci. Technol., 51, 6131–6138, https://doi.org/10.1021/acs.est.7b00144, 2017.

Allonier, A.-S., Khalanski, M., and Camel, R.: Characterization of Chlorination By-products in Cooling E,ffluents of Coastal Nuclear Power Stations, Marine Pollution Bulletin, 38, 1999.

Andreae, M. O., Acevedo, O. C., Araùjo, A., Artaxo, P., Barbosa, C. G. G., Barbosa, H. M. J., Brito, J., Carbone, S., Chi, X., Cintra, B. B. L., da Silva, N. F., Dias, N. L., Dias-Júnior, C. Q., Ditas, F., Ditz, R., Godoi, A. F. L., Godoi, R. H. M., Heimann, M., Hoffmann, T., Kesselmeier, J., Könemann, T., Krüger, M. L., Lavric, J. V., Manzi, A. O., Moran-Zuloaga, D., Nölscher, A. C., Santos Nogueira, D., Piedade, M. T. F., Pöhlker, C., Pöschl, U., Rizzo, L. V., Ro, C.-U., Ruckteschler, N., Sá, L. D. A., Sá, M. D. O., Sales, C. B., Santos, R. M. N. D., Saturno, J., Schöngart, J., Sörgel, M., de Souza, C. M., de Souza, R. A. F., Su, H., Targhetta, N., Tóta, J., Trebs, I., Trumbore, S., van Eijck, A., Walter, D., Wang, Z., Weber, B., Williams, J., Winderlich, J., Wittmann, F., Wolff, S., and Yáñez-Serrano, A. M.: The Amazon Tall Tower Observatory (ATTO) in the remote Amazon Basin: overview of first results from ecosystem ecology, meteorology, trace gas, and aerosol measurements, https://doi.org/10.5194/acpd-15-11599-2015, 21 April 2015.

Anon: arl-230.pdf, n.d.

NOAA's Climate Prediction Center: https://origin.cpc.ncep.noaa.gov/products/analysis_monitoring/ensostuff/ONI_v5.php, last access: 16 September 2024.

Aschmann, J.: Modeling the transport of very short-lived substances into the tropical upper troposphere and lower stratosphere, Atmos. Chem. Phys., 2009.

Aucott, M. L., McCulloch, A., Graedel, T. E., Kleiman, G., Midgley, P., and Li, Y.-F.: Anthropogenic emissions of trichloromethane (chloroform, CHCl3) and chlorodifluoromethane (HCFC-22): Reactive Chlorine Emissions Inventory, Journal of Geophysical Research: Atmospheres, 104, 8405–8415, https://doi.org/10.1029/1999JD900053, 1999.

Bahlmann, E., Stolle, C., Weinberg, I., Seifert, R., Schulz-Bull, D. E., and Michaelis, W.: Isotopic composition of polyhalomethanes from marine macrophytes – systematic effects of the halogen substituents on isotopic composition, Environ. Chem., 12, 504, https://doi.org/10.1071/EN14210, 2015.

Berberich, G. M., Sattler, T., Klimetzek, D., Benk, S. A., Berberich, M. B., Polag, D., Schöler, H. F., and Atlas, E.: Halogenation processes linked to red wood ant nests (Formica spp.) and tectonics, J Atmos Chem, 74, 261–281, https://doi.org/10.1007/s10874-016-9358-0, 2017.

Bondu, S., Cocquempot, B., Deslandes, E., and Morin, P.: Effects of salt and light stress on the release of volatile halogenated organic compounds by *Solieria chordalis*: a laboratory incubation study, botm, 51, 485–492, https://doi.org/10.1515/BOT.2008.056, 2008.

Booge, D., Tjiputra, J. F., Olivié, D. J. L., Quack, B., and Krüger, K.: Natural marine bromoform emissions in the fully coupled ocean–atmosphere model NorESM2, Earth Syst. Dynam., 15, 801–816, https://doi.org/10.5194/esd-15-801-2024, 2024.

Breider, F. and Hunkeler, D.: Investigating Chloroperoxidase-Catalyzed Formation of Chloroform from Humic Substances Using Stable Chlorine Isotope Analysis, Environ. Sci. Technol., 48, 1592–1600, https://doi.org/10.1021/es403879e, 2014.

Butler, J. H., King, D. B., Lobert, J. M., Montzka, S. A., Yvon-Lewis, S. A., Hall, B. D., Warwick, N. J., Mondeel, D. J., Aydin, M., and Elkins, J. W.: Oceanic distributions and emissions of short-lived halocarbons, Global Biogeochemical Cycles, 21, 2006GB002732, https://doi.org/10.1029/2006GB002732, 2007.

Cappelletti, M., Frascari, D., Zannoni, D., and Fedi, S.: Microbial degradation of chloroform, Appl Microbiol Biotechnol, 96, 1395–1409, https://doi.org/10.1007/s00253-012-4494-1, 2012.

Chipperfield, M. P. and Pyle, J. A.: Model sensitivity studies of Arctic ozone depletion, Journal of Geophysical Research: Atmospheres, 103, 28389–28403, https://doi.org/10.1029/98JD01960, 1998.

Ciavarelli, R., Cappelletti, M., Fedi, S., Pinelli, D., and Frascari, D.: Chloroform aerobic cometabolism by butane-growing Rhodococcus aetherovorans BCP1 in continuous-flow biofilm reactors, Bioprocess Biosyst Eng, 35, 667–681, https://doi.org/10.1007/s00449-011-0647-3, 2012.

Crutzen, P. J.: My Life with O3, NOx and Other YZOxs. Nobel Lecture 1995. https://www.nobelprize.org/prizes/chemistry/1995/crutzen/lecture/ 1995.

Daniel, J. S., Solomon, S., Portmann, R. W., and Garcia, R. R.: Stratospheric ozone destruction: The importance of bromine relative to chlorine, Journal of Geophysical Research: Atmospheres, 104, 23871–23880, https://doi.org/10.1029/1999JD900381, 1999.

Dimmer, C. H., Simmonds, P. G., Nickless, G., and Bassford, M. R.: Biogenic fluxes of halomethanes from Irish peatland ecosystems, Atmospheric Environment, 2001.

Draxler, R.R., 1999: HYSPLIT4 user's guide. NOAA Tech. Memo. ERL ARL-230, NOAA Air Resources Laboratory, Silver Spring, MD, 1999.

Draxler, R. R. and Hess, G. D.: Description of the HYSPLIT_4 modeling system, NOAA Tech. Memo. ERL ARL-224, NOAA Air Resources Laboratory, Silver Spring, MD, 24 pp, 1997.

Draxler, R. R. and Hess, G. D.: An Overview of the HYSPLIT_4 Modelling System for Trajectories, Dispersion, and Deposition, Aust. Meteor. Mag., 47, 295-308, 1998.

Edtbauer, A., Pfannerstill, E. Y., Pires Florentino, A. P., Barbosa, C. G. G., Rodriguez-Caballero, E., Zannoni, N., Alves, R. P., Wolff, S., Tsokankunku, A., Aptroot, A., de Oliveira Sá, M., de Araújo, A. C., Sörgel, M., de Oliveira, S. M., Weber, B., and Williams, J.: Cryptogamic organisms are a substantial source and sink for volatile organic compounds in the Amazon region, Commun Earth Environ, 2, 258, https://doi.org/10.1038/s43247-021-00328-y, 2021.

Ernle, L., Ringsdorf, M. A., and Williams, J.: Influence of ozone and humidity on PTR-MS and GC-MS VOC measurements with and without a $Na_2S_2O_3$ ozone scrubber, Atmos. Meas. Tech., 16, 1179–1194, https://doi.org/10.5194/amt-16-1179-2023, 2023.

Finck, J., Lange, D. F., Quesada, B., Portela, B. T. T., Ferreira, S. J. F., Andreote, F. D., Kothe, E., and Gleixner, G.: Seasonal drought reduces microbial diversity and functional richness in the Amazon, , https://doi.org/10.5194/egusphere-egu24-11089, 2024.

Forczek, S. T., Laturnus, F., Doležalová, J., Holík, J., and Wimmer, Z.: Emission of climate relevant volatile organochlorines by plants occurring in temperate forests, Plant, Soil and Environment, 61, 103–108, https://doi.org/10.17221/900/2014-PSE, 2015.

Frische, M., Garofalo, K., Hansteen, T. H., and Borchers, R.: Fluxes and origin of halogenated organic trace gases from Momotombo volcano (Nicaragua), Geochemistry, Geophysics, Geosystems, 7, https://doi.org/10.1029/2005GC001162, 2006.

Fueglistaler, S., Dessler, A. E., Dunkerton, T. J., Folkins, I., Fu, Q., and Mote, P. W.: Tropical tropopause layer, Reviews of Geophysics, 47, https://doi.org/10.1029/2008RG000267, 2009.

Gebhardt, S., Colomb, A., Hofmann, R., Williams, J., and Lelieveld, J.: Halogenated organic species over the tropical South American rainforest, Atmospheric Chemistry and Physics, 8, 3185–3197, https://doi.org/10.5194/acp-8-3185-2008, 2008.

von Glasow, R., von Kuhlmann, R., Lawrence, M. G., Platt, U., and Crutzen, P. J.: Impact of reactive bromine chemistry in the troposphere, Atmospheric Chemistry and Physics, 4, 2481–2497, https://doi.org/10.5194/acp-4-2481-2004, 2004.

Grøn, C., Laturnus, F., and Jacobsen, O. S.: Reliable test methods for the determination of a natural production of chloroform in soils, Environ Monit Assess, 184, 1231–1241, https://doi.org/10.1007/s10661-011-2035-5, 2012.

Gusareva, E. S., Acerbi, E., Lau, K. J. X., Luhung, I., Premkrishnan, B. N. V., Kolundžija, S., Purbojati, R. W., Wong, A., Houghton, J. N. I., Miller, D., Gaultier, N. E., Heinle, C. E., Clare, M. E., Vettath, V. K., Kee, C., Lim, S. B. Y., Chénard, C., Phung, W. J., Kushwaha, K. K., Nee, A. P., Putra, A., Panicker, D., Yanqing, K., Hwee, Y. Z., Lohar, S. R., Kuwata, M., Kim, H. L., Yang, L., Uchida, A., Drautz-Moses, D. I., Junqueira, A. C. M., and Schuster, S. C.: Microbial communities in the tropical air ecosystem follow a precise diel cycle, Proc. Natl. Acad. Sci. U.S.A., 116, 23299–23308, https://doi.org/10.1073/pnas.1908493116, 2019.

Hepach, H., Quack, B., Ziska, F., Fuhlbrügge, S., Atlas, E. L., Krüger, K., Peeken, I., and Wallace, D. W. R.: Drivers of diel and regional variations of halocarbon emissions from the tropical North East Atlantic, Atmos. Chem. Phys., 14, 1255–1275, https://doi.org/10.5194/acp-14-1255-2014, 2014.

Hernandez, R. R. and Allen, M. F.: Diurnal patterns of productivity of arbuscular mycorrhizal fungi revealed with the Soil Ecosystem Observatory, New Phytologist, 200, 547–557, https://doi.org/10.1111/nph.12393, 2013.

Hoekstra, E. J., de Leer, E. W. B., and Brinkman, U. A. Th.: Natural Formation of Chloroform and Brominated Trihalomethanes in Soil, Environ. Sci. Technol., 32, 3724–3729, https://doi.org/10.1021/es980127c, 1998a.

Hoekstra, E. J., Verhagen, F. J. M., Field, J. A., Leer, E. W. B. D., and Brinkman, U. A. T.: Natural Production Of Chloroform By Fungi, Phytochemistry, 49, 91–97, https://doi.org/10.1016/S0031-9422(97)00984-9, 1998b.

Hoekstra, E. J., Duyzer, J. H., de Leer, E. W. B., and Brinkman, U. A. T.: Chloroform – concentration gradients in soil air and atmospheric air, and emission fluxes from soil, Atmospheric Environment, 35, 61–70, https://doi.org/10.1016/S1352-2310(00)00285-5, 2001.

Hossaini, R., Atlas, E., Dhomse, S. S., Chipperfield, M. P., Bernath, P. F., Fernando, A. M., Mühle, J., Leeson, A. A., Montzka, S. A., Feng, W., Harrison, J. J., Krummel, P., Vollmer, M. K., Reimann, S., O'Doherty, S., Young, D., Maione, M., Arduini, J., and Lunder, C. R.: Recent Trends in Stratospheric Chlorine From Very Short-Lived Substances, Journal of Geophysical Research: Atmospheres, 124, 2318–2335, https://doi.org/10.1029/2018JD029400, 2019.

Huber, S. G., Kotte, K., Schöler, H. F., and Williams, J.: Natural Abiotic Formation of Trihalomethanes in Soil: Results from Laboratory Studies and Field Samples, Environ. Sci. Technol., 43, 4934–4939, https://doi.org/10.1021/es8032605, 2009.

Johnsen, A. R., Jacobsen, O. S., Gudmundsson, L., and Albers, C. N.: Chloroform emissions from arctic and subarctic ecosystems in Greenland and Northern Scandinavia, Biogeochemistry, 130, 53–65, https://doi.org/10.1007/s10533-016-0241-5, 2016.

Jordan, A., Harnisch, J., Borchers, R., Le Guern, F., and Shinohara, H.: Volcanogenic Halocarbons, Environ. Sci. Technol., 34, 1122–1124, https://doi.org/10.1021/es990838q, 2000.

Khalil, M. A. K., Rasmussen, R. A., Wang, M.-X., and Ren, L.: Emissions of trace gases from Chinese rice fields and biogas generators: CH4, N2O, CO, CO2, chlorocarbons, and hydrocarbons, Chemosphere, 20, 207–226, https://doi.org/10.1016/0045-6535(90)90097-D, 1990a.

Khalil, M. a. K., Rasmussen, R. A., French, J. R. J., and Holt, J. A.: The influence of termites on atmospheric trace gases: CH4, CO2, CHCl3, N2O, CO, H2, and light hydrocarbons, Journal of Geophysical Research: Atmospheres, 95, 3619–3634, https://doi.org/10.1029/JD095iD04p03619, 1990b.

Ko, M. K. W. and Poulet, G.: Very Short-Lived Halogen and Sulfur Substances, in: Scientific assessment of ozone depletion: 2002, vol. Report No. 47, World Meteorological Organization, Geneva, 2003.

Krysztofiak, G., Catoire, V., Poulet, G., Marécal, V., Pirre, M., Louis, F., Canneaux, S., and Josse, B.: Detailed modeling of the atmospheric degradation mechanism of very-short lived brominated species, Atmospheric Environment, 59, 514–532, https://doi.org/10.1016/j.atmosenv.2012.05.026, 2012.

Kuhn, U., Dindorf, T., Ammann, C., Rottenberger, S., Guyon, P., Holzinger, R., Ausma, S., Kenntner, T., Helleis, F., and Kesselmeier, J.: Design and field application of an automated cartridge sampler for VOC concentration and flux measurements, J. Environ. Monit., 7, 568, https://doi.org/10.1039/b500057b, 2005.

Laturnus, F.: Marine macroalgae in polar regions as natural sources for volatile organohalogens, Environ Sci & Pollut Res, 8, 103–108, https://doi.org/10.1007/BF02987302, 2001.

Leedham, E. C., Hughes, C., Keng, F. S. L., Phang, S.-M., Malin, G., and Sturges, W. T.: Emission of atmospherically significant halocarbons by naturally occurring and farmed tropical macroalgae, Biogeosciences, 10, 3615–3633, https://doi.org/10.5194/bg-10-3615-2013, 2013.

Liang, Q., Atlas, E., Blake, D., Dorf, M., Pfeilsticker, K., and Schauffler, S.: Convective transport of very short lived bromocarbons to the stratosphere, Atmos. Chem. Phys., 14, 5781–5792, https://doi.org/10.5194/acp-14-5781-2014, 2014.

Lim, Y.-K., Phang, S.-M., Abdul Rahman, N., Sturges, W. T., and Malin, G.: Halocarbon emissions from marine phytoplankton and climate change, Int. J. Environ. Sci. Technol., 14, 1355–1370, https://doi.org/10.1007/s13762-016-1219-5, 2017.

Lim, Y.-K., Phang, S.-M., Sturges, W. T., Malin, G., and Rahman, N. B. A.: Emission of short-lived halocarbons by three common tropical marine microalgae during batch culture, J Appl Phycol, 30, 341–353, https://doi.org/10.1007/s10811-017-1250-z, 2018.

Lin, C. Y. and Manley, S. L.: Bromoform production from seawater treated with bromoperoxidase, Limnology and Oceanography, 57, 1857–1866, https://doi.org/10.4319/lo.2012.57.6.1857, 2012.

Lobert, J. M., Keene, W. C., Logan, J. A., and Yevich, R.: Global chlorine emissions from biomass burning: Reactive Chlorine Emissions Inventory, Journal of Geophysical Research: Atmospheres, 104, 8373–8389, https://doi.org/10.1029/1998JD100077, 1999.

Macdonald, M. L., Wadham, J. L., Young, D., Lunder, C. R., Hermansen, O., Lamarche-Gagnon, G., and O'Doherty, S.: Consumption of CH3Cl, CH3Br and CH3I and emission

of CHCl3, CHBr3 and CH2Br2 from a retreating Arctic glacier's forefield, https://doi.org/10.5194/acp-2019-943, 6 December 2019.

McCulloch, A.: Chloroform in the environment: occurrence, sources, sinks and effects, Chemosphere, 50, 1291–1308, https://doi.org/10.1016/s0045-6535(02)00697-5, 2003.

Moore, R. M., Webb, M., Tokarczyk, R., and Wever, R.: Bromoperoxidase and iodoperoxidase enzymes and production of halogenated methanes in marine diatom cultures, Journal of Geophysical Research: Oceans, 101, 20899–20908, https://doi.org/10.1029/96JC01248, 1996.

Mtolera, M. S. P., Collén, J., Pedersén, M., Ekdahl, A., Abrahamsson, K., and Semesi, A. K.: Stress-induced production of volatile halogenated organic compounds in *Eucheuma denticulatum* (Rhodophyta) caused by elevated pH and high light intensities, European Journal of Phycology, 31, 89–95, https://doi.org/10.1080/09670269600651241, 1996.

Nightingale, P. D., Malin, G., and Liss, P. S.: Production of chloroform and other low molecular-weight halocarbons by some species of macroalgae, Limnology and Oceanography, 40, 680–689, https://doi.org/10.4319/lo.1995.40.4.0680, 1995.

Orlikowska, A., Stolle, C., Pollehne, F., Jürgens, K., and Schulz-Bull, D. E.: Dynamics of halocarbons in coastal surface waters during short term mesocosm experiments, Environ. Chem., 12, 515, https://doi.org/10.1071/EN14204, 2015.

Papanastasiou, D. K., McKeen, S. A., and Burkholder, J. B.: The very short-lived ozone depleting substance CHBr₃ (bromoform): revised UV absorption spectrum, atmospheric lifetime and ozone depletion potential, Atmos. Chem. Phys., 14, 3017–3025, https://doi.org/10.5194/acp-14-3017-2014, 2014.

Pfannerstill, E. Y., Nölscher, A. C., Yáñez-Serrano, A. M., Bourtsoukidis, E., Keßel, S., Janssen, R. H. H., Tsokankunku, A., Wolff, S., Sörgel, M., Sá, M. O., Araújo, A., Walter, D., Lavrič, J., Dias-Júnior, C. Q., Kesselmeier, J., and Williams, J.: Total OH Reactivity Changes Over the Amazon Rainforest During an El Niño Event, Front. For. Glob. Change, 1, 12, https://doi.org/10.3389/ffgc.2018.00012, 2018.

Pöhlker, C., Walter, D., Paulsen, H., Könemann, T., Rodríguez-Caballero, E., Moran-Zuloaga, D., Brito, J., Carbone, S., Degrendele, C., Després, V. R., Ditas, F., Holanda, B. A., Kaiser, J. W., Lammel, G., Lavrič, J. V., Ming, J., Pickersgill, D., Pöhlker, M. L., Praß, M., Löbs, N., Saturno, J., Sörgel, M., Wang, Q., Weber, B., Wolff, S., Artaxo, P., Pöschl, U., and Andreae, M. O.: Land cover and its transformation in the backward trajectory footprint region of the Amazon Tall Tower Observatory, Atmos. Chem. Phys., 19, 8425–8470, https://doi.org/10.5194/acp-19-8425-2019, 2019.

Prinn, R. G., Weiss, R. F., Arduini, J., Arnold, T., DeWitt, H. L., Fraser, P. J., Ganesan, A. L., Gasore, J., Harth, C. M., Hermansen, O., Kim, J., Krummel, P. B., Li, S., Loh, Z. M., Lunder, C. R., Maione, M., Manning, A. J., Miller, B. R., Mitrevski, B., Mühle, J., O'Doherty, S., Park, S., Reimann, S., Rigby, M., Saito, T., Salameh, P. K., Schmidt, R., Simmonds, P. G., Steele, L. P., Vollmer, M. K., Wang, R. H., Yao, B., Yokouchi, Y., Young, D., and Zhou, L.: History of chemically and radiatively important atmospheric gases from the Advanced Global Atmospheric Gases Experiment (AGAGE), Earth Syst. Sci. Data, 10, 985–1018, https://doi.org/10.5194/essd-10-985-2018, 2018.

Quack, B. and Wallace, D. W. R.: Air-sea flux of bromoform: Controls, rates, and implications, Global Biogeochemical Cycles, 17, https://doi.org/10.1029/2002GB001890, 2003.

Rhew, R. C., Miller, B. R., and Weiss, R. F.: Chloroform, carbon tetrachloride and methyl chloroform fluxes in southern California ecosystems, Atmospheric Environment, 42, 7135–7140, https://doi.org/10.1016/j.atmosenv.2008.05.038, 2008a.

Rhew, R. C., Teh, Y. A., Abel, T., Atwood, A., and Mazéas, O.: Chloroform emissions from the Alaskan Arctic tundra, Geophysical Research Letters, 35, https://doi.org/10.1029/2008GL035762, 2008b.

Scheeren, H. A., Lelieveld, J., Williams, J., Fischer, H., and Warneke, C.: Measurements of reactive chlorocarbons over the Surinam tropical rain forest: indications for strong biogenic emissions, https://doi.org/10.5194/acpd-3-5469-2003, 2003.

Scheffer, F., Stricker, G., Kickuth, R., and Scheffer, F.: Organische Verbindungen in der Guttationsflüssigkeit einiger Wild- und Kulturweizen, Zeitschrift für Pflanzenernährung, Düngung, Bodenkunde, 109, 240–248, https://doi.org/10.1002/jpln.19651090306, 1965.

Sinnhuber, B.-M. and Folkins, I.: Estimating the contribution of bromoform to stratospheric bromine and its relation to dehydration in the tropical tropopause layer, Atmospheric Chemistry and Physics, 6, 4755–4761, https://doi.org/10.5194/acp-6-4755-2006, 2006.

Sinnhuber, B.-M., Sheode, N., Sinnhuber, M., Chipperfield, M. P., and Feng, W.: The contribution of anthropogenic bromine emissions to past stratospheric ozone trends: a modelling study, Atmospheric Chemistry and Physics, 9, 2863–2871, https://doi.org/10.5194/acp-9-2863-2009, 2009.

Staley, C., Ferrieri, A. P., Tfaily, M. M., Cui, Y., Chu, R. K., Wang, P., Shaw, J. B., Ansong, C. K., Brewer, H., Norbeck, A. D., Markillie, M., do Amaral, F., Tuleski, T., Pellizzaro, T., Agtuca, B., Ferrieri, R., Tringe, S. G., Paša-Tolić, L., Stacey, G., and Sadowsky, M. J.: Diurnal cycling of rhizosphere bacterial communities is associated with shifts in carbon metabolism, Microbiome, 5, 65, https://doi.org/10.1186/s40168-017-0287-1, 2017.

Stein, A. F., Draxler, R. R., Rolph, G. D., Stunder, B. J. B., Cohen, M. D., and Ngan, F.: NOAA's HYSPLIT Atmospheric Transport and Dispersion Modeling System, Bulletin of the American Meteorological Society, 96, 2059–2077, https://doi.org/10.1175/BAMS-D-14-00110.1, 2015.

Stemmler, I., Hense, I., and Quack, B.: Marine sources of bromoform in the global open ocean – global patterns and emissions, Biogeosciences, 12, 1967–1981, https://doi.org/10.5194/bg-12-1967-2015, 2015.

Villamayor, J., Iglesias-Suarez, F., Cuevas, C. A., Fernandez, R. P., Li, Q., Abalos, M., Hossaini, R., Chipperfield, M. P., Kinnison, D. E., Tilmes, S., Lamarque, J.-F., and Saiz-Lopez, A.: Very short-lived halogens amplify ozone depletion trends in the tropical lower stratosphere, Nat. Clim. Chang., 13, 554–560, https://doi.org/10.1038/s41558-023-01671-y, 2023.

Weigold, P., El-Hadidi, M., Ruecker, A., Huson, D. H., Scholten, T., Jochmann, M., Kappler, A., and Behrens, S.: A metagenomic-based survey of microbial (de)halogenation potential in a German forest soil, Sci Rep, 6, 28958, https://doi.org/10.1038/srep28958, 2016.

World Meteorological Organization (WMO) (Ed.): Scientific Assessment of Ozone Depletion: 2018, Geneva, Switzerland, 588 pp. pp., 2018.

World Meteorological Organization (WMO) (Ed.): Scientific Assessment of Ozone Depletion: 2022, Geneva, 509 pp. pp., 2022.

Worton, D. R., Sturges, W. T., Schwander, J., Mulvaney, R., Barnola, J.-M., and Chappellaz, J.: 20th century trends and budget implications of chloroform and related tri-and dihalomethanes inferred from firn air, Atmos. Chem. Phys., 6, 2847–2863, https://doi.org/10.5194/acp-6-2847-2006, 2006.

Zhang, W., Jiao, Y., Zhu, R., Rhew, R. C., Sun, B., and Dai, H.: Chloroform ($CHCl_3$) Emissions From Coastal Antarctic Tundra, Geophysical Research Letters, 48, e2021GL093811, https://doi.org/10.1029/2021GL093811, 2021.

4 Establishment of a Setup for Long-Term Online Measurements of Halogenated VOCs in the Amazon Rainforest

4.1 Introduction

The Amazon rainforest is recognized as one of the most significant natural sources of halogenated volatile organic compounds (XVOCs), particularly chloromethane (CH_3Cl). As highlighted by Carpenter et al. (2014) and Yokouchi et al. (2002), plants are the largest global source of chloromethane, yet there remain substantial uncertainties regarding the exact magnitudes of these emissions. These uncertainties are particularly pronounced in tropical forested regions like the Amazon, where the complex interplay of vegetation, soil, and microbial processes can lead to strong variations in emissions. Understanding and quantifying these emissions is crucial for accurately assessing the role of the Amazon rainforest in the global halogen cycle and its impact on atmospheric chemistry and climate.

In addition to chloromethane, there are observations indicating that chloroform ($CHCl_3$) also has local sources within the Amazon ecosystem, as discussed in Chapter 3. These local sources could include yet unknown sources, such as specific plant species or even termite colonies, which are abundant in the rainforest, in addition to biotic or abiotic emissions from soils. The identification and quantification of these sources are crucial for understanding the contribution of the Amazon to global chloroform levels, as well as for identifying potential hotspots of emissions that might significantly influence local and regional atmospheric composition.

Similarly, bromoform ($CHBr_3$) is another halogenated compound that is suspected to have small, yet uncharacterized, sources within the Amazon (Chapter 3). Given the structural similarities between chloroform and bromoform, and the known production of halogenated compounds by terrestrial organisms, it is plausible that bromoform emissions can potentially occur in the Amazon as well, even though probably to a much smaller extent based on the relative abundances of chlorine and bromine in the soil. Identifying and quantifying these emissions would not only improve our understanding of bromoform dynamics but also help in identifying other potential halogenated very short-lived substances (VSLSs) or XVOCs with a longer lifetime that the forest ecosystem might emit.

The Amazon rainforest's potential to act as a sink for other halogenated VOCs is another area of interest but there is little experimental data. While some XVOCs are known to be emitted by the forest, others may be absorbed or degraded by the dense vegetation, soils, or microbial communities (see **Figure 1-1**). Investigating the rainforest's role as a sink is important for understanding the full impact of the Amazon on atmospheric halogen levels. This could involve studying the degradation pathways of XVOCs within the forest and identifying the conditions under which these compounds are absorbed or broken down.

For halogenated VOCs that are relatively inert and for which the Amazon does not act as a significant source or sink (e.g., CFCs), the remote location of the ATTO site provides an ideal environment for monitoring their global atmospheric background levels. The ATTO site, situated far from significant anthropogenic influences, allows for the collection of data that reflect the broader atmospheric composition, comparable to the AGAGE network or NOAA measurement stations (Hossaini et al., 2019; Prinn et al., 2018; NOAA/GMD/ESRL halocarbons in situ program). This is particularly valuable for compounds that are part of the global halogen budget but whose local sources or sinks in the Amazon are minimal or nonexistent.

Finally, for every halogenated VOC, whether it is emitted, absorbed, or inert within the Amazon, accurate quantification of its emissions or degradation is essential. This quantification forms the basis of a bottom-up approach that is crucial for atmospheric modelers. It should be noted that the Amazon rainforest ecosystem is located such that any halogenated emissions will be liable to be

convected rapidly to the upper troposphere and thereafter enter the stratosphere through the tropical upward branch of the Brewer-Dobson circulation. By providing detailed emission inventories and degradation rates, researchers can improve the accuracy of global atmospheric models, which are used to predict the impacts of these compounds on climate, ozone depletion, and other aspects of atmospheric chemistry.

4.2 Motivation for the Method Specifics

Many paths lead to the goal, and each path has its advantages and disadvantages. The following subsections explain the underlying arguments that lead to the final method used in this thesis.

4.2.1 Benefits of the ATTO Site

The Amazon Tall Tower Observatory (ATTO) offers unique opportunities for atmospheric research. One of the key advantages of ATTO is its ability to provide measurements not only at ground level but also at various heights above the forest canopy (up to 325 m). This vertical stratification allows researchers to calculate concentration gradients, offering insights into the dynamics of VOC exchange between the forest and the atmosphere. By sampling at different heights, it becomes possible to determine which specific compounds are being emitted from the forest and which are being absorbed or degraded, ultimately providing a more comprehensive understanding of the net fluxes of VOCs in this ecosystem. At higher altitudes, the air sampled by the tower is representative of a larger region, reducing the influence of localized emission or degradation processes that could otherwise distort the data (Gloor et al., 2001). In contrast, single-point measurements at or below canopy heights are more susceptible to the effects of immediate local sources or sinks, which can lead to overestimation or underestimation of the ecosystem's overall impact on atmospheric chemistry. By capturing a wider range of air masses, the ATTO tower provides a more accurate representation of the Amazon rainforest's contribution to global (X)VOC levels.

The ATTO site is also uniquely positioned as the only place in the Amazon rainforest that combines a quasi-pristine environment with the necessary infrastructure for long-term scientific research. The site's remote location ensures minimal anthropogenic influence, which is crucial for studying natural VOC emissions and interactions. At the same time, ATTO is equipped with essential infrastructure, including a reliable water supply, food provisions with a dedicated cook, and the necessary facilities for material transport and electricity. This combination of remoteness and infrastructure makes ATTO an ideal location for continuous, long-term atmospheric monitoring, providing data that are both scientifically valuable and logistically feasible to collect.

Additionally, ATTO supports a "lab in the jungle" approach, allowing researchers to conduct experiments directly within the Amazon rainforest. This capability is particularly valuable for studying local sources of halogenated VOCs, such as specific plants, soils, or insect colonies, in their natural environment. By conducting experiments in situ, researchers can observe the immediate effects of environmental conditions on VOC emissions without the need for extensive sample transportation, which could compromise sample integrity. This approach ensures that samples remain fresh, minimizing storage artifacts, and that the data collected accurately reflect the natural processes occurring within the forest, providing deeper insights into the factors driving XVOC emissions in this unique ecosystem.

4.2.2 Comparison: Continuous In Situ Measurements vs. Adsorbent Tubes

One of the primary advantages of continuous in situ measurements at a site like ATTO is the ability to maintain a permanent setup that operates independently of short-term measurement

campaigns, spanning different seasons and even years. Historically, research on XVOCs in the Amazon has relied heavily on campaign-based approaches, where data collection is limited to specific periods, often only a few weeks in duration, whether airborne or ground-based. For example, past studies have utilized aircraft campaigns to capture XVOC emissions over large spatial scales or have conducted ground-based sampling during specific seasons (e.g. Gebhardt et al., 2008; Scheeren, 2003). While these campaigns have provided valuable insights, they are inherently limited in their ability to capture long-term trends and seasonal variations. Such flight campaigns are also unable to measure close to the rainforest by night. A permanent, continuous measurement system circumvents these limitations by allowing for the collection of data over extended periods, providing a more comprehensive understanding of XVOC dynamics in the Amazon. In addition, long-term measurements provide in total more data points, enabling better statistics and giving less weight to short-term events which is especially helpful when comparing different seasons.

Continuous in situ measurement systems also offer superior time resolution compared to adsorbent tubes. To achieve a comparable time resolution with adsorbent tubes, researchers would need to perform frequent sampling and engage in extensive sample preparation, which is both labor-intensive and prone to variability. The high time resolution provided by continuous measurements allows for the detection of rapid changes in XVOC concentrations, which can be crucial for understanding the factors that influence emissions. For instance, continuous monitoring can capture the immediate effects of environmental changes, such as a sudden increase in temperature, rainfall, or a shift in wind patterns, on XVOC emissions. This capability is particularly valuable in the dynamic and complex environment of the Amazon rainforest.

Another significant benefit of continuous in situ measurements is the ability to detect sampling problems instantly. At a remote site like ATTO, where access to the equipment may be limited, real-time monitoring allows researchers to identify and address issues as they arise. For example, if there is a malfunction in the sampling system or a calibration drift in the instruments, these problems can be detected immediately and corrected, ensuring the integrity of the data collected. This is in contrast to adsorbent tube sampling, where problems might only become apparent after the samples have been returned to the laboratory and analyzed, potentially leading to the loss of valuable data and time.

Continuous systems also reduce the sources of error and data variability associated with sample processing. Adsorbent tubes require careful handling and preparation both during and after sampling, and any inconsistencies in these processes can lead to variability of the results. By eliminating the need for extensive sample processing, continuous in situ measurements provide a more direct and reliable measure of XVOC concentrations, reducing the potential for human error and ensuring greater consistency in the data.

However, there are also challenges associated with continuous in situ measurements. Developing and testing a new method for trace gas analysis, especially in a remote setting like ATTO, can be complex and time-consuming. The remote location and the highly sensitive nature of the analytical devices used in XVOC measurements mean that any technical issues cannot always be fixed immediately. Some advanced spare parts take time to be delivered to such a place, and the location is not easily accessible to external engineers who can diagnose and repair devices. Additionally, managing these systems remotely requires robust diagnostic and communication tools, including a stable internet connection, to ensure that any problems can be identified and resolved without the need for constant on-site presence.

In contrast, adsorbent tubes offer a more basic approach to sampling, with fewer immediate logistical challenges. They are relatively easy to deploy, with a sampling process that is less

technically sophisticated. The samples can be collected and stored for later analysis in a controlled laboratory environment. This method is particularly useful for verifying the results obtained from continuous in situ measurements and for conducting focused studies on specific sources or sinks of XVOCs, such as particular soil types, plant species, or insect colonies. By using adsorbent tubes in conjunction with continuous measurements, data can be cross-verified and specific sources identified so that the overall picture of relevant processes within the ecosystem can be investigated better on multiple levels.

4.2.3 Comparison of Cryogenic and Cryogen-Free Preconcentration Units

After the decision had been made to pursue the goal of implementing long-term XVOC measurements at ATTO, the search for appropriate instrumentation began. This search mainly concerned the front-end instrumentation, as the back-end was already available in the form of a robust, tried-and-tested GC-MS system (Chapters 4.3.3 and 4.3.4). Since the atmospheric XVOC background concentrations are usually in the pptv range, some kind of preconcentration is required prior to the regular GC-MS analysis in order to detect small changes in the XVOC VMRs.

Often, a preconcentration unit relies on a cryo-trap. During the preconcentration process, the air sample is cooled using liquid nitrogen (LN), causing the volatile compounds to freeze and become trapped, while the primary components of air, such as oxygen and nitrogen, pass through. In the next step, the LN is removed and the trap is heated, releasing the trapped trace gases, which are then transferred to the GC-MS for analysis. This method of preconcentration has proven itself in multiple studies of trace gases (e.g. Heard, 2007; Schwandner et al., 2013). However, there has been the development of non-cryogenic preconcentration techniques, and both methods have their reason for existence:

Preconcentration systems using liquid nitrogen (LN) reach extremely low temperatures, which allows them to condense and trap a wide range of VOCs, including highly volatile compounds (below 50°C). Non-cryogenic systems do not reach the low temperatures of LN systems, which is why they are limited in their ability to efficiently capture highly volatile or halogenated compounds that require colder conditions to be trapped effectively. Depending on the instrument and method that is used for the preconcentration, non-cryogenic instruments can trap very volatile compounds only down to a boiling point (BP) of -30 or -50 °C.

In regards to potential detection limits, cryogenic preconcentration systems are known for their ability to enhance sensitivity by effectively trapping and concentrating even ultra-trace levels of VOCs. Non-cryogenic systems may struggle to achieve the same levels of concentration, particularly for VOCs present in extremely low concentrations, which is often the case with halogenated VOCs in remote environments like the Amazon rainforest. Furthermore, the basic technical setup of cryogenic preconcentration systems is usually simpler than that of non-cryogenic systems. When dealing with a complex mixture of halogenated VOCs, cryogenic systems can effectively trap a wide range of compounds simultaneously. Non-cryogenic systems may require more complex setups or multiple adsorbent materials to achieve the same level of performance, complicating the analysis process. Furthermore, non-cryogenic systems often rely on adsorbent materials that can become saturated over time, leading to potential carryover or memory effects. This is less of an issue with cryogenic systems where VOCs are physically trapped by freezing on an inert surface rather than adsorption, reducing the risk of cross-contamination between samples. On the other hand, the consistency of the preconcentration efficiency can be affected by fluctuations in LN supply or temperature, making it less reliable than non-cryogenic

systems. This doesn't only affect regular measurements but can also lead to inconsistent calibrations, leading to larger uncertainties in the generated data.

The technological progress of the development of non-cryogenic preconcentration systems nowadays, however, is so advanced that many of the disadvantages have been tackled and are now manageable. This applies in particular to water management, a field where cryogenic systems used to be superior to non-cryogenic systems and that is highly relevant, especially in environments with high humidity like the Amazon rainforest. Non-cryogenic systems used to struggle with water vapor, which can compete with VOCs for adsorption sites or lead to condensation issues. The use of LN can more effectively separate water vapor from VOCs due to its extreme cooling capacity but modern non-cryogenic systems implemented technical solutions that made them able to compete. The limited range of preconcentrated compounds is negligible for this work, as most of the compounds of highest interest, including chloromethane (BP of -24.18 °C; Ganeff and Jungers, 1948), are still within this range.

To set up a cryogenic preconcentration unit at ATTO would have had several disadvantages: First of all, LN is inconvenient to handle, especially in remote field conditions like those in the Amazon. Due to its hazardous nature, it poses risks of burns and asphyxiation. This applies not only to the cramped laboratory container, but especially along the necessary transportation route, in which the LN has to be transported from Manaus over bumpy roads, loaded onto a small ship and unloaded again, and transported over an unpaved road using off-road vehicles, all that at tropical conditions. Even if there would be an LN generator on site, eradicating the transportation disadvantages, such an infrastructure would have had to be built from scratch, including all occupational safety requirements and appropriate training for technical staff, as LN requires a constant supply. Cryogenic systems need to stop for LN refills, so they can't operate continuously. This is particularly disadvantageous in capturing dynamic changes in XVOC concentrations over time, which is important for studies on diurnal or seasonal patterns in the Amazon.

Overall, a non-cryogenic preconcentration system offers safer, more reliable, and continuous operation, making it ideal for remote field conditions like those at ATTO. It eliminates the need for complex infrastructure, allows uninterrupted monitoring of XVOC concentrations, and ensures consistent and accurate data collection.

4.3 Final Instrumental Setup

This chapter describes the final stage of the instrumental design and the methodology used to generate the data presented in Chapter 4.5. However, the development and refinement of the instrument will continue, with further adjustments and improvements to be carried out in the future.

4.3.1 Inlet System

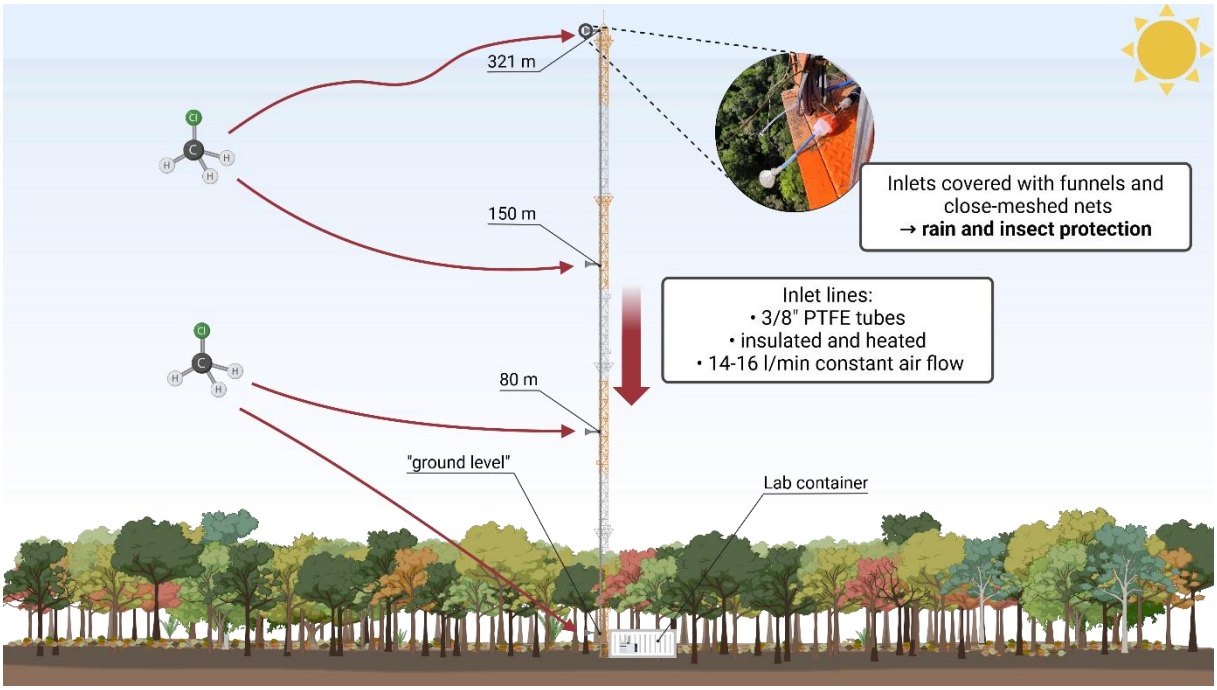

Figure 4-1. *Schematic design of the ATTO tall tower inlet system. Figure created in Biorender.com*

There are four inlet lines, three of which are attached to the ATTO tall tower, and one at ground level **(Figure 4-1)**. The openings of all inlet tubes are covered with a polyethylene (PE) funnel. These funnels act as rain protection as they prevent raindrops from entering the inlet line. The funnels themselves are covered in a close-meshed net fabric which prevents insects from entering the inlet lines. The tower inlet lines start at 321 m, 150 m, and 80 m height, respectively. These lines are made of 3/8 in (0,9525 cm) polytetrafluoroethylene (PTFE) tubes and run along the core of the tower. They are opaque to prevent sunlight from photochemically altering the trace gases within the sampled air mass. Furthermore, the tubing is insulated with PE foam and heated to prevent condensation of water vapor.

The "ground level" inlet line is not directly connected to the tall tower but is instead mounted below a roof approximately 3 meters above the ground at the base of the tower, covering the laboratory containers. The inlet is placed so that it faces the rainforest. Its tubing consists of a 6 m, 0.25 in (0.635 cm) SilcoNert® steel tube that connects directly to the Entech 7200CTS inlet (Chapter 4.3.2). This line is also equipped with PE foam insulation and a tube heating system to prevent water vapor condensation when the supply line enters the air-conditioned laboratory container.

In contrast to the ground-level inlet line, the tower inlet lines are constantly flushed. They are attached to high flow membrane pumps, positioned in the laboratory container, that draw air at a rate of 14 l min^{-1} and 16 l min^{-1}, respectively, depending on the pump model used. This rate leads to a residence time of the sample inside the inlet line of about 1.4 min for the 320 m line, 0.7 min for the 150 m line, and 0.4 min for the 80 m line. Just before the pumps, bypasses made of about 2 m of 1/8 in (0.3175 cm) SilcoNert® steel tube are attached to each of the tower lines, which then connect

to the Entech 7200CTS inlet. These bypasses are flushed only before the actual sampling (see next chapter).

4.3.2 Preconcentration System

As described in Chapter 4.2.3, a preconcentration system is used in XVOC analysis of gas samples, making it possible to detect very low concentrations that would be difficult or impossible to measure directly. The 7200CTS (Entech Instruments, Simi Valley, CA, USA) is a preconcentration system that operates without cryogenics like LN. Instead, the instrument uses a multi-capillary column trapping system (MCCTS) to concentrate the volatile trace gases from the air sample. It can be used for compounds within the BP range of -50°C to >230°C. After trapping the XVOCs, the system uses thermal desorption to release the concentrated compounds into a gas chromatograph (GC) for analysis (**Figure 4-2**, left side). The 7200CTS can be programmed for automated sampling, allowing for continuous or periodic collection of air samples over extended periods, which is particularly useful for long-term environmental monitoring or studies requiring temporal resolution of XVOC emissions.

***Figure 4-2**. Instrumental setup in a laboratory container at the ATTO site. Center: 7200CTS preconcentration unit with operating software (right) and attached GC (left).*

In **Figure 4-3**, the basic flow path of the 7200CTS is shown. The reservoir (bottom left) is a stainless-steel canister that is evacuated by default. The reservoir is crucial, as its vacuum passively controls the airflow through the instrument at different stages of the trapping process. Module 1 (M1, bottom-center) refers to the first of the two traps. It consists of three capillary columns: a weak, a moderate, and a strong column. The main function of this trap is to reduce the sample volume from up to 250 ml to just 1-2 µL. It is also used to remove water from the sample (see further below). The second trap, Module 2 (M2), is the focus trap, also consisting of various capillary columns but with shorter column lengths. The three digitally controlled multiport rotary valves (see **Figure 4-3** top row from right to left: Stream Select Valve (SSV), Trap Select Valve (TSV), Loop Valve (LV)) control the path of the sample within the instrument at every step of the run. All lines and tubing throughout the flow path are coated with Silonite™-D to reduce the potential for chemical adsorption.

There are 21 different run steps for a single 7200CTS analysis, some of which are optional, depending on the method used. To simplify matters, the path of a sample through the device during enrichment is described in the following: before the actual trapping, the corresponding inlet line, of which the 7200CTS has four, is pre-flushed with the air to be sampled so that no previous sample is left in the line. The duration of that pre-flushing is dependent on the length of the used inlet line. As described in Chapter 4.3.1, the entire inlet line is flushed during this step for the ground-level inlet. However, for the tower inlet, only the bypass line is flushed during this step, while the main tower inlet lines are continuously flushed by the external membrane pumps. After the pre-flush, the air sample enters the 7200CTS through one of the four inlet lines connected to the SSV (see **Figure 4-3**, connections 5-8). The other connections at the SSV are a blind stream (1), carrier gas inlet (2), internal standard inlet (3), calibration standard inlet (4), and the common port (C) which connects to the downstream flow path.

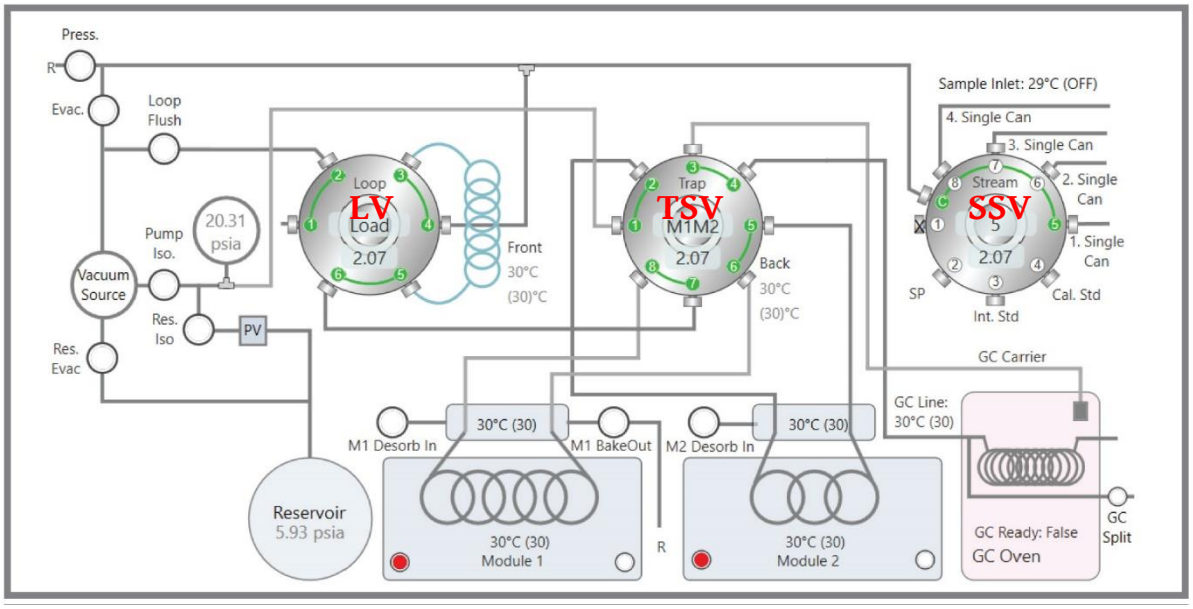

Figure 4-3. *Simplified flow path diagram of the Entech 7200CTS preconcentration system. Kindly provided by Entech Instruments Inc.*

From the SSV, the sample is transported to the LV (4→3→5→6) and from there through the TSV (7→6) to M1. The volatile trace gases are trapped here at a temperature of 35 °C. The fundamental principle is that as the gas sample flows through the trap, the compounds within the sample interact with the surface of the capillary columns. This interaction causes the compounds to be adsorbed and temporarily retained on the column surfaces. However, because the compounds, especially the very volatile ones, are not strongly adsorbed, they are only slowed down rather than permanently retained. Therefore, there are limitations regarding this trapping mechanism. For example, when using the instrument's optimal sampling flow rate of 20 cc min^{-1}, it is recommended to limit the sample volume to 250 cc. If the sample volume exceeds this, the extended sampling time could cause very volatile compounds like chloromethane to break through the trap before the sampling is complete. As a result, these compounds would not be preconcentrated and would be lost, escaping into the reservoir. The range specified by the manufacturer for the 7200CTS is therefore limited to compounds with a BP of -50°C to >230°C. The exact properties and configuration of the installed columns are subject to trade secrecy and therefore not known to the author.

As mentioned in Chapter 4.2.3, good water management is an essential task of the preconcentration system. A sample containing high humidity introduced to a GC leads to increased “column bleed”. Column bleed means the degradation of the polymer used in the column’s stationary phase, whose

degradation products elute along with the sample analytes, contaminating the detector and potentially interfering with the analysis by appearing as baseline noise or unwanted peaks in the chromatogram. So, the better the water management of the preconcentration system, the better the back-end instrumentation (i.e., the GC-MS) is protected as less column bleed leads to longer GC column lifetimes and fewer MS source cleanings.

Within the 7200CTS, the first trap (M1) is used to remove the water from the sample. After the first stage of preconcentration, the system initiates a dry purge process. In this step, a stream of dry, inert gas (helium) is passed through the trap. This gas helps to remove any water that has co-trapped with the VOCs by selectively desorbing the water molecules from the adsorbent material. This ensures that only the VOCs remain, which are then ready for thermal desorption. The use of selective adsorbent materials in the trap that preferentially retain VOCs over water reduces the amount of water that needs to be removed during the dry purge step, enhancing the efficiency of the water removal process.

The main gases flow unretained through M1 to the TSV (8→1) into the reservoir. The sampled volume is derived from the pressure change within the reservoir, using an Electronic Volume Controller (EVC). The EVC also determines the flow rates by measuring the rate of change in the sampled volume. Once the set volume has been sampled, M1 is heated and back-flushed with helium (SSV 2→C; LV 4→3→5→6; TSV 7→8; M1). The helium stream transports the now mobilized, preconcentrated sample to "cold" (35 °C) M2 (M1; TSV 6→5; M2), which is the focus trap. This trap follows the same basic principles as M1, just with shorter capillary columns. It refocuses the already preconcentrated compounds so that they are released to the GC in a more focused, narrow pulse, which leads to sharper peaks and better resolution in the chromatogram. This is particularly important for separating compounds that are very similar in their physical properties. After this step, the TSV changes position again so that the GC carrier gas, which flows in idle mode through TSV 3→4 onto the GC column, is now flowing through TSV 3→2 to heated M2, backflushing the trap and transporting the focused sample through TSV 5→4 into the GC via splitless injection. Simultaneously, this step triggers the GC method to start.

All parameters controlling the preconcentration are adjustable for each single step and displayed in **Figure 4-4**. As the instrument has been developed for the EPA method TO-15 (EPA, 1999), its default method is specialized for the analysis of some halogenated VOCs. Hence, not many method changes had to be implemented for this device in the scope of the objective of this work. This applies in particular to the temperatures, as these are crucial for a functioning preconcentration. Changes in the pre-set temperatures need to be considered carefully as they could lead to a premature breakthrough of compounds, insufficient system maintenance, or damage to the traps. However, the changes made during the development of the method mainly relate to the duration of heating events and flushing as well as changes in flow rates and volumes. These changes had the overall goal of aligning the timing of the enrichment method with the timing of the GC method. The 7200CTS method has a total runtime of 36.5 minutes.

CTS Method - Temperature Zone Control

File: ATTO 80m Inlet.CTS

Zones	Trapping	M1 Preheat	M1 Cool Purge	M1->M2	M2 Preheat	M2 Inject	M1 & M2 Bake Out
Mod 1	35°C	90°C	--	120°C	--	--	160°C
Mod 1 Bulkhead	150°C	150°C	--	150°C	150°C	--	150°C
Mod 2	35°C	--	0°C	35°C	160°C	180°C	180°C
Mod 2 Bulkhead	150°C	--	--	--	150°C	150°C	150°C
Rotary Valve Plate	150°C	150°C	--	150°C	150°C	--	150°C

7200	
Sample Transfer Line	0°C
GC Transfer Line	140°C

Event Durations	
Preheat Hold	0.2 min
Inject Duration	1.2 min
Post Injection Delay	8.0 min

Preflush Duration	
Int. Std.	5 sec
Cal. Std.	5 sec
Sample	70 sec
Swp/Prg Gas	5 sec
Pre M1 Gas Flush	15 sec
Loop Flush (<= 5cc)	0 sec

Volume	
S11) Flush Volume	40 cc
S12) M1 Cool Purge	15 cc
S13) M1 To M2 Volume	30 cc

Flow Rate	
S5) Int. Std. Trapping	20 cc/min
S7) Cal. Std. Trapping	20 cc/min
S9) Sample Trapping	20 cc/min
S11) Flush	20 cc/min
S13) M1 To M2 Transfer	10 cc/min

Figure 4-4. *Compilation of 7200CTS method parameters used for the sampling of the ATTO tower inlet lines. The sample preflush duration for the ground-level inlet line is 60 sec; all other parameters are kept the same for both methods. Explanations for the temperatures: "Trapping" refers to the temperatures during the actual trapping of M1. "M1 preheat" refers to the heating of M1 to 90 °C at zero flow before the actual desorption step to allow faster desorption. "M1 Cool Purge" doesn't apply to the method used. "M1->M2" are the temperatures during M1 desorption and sample transfer to M2. "M2 preheat" is comparable to the same step for M1. "M2 Inject" refers to the desorption temperature of M2 with the subsequent GC injection. "M1 & M2 Bakeout" are the temperatures during the bakeout of both traps which mobilizes any compounds remaining on the trap after regular desorption.*

4.3.3 Gas Chromatography (GC)

After preconcentration, the sample is transported with the carrier gas stream through a heated transfer line which connects the 7200CTS and a 6890A Gas Chromatograph (GC) (Agilent Technologies, Inc., Santa Clara, CA, USA). The carrier gas used is ultra-high purity (UHP) helium (ALPHAGAZ™ 2 Helium 99.9999 %, AirLiquide, France), purified by streaming through an Agilent Gas Clean carrier gas purifier (Agilent Part-Number: CP17973). Once introduced into the system, the sample is carried into a capillary column (J&W DB-1 GC column; 60 m length, 0.25 mm ID, 1.0 µm film thickness; Agilent) housed within the GC oven. The column is coated with a solid stationary phase (100% dimethylpolysiloxane), and as the mobile phase (i.e., the sample) travels through it, the compounds interact differently with the stationary phase based on their physical properties, primarily their volatility, and polarity. Compounds with lower boiling points or weaker interactions with the stationary phase travel more quickly through the column and elute earlier. Conversely, compounds with higher boiling points or stronger interactions are retained longer and elute later. As the DB-1 column is considered to be a non-polar column, polar compounds are less retained than non-polar compounds. The interaction of each compound with the stationary phase results in compound-specific retention times, which refer to the time it takes for a compound to travel from the injection point onto the GC column to its arrival at the detector.

The temperature of the GC oven can be controlled and changed while the sample is running through the column. It is often programmed to increase gradually during the analysis. This temperature ramping allows for more efficient separation of a wide range of compounds, from highly volatile to

less volatile species. Early-eluting compounds are separated at lower temperatures, while higher-boiling compounds are eluted as the oven temperature increases. The temperature program used in this method is shown in **Figure 4-5**. The GC temperature program recommended by the 7200CTS manufacturer for the TO-15 method had to be adjusted to retrieve a better resolution of the early eluting compounds. The initial temperature of 35 °C is maintained for 7.5 minutes, followed by a ramp of 10 °C min^{-1} until 200 °C is reached. A second ramp of 40 °C min^{-1} leads to the final temperature of 250 °C, which is held for a further 1.5 minutes and marks the end of the method.

The initial helium flow of 0.3 ml min^{-1} is held for 0.9 minutes, then ramped with 3.0 ml min^{-1} to a final flow of 1.2 minutes. The total run time of this GC method is 26.75 min. The difference in time between the preconcentration method and the GC method of about 9 minutes is due to the time it takes for the GC to cool down from its final temperature of 250 °C to its initial temperature of 35 °C to start the next run.

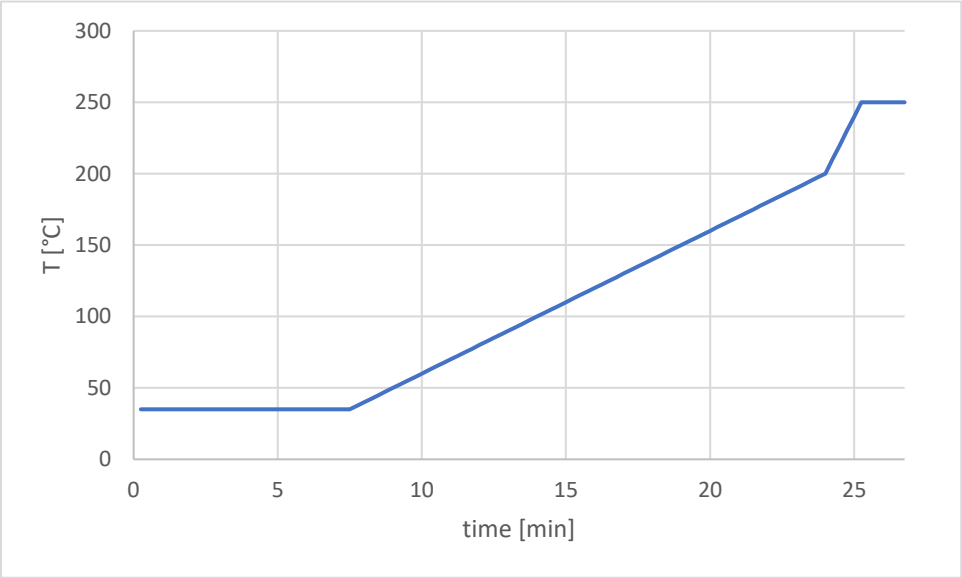

Figure 4-5. *Temperature profile of the GC.*

4.3.4 Mass Spectrometry (MS)

As the compounds exit the GC column, they enter the transfer line that connects the GC to the Mass Selective Detector (MSD) and finally the analyzer chamber of the MSD. Inside the analyzer chamber, there is a high vacuum (about 10^{-5} to 10^{-6} mbar; *5973N MSD Hardware Manual*, 1999). The sample molecules are now ionized by electron impact ionization (EI). In this process, an electrically heated filament emits electrons which are then accelerated by an applied voltage difference. The resulting stream of high-energy electrons hits the analyte's neutral molecules. This collision knocks electrons out of the molecules and generates positively charged ions. This ionization results also in the fragmentation of the molecules, producing a characteristic pattern of ions that can be used to identify the specific compound.

After ionization, the fragments reach the quadrupole mass filter. As the name suggests, the quadrupole filters masses based on their mass-to-charge ratio (m/z). It consists of four parallel quartz rods, covered with gold (*5973N MSD Hardware Manual*, 1999), that create an oscillating electric field, which allows only ions of a specific m/z ratio to pass through. By rapidly varying the electric field, the quadrupole can scan a whole range of m/z ratios in a very short time (several thousand atomic mass units per second). When the sum of all ion signals detected across a range of m/z ratios is recorded, that mode is called total ion current (TIC). It is used to analyze samples with unknown compounds. In contrast, the user can pre-select m/z ratios before the analysis, which is called

selected ion monitoring (SIM mode). SIM mode is used when the identity of the target analytes is known and precise quantification of those specific ions is required, as it has the advantage of a higher sensitivity and lower detection limits for those particular compounds.

The ions that successfully pass through the quadrupole reach the detector. When an ion hits the detector, an electronic signal is generated and amplified by an electron multiplier. This signal then is carried to and read out by a computer. It contains two relevant pieces of information: First, the mass spectrum, which is the intensity of ion signals detected in a mass spectrometer as a function of their mass-to-charge (m/z) ratios. The mass spectrum serves as a fingerprint for each compound and can be used for compound identification through comparison with a spectral library. Next to this qualitative information, the detector signal also contains quantitative information, as its intensity is proportional to the number of ions striking the detector.

The graphical representation of the detector signal over time is called a chromatogram. As a result of the compound separation during the gas chromatography, a chromatogram includes peaks, where each peak corresponds to a different compound. Quantitative chromatogram analysis compares the peak areas with those of calibration standards with known composition and known concentrations.

The data from the GC and MSD are collected and processed using Agilent ChemStation software, which is also used to control both instruments and change the respective method parameters (see Chapter 4.3.3 for GC parameters and **Table 4-1** for MS parameters).

Table 4-1. *Mass Spec parameters for TIC mode.*

Parameter	Value
Solvent Delay	1.2 min
AUX Temperature	230 °C
MS Source Temperature	230 °C
MS Quadrupole Temperature	150 °C
Scan Parameters	
Time Range 1	2.0-15.5 min
Mass Range 1	45-190 m/z
Time Range 2	15.5-26.75 min
Mass Range 2	45-264 m/z
Threshold	50 counts
A/D Samples	4

In the mass spectrometry method, a solvent delay of 1.2 minutes was applied to prevent the mass spectrometer from analyzing and being overwhelmed by early-eluting, non-analyte components, which could potentially damage the detector or complicate the data analysis. The AUX temperature, set to 230°C, refers to the temperature of the transfer line that connects the GC to the MS. This temperature ensures efficient transfer of analytes from the GC to the MS without condensation or loss.

A method has been developed for SIM mode to achieve better sensitivity for a few XVOCs of interest. This method has not been used at ATTO yet, since the first goal has been to get an overview of XVOCs present and detectable in the Amazon rainforest. Measurements in SIM mode should be carried out in the future to decrease the limits of detection (LOD) and quantification (LOQ) and to track changes of XVOCs in the single pptv range like chloroform or bromoform. The parameters of the developed SIM mode are presented in **Table 4-2**.

Table 4-2. *Mass Spec parameters for SIM mode*

Parameter	Value
Solvent Delay	1.2 min
AUX Temperature	230 °C
MS Source Temperature	230 °C
MS Quadrupole Temperature	150 °C
Scan Parameters	
Time Range 1	1.0-6.0 min
Masses Group 1	50, 51, 52, 60, 62, 67, 85, 87, 135, 137 m/z
Time Range 2	6-26.75 min
Masses Group 2	49, 51, 84, 86, 101, 103, 117, 119, 120 m/z
Threshold	50 counts
A/D Samples	4
Dwell time	50 ms

4.3.5 Calibration Method

To quantify the data, the 7200CTS-GC-MS setup has been calibrated. For this purpose, a multi-compound gas-phase calibration standard (APEL-RIEMER ENVIRONMENTAL, INC.; Miami, FL, USA) has been measured repeatedly with the same setup and parameters as the samples. The list of the compounds included are shown in the **Table 4-3**:

Table 4-3. *Multi-component calibration mixture in ultra-pure nitrogen.*

Compound	CAS#	Concentration [ppbv]	Uncertainty
1,1,1,2-Tetrafluoroethane (HCFC-134a)	811-97-2	10.87	±5%
Chlorodifluoromethane (HCFC-22)	75-45-6	10.54	±5%
Carbonyl Sulfide	463-58-1	10.34	±5%
Dichlorodifluoromethane (CFC-12)	75-71-8	10.03	±5%
1-Chloro-1,1-difluoroethane (HCFC-142b)	75-68-3	10.63	±5%
Chloromethane	74-87-3	10.44	±5%
1,2-Dichloro-1,1,2,2-tetrafluoroethane (CFC-114)	76-14-2	10.46	±5%
2-Chloro-1,1,1-trifluoroethane (HCFC-133a)	75-88-7	10.41	±5%
Vinyl Chloride	75-01-4	10.51	±5%
Bromomethane	74-83-9	10.84	±5%
Chloroethane	75-00-3	10.73	±5%
Vinyl Bromide	593-60-2	10.83	±5%
Trichlorofluoromethane (CFC-11)	75-69-4	9.89	±5%
Isoprene	78-79-5	11.39	±5%
Methyl Iodide	74-88-4	10.90	±5%
1,1-Dichloroethene	75-35-4	11.43	±5%
Dichloromethane	75-09-2	10.72	±5%
1,2-Dichloro-1,1-difluoroethane (HCFC-132b)	1649-08-7	10.56	±5%
1,1,2-Trichloro-1,2,2-trifluoroethane (CFC-113)	76-13-1	10.68	±5%
trans-1,2-Dichloroethene	156-60-5	10.53	±5%
1,1-Dichloroethane	75-34-3	10.86	±5%
2-Chloro-1,3-Butadiene	126-99-8	6.57	±5%
cis-1,2-Dichloroethene	156-59-2	10.60	±5%
2-Chlorobutane	78-86-4	10.79	±5%
Chloroform	67-66-3	9.65	±5%
1,2-Dichloroethane	107-06-2	9.56	±5%
1,1,1-Trichloroethane	71-55-6	9.51	±5%
Benzene	71-43-2	9.79	±5%
Tetrachloromethane	56-23-5	9.65	±5%
Dibromomethane	74-95-3	10.06	±5%
Bromodichloromethane	75-27-4	8.60	±5%
Trichloroethylene	79-01-6	9.06	±5%
cis-1,3-Dichloropropene	10061-01-5	0.26	±5%
trans-1,3-Dichloropropene	10061-02-6	17.15	±5%
1,1,2-Trichloroethane	79-00-5	8.79	±5%
Toluene	108-88-3	8.60	±5%
1,2-Dibromoethane	106-93-4	8.81	±5%
Tetrachloroethylene	127-18-4	8.64	±5%
1,1,1,2-Tetrachloroethane	630-20-6	8.63	±5%
Chlorobenzene	108-90-7	8.73	±5%
Bromoform	75-25-2	9.07	±5%
1,1,2,2-Tetrachloroethane	79-34-5	8.96	±5%
Bromobenzene	108-86-1	9.02	±5%
1,3-Dichlorobenzene	541-73-1	8.40	±5%
Benzyl Chloride	100-44-7	8.62	±5%
1,4-Dichlorobenzene	106-46-7	16.39	±5%
1,3-Dibromobenzene	108-36-1	7.72	±5%
1,4-Dibromobenzene	106-37-6	14.68	±5%

Many of the listed compounds occur in lower concentrations in nature. To ensure an appropriate calibration, the calibration range should cover the range of natural abundances. Chloromethane, for example, has an atmospheric background of around 550 pptv (WMO, 2022). An appropriate calibration could therefore cover a range between 200 and 1000 ppt. To achieve this, two approaches have been tested with the given setup: The first approach involved preconcentrating varying volumes of the calibration standard to adjust for different analyte concentrations. The CalGas used for this process has a chloromethane concentration of 10,440 parts per trillion by volume (pptv). For the standard procedure, a sample volume of 250 cubic centimeters (cc) is preconcentrated. To achieve calibration at lower concentrations, we reduced the volume of the calibration gas sampled, for example by a factor of 10 to 25 cc. This reduction means that the volume of chloromethane analyzed corresponds to a 250 cc gas sample with a concentration of 1,044 pptv.

However, this method requires low preconcentration volumes. For example, to calibrate the concentration step of 200 pptv, only about 5 cc of CalGas would need to be preconcentrated. In this range, the relative uncertainties of the preconcentration process are too high, which is why this method is only feasible for compounds with higher natural abundancies and consequently higher calibration ranges.

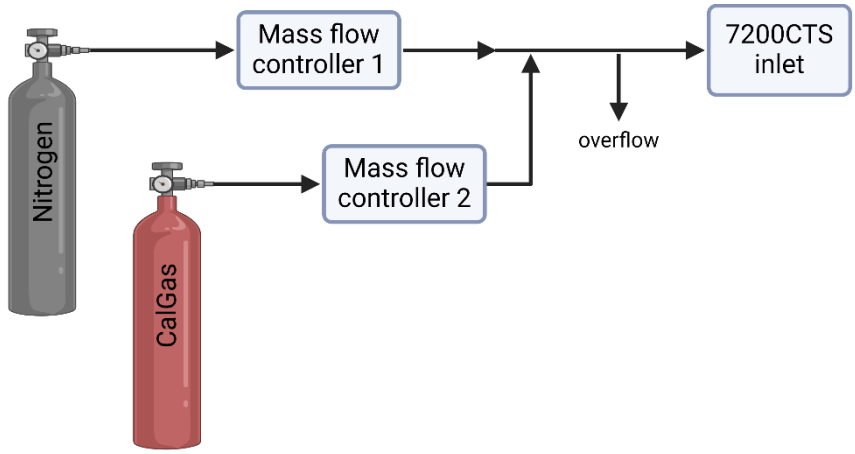

Figure 4-6. *Flow path of the calibration setup. Figure created in Biorender.com*

A different calibration method was used for lower calibration ranges. In this method, the CalGas was diluted with nitrogen. Subsequently, different dilution levels of this gas mixture were measured to calibrate the system. The dilution was achieved by the flow setup shown in **Figure 4-6**. Mass flow controller (MFC) 2 has been constantly kept at 5 sccm, while the flow of MFC 1 was adjusted for every step to obtain the desired dilution. The resulting calibration curve for chloromethane is given as an example in **Figure 4-7**. This calibration has proven itself to be more applicable for a lower mixing ratio range and therefore has been used for the quantification of the data shown in Chapter 4.5. However, the original y-intercept had to be subtracted from all data points to correct for an offset that has its cause probably in the calibration setup, more precisely in the chosen gas flows controlled by the MFCs. Keeping the CalGas flow consistent while adjusting the nitrogen flow resulted in large variation of the flow difference. For example, while for one dilution step the flow ratio was 5 sccm CalGas to 40 sccm nitrogen, this ratio was 5 sccm CalGas to 210 sccm nitrogen for another dilution step. As a result, it turned out that sufficient mixing of the very different flows cannot be guaranteed, especially with smaller flow ratios.

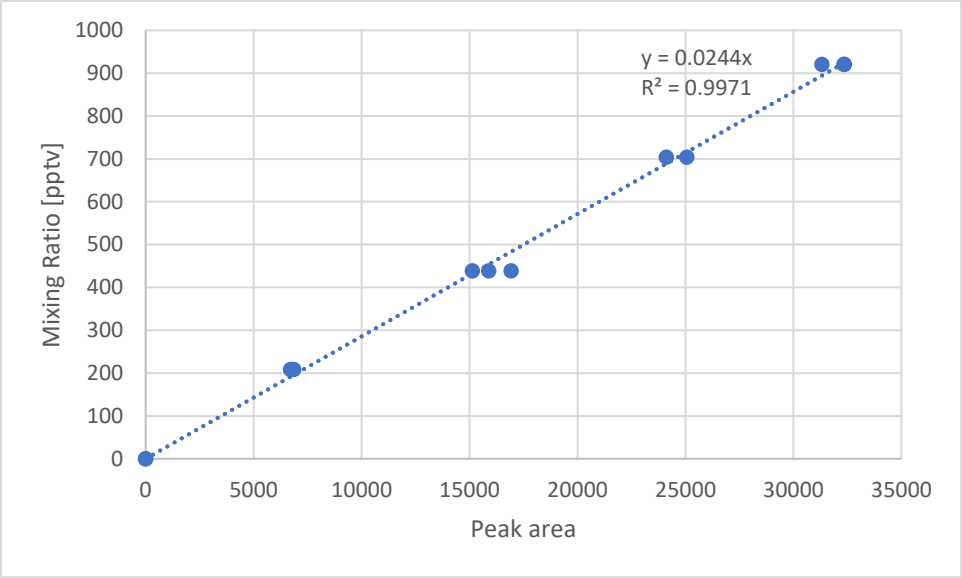

Figure 4-7. *Chloromethane calibration curve derived from MFC setup shown in Figure 4-6.*

The resulting offset, by which the calibration was corrected, in turn leads to a comparatively high limit of detection (LOD) and limit of quantification (LOQ). This is not a problem for chloromethane with an LOD of 62.2 pptv and an LOQ of 188.5 pptv, as its atmospheric background is in the range of 550 pptv (WMO, 2022). However, for compounds with lower atmospheric abundances, such an offset is problematic. To reduce this offset, the procedure should be changed for future calibrations by keeping the nitrogen flow constant and varying the CalGas flow to achieve different dilutions. By this setup change, the absolute differences between CalGas flow and nitrogen flow would be smaller, enabling a potentially lower offset through better mixing of the two flows. Despite the offset correction, the derived calibration curve provides a good linear regression and can therefore be used for quantification within the displayed mixing ratio range above the LOQ. **Figure 4-8** shows a chromatogram of the analyzed CalGas with a tenfold dilution. Despite a certain co-elution of peaks between 4 and 5 minutes, the overall separation of the peaks is sufficient. The co-elution impacts only the total ion count chromatogram; this issue can be resolved by integrating only the unique masses specific to each compound.

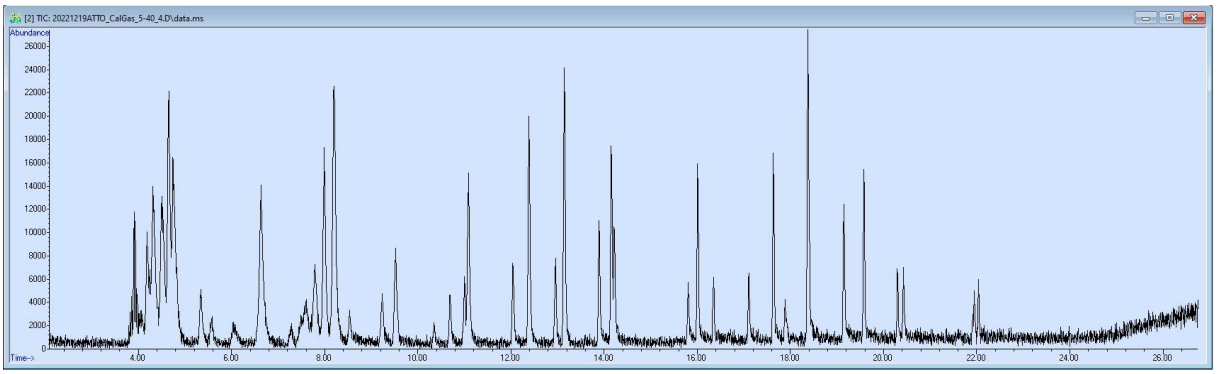

Figure 4-8. *Chromatogram of a tenfold diluted CalGas in TIC mode.*

4.3.6 Error Assessment

The necessity of quantifying the systematic error of an analytical setup is evident. However, this is only feasible to a certain extent for the described setup. The systematic error of the 7200CTS-GC-MS setup itself is quantifiable by calculating the uncertainty of the described calibration because the path of a sample is the same for the CalGas and a natural sample, at least from the inlet of the preconcentrating system to the MS detection. This error can be calculated with Equation 9 and equals 8.66 %.

$$\sigma_{total} = \sqrt{{\sigma_{MFC1}}^2 + {\sigma_{MFC2}}^2 + {\sigma_{CalGas}}^2} \qquad \text{Equation 9}$$

Where:

σ_{MFC1}=uncertainty of nitrogen MFC (5 %),

σ_{MFC2}=uncertainty of CalGas MFC (5 %)

σ_{CalGas}=uncertainty of the calibration standard (5 %)

There are other potential sources of uncertainty. For example, target analytes may be lost to some extent in the tower inlet lines due to interaction with the tubing material. In contrast to the error derived from the calibration, an error due to line loss would be individual for each compound. However, since the magnitude of this influence has not yet been quantified, this aspect can not be included into the error calculation.

4.4 Method Development – from an Idea to Realization

The method used in the scope of this PhD project has been developed for the first time in a highly challenging environment, i.e., the Amazon rainforest. However, the instrumental setup is designed and built for a regular laboratory environment. Setting up such an instrumental setup in a laboratory container at ATTO presented a unique set of challenges, compounded by the global COVID-19 pandemic. The pandemic led to significant delays due to laboratory access restrictions and travel bans, which severely impacted both the preparation and execution phases. These delays not only postponed the start of the data acquisition but also created a ripple effect on the execution of subsequent campaigns. The goal of being able to provide a dataset of several seasons at the end of this PhD project was therefore out of reach.

From the analytical point of view, there have been some unforeseen complications as well. The use of PFA (Perfluoroalkoxy alkanes) Teflon tubing for inlet lines, chosen for its chemical inertness and tried and tested for many other applications at ATTO, e.g., a PTR-TOF-MS setup, turned out to be problematic for the measurement of halogenated VOCs under certain conditions. For the setup at ATTO, a few meters of new 1/8 in (0.3175 cm) PFA tubes were used for the bypass of the tower inlet tubing connecting to the 7200CTS inlet (see Chapter 4.3.1) and the ground-level inlet line. These new lines outgassed significantly, causing a large background signal in the MS data and making it impossible to quantitatively and qualitatively analyze the samples (**Figure 4-9**). Even after months of conditioning, the background signal remained too high. This issue was ultimately resolved by replacing these PFA tubing with the silica-coated stainless steel lines described in Chapter 4.3.1. During the method development phase at the MPIC in Mainz, this issue did not emerge because older PFA tubes from the laboratory stock were used; these had been in service for several years and were well-conditioned. The tubing of the PTFE tower inlet lines did not cause any such problems, probably because these lines have a larger diameter (and therefore a lower surface-to-volume ratio) and were installed already in 2015, meaning they had enough time to condition.

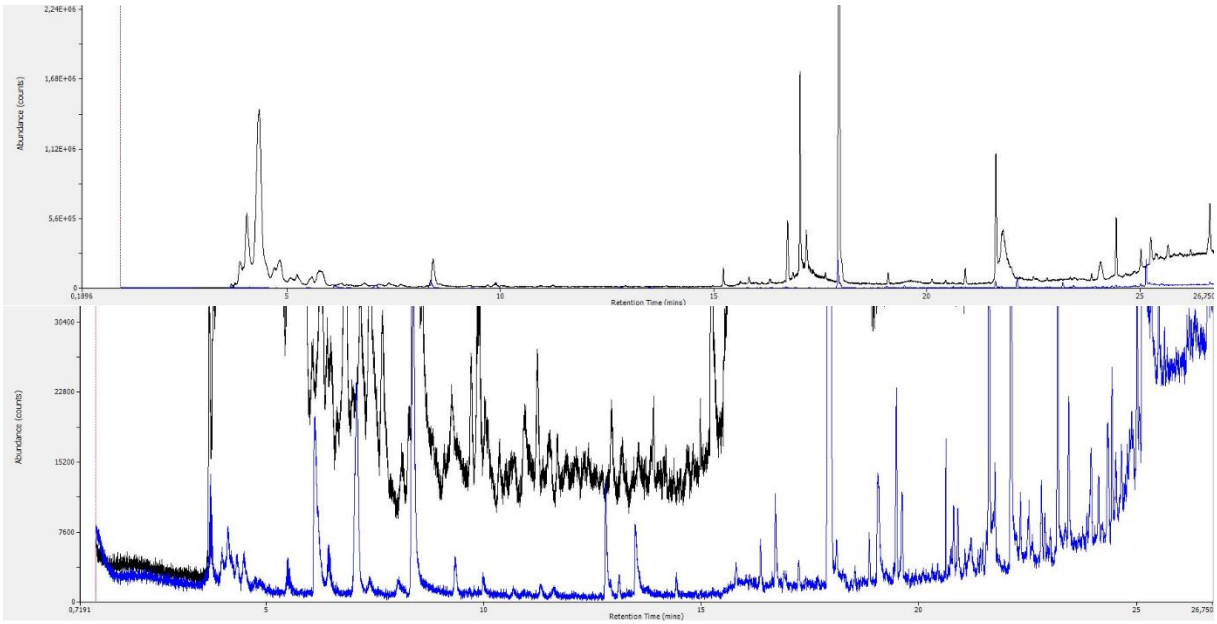

Figure 4-9. *Comparison of two chromatograms of ambient air, one with PFA tubing (black) and one with SilcoNert®-coated stainless steel tubing (blue). Both images show the same chromatograms, whereby the lower image has only been zoomed.*

A similar problem occurred when a Teflon housing for quartz filters or ozone scrubbers was attached to the inlet. This problem was already identified during the first field test of the instrument setup at the Kleiner Feldberg observatory north of Frankfurt in 2021. As a consequence, these filter housings are not part of the final setup at ATTO.

Another major challenge was and remains the power cuts at the ATTO site. There are multiple Uninterruptible Power Supply (UPS) modules installed at the site, which can bridge short power outages of up to 30 minutes. However, longer power cuts, triggered for example by fallen trees that damage the power lines, lead to forced shutdowns of the delicate instruments and subsequent issues with restarting the equipment under optimal conditions. Such power cuts affected for example the turbo pump of the MS, which normally needs to be shut down slowly and controlled. Another power cut led to severe damage to the preconcentration system: Whenever this system is shut down, it should be put into safety mode beforehand. One aspect of this safety mode is the multiport rotary valves being set into "in between" positions, interrupting the instrument's flow path. Due to a sudden shut-down caused by a power cut, a pressure spike has flowed through the flow path in the wrong direction, resulting in contamination with filter material and other debris throughout large parts of the flow path. As a consequence, the instrument had to be sent to the manufacturer for a complete replacement of the flow path. Some upgrades have been integrated into the new flow path, such as physical barriers and frits to prevent this problem from occurring again in the future.

The logistical constraints of operating in such a remote environment meant that some major equipment failures could not be addressed promptly. After each campaign, the equipment had to be left in situ, and any malfunctions discovered could often only be fixed months later during the next planned campaign. Only smaller issues could be fixed by instructing a site engineer and assisting him remotely in the repair process. This delay in repairs reduced the amount of usable data collected and increased the risk of further damage to the equipment.

In summary, issues that could be solved in a few days in a regular lab may mean a delay of several months for such a project. The combination of the described technical and logistical hurdles emphasizes that maintaining high-precision instrumentation in such an environment requires meticulous planning, robust backup systems, and the ability to adapt to unexpected challenges.

4.5 Proof of Concept and First Results

Despite the challenges described above, some data was collected that proves that the setup works in principle and that the data collected is valid and has great potential to answer open questions in the future. This chapter presents the results of the data obtained in the context of the CAFE Brazil campaign (campaign features described in detail in Ort et al., 2024, for example) between December 2022 and January 2023.

4.5.1 Comparison of Chloromethane and CFC-12 Data

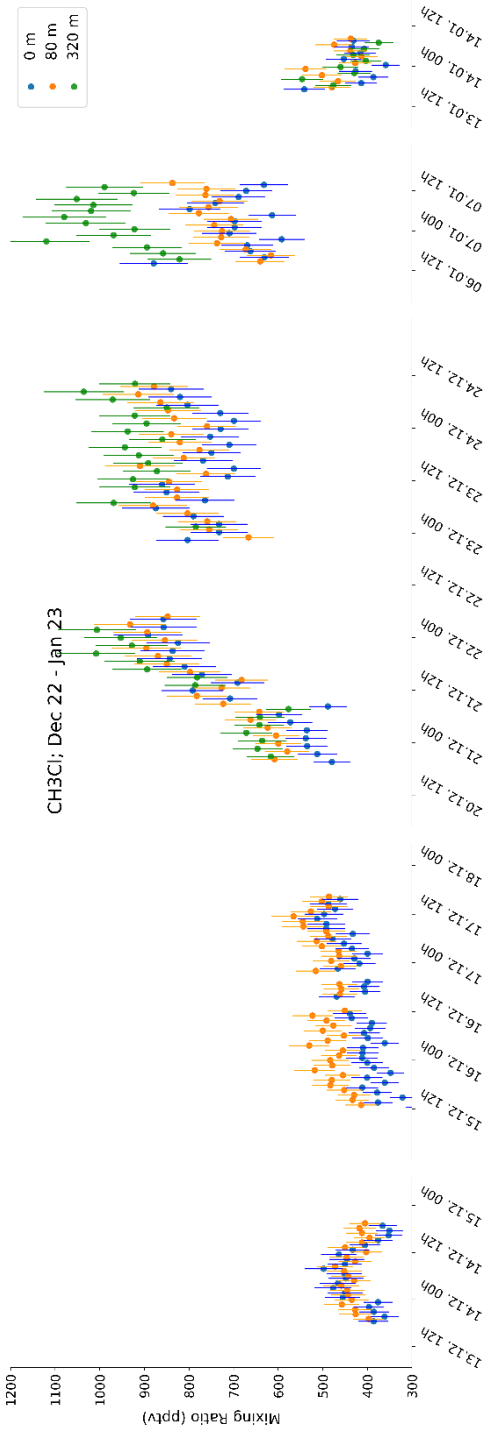

Figure 4-10. *Chloromethane mixing ratios of ambient air measured at the ATTO tower at ground level ("0 m"), 80 m, and 320 m, respectively, between mid-December 2022 and mid-January 2023. Error bars indicate a systematic uncertainty of 8.66 % for each data point. All times are given in UTC.*

Figure 4-10 shows the chloromethane data of this period in the form of volume mixing ratios (VMRs) plotted against the time, measured at ground level ("0 m"), 80 m, and 320 m height, respectively. On the first days, only 0 m and 80 m were sampled, as this was still a test phase and the aim was to achieve a better temporal resolution. All shown data is based on only one single calibration, carried out on the 19th of December (see Chapter 4.3.5). The reason for this is that a permanent calibration setup has not yet been implemented for this system.

All reported chloromethane VMRs were well above the LOQ of 188.5 pptv. During the first days, values were between 300 and 600 pptv and therefore well within a range reported for the global atmospheric background (e.g., by AGAGE (Hossaini et al., 2019; Prinn et al., 2018)). Starting with the 20th of December, there was a striking increase in chloromethane VMR over almost two days, peaking in a range of about 1000 pptv. The values remained at this high level until the first week of January, whereas in the second week of January, the values were back at the initial level.

Before the underlying causes of the data shown could be interpreted, the data quality had to be confirmed to ensure that the VMR changes observed were real and not a systematic error or any kind of sampling artifact. This applied in particular to the large increase of more than 100 % between the 20th and 22nd of December. For that reason, we compared this chloromethane data with the data of another compound, i.e., CFC-12 (dichlorodifluoromethane, CCl_2F_2).

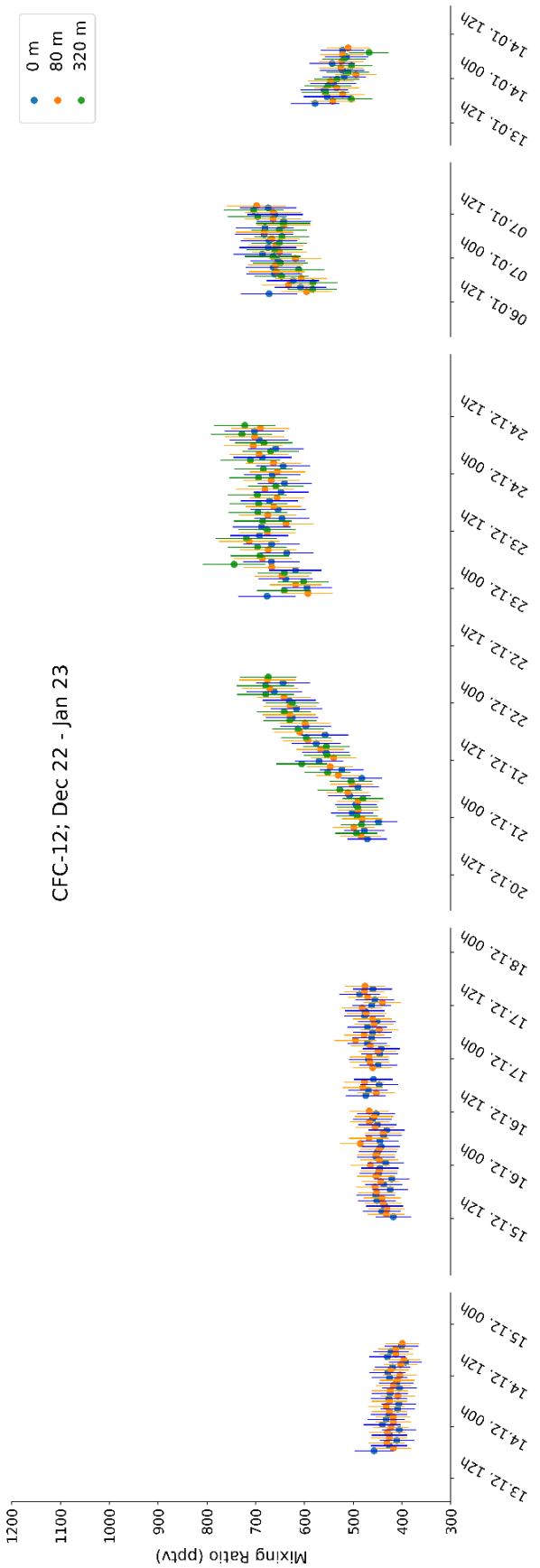

Figure 4-11. *CFC-12 mixing ratios of ambient air measured at the ATTO tower at ground level ("0 m"), 80 m, and 320 m, respectively, between mid-December 2022 and mid-January 2023. Error bars indicate a systematic uncertainty of 8.66 % for each data point. All times are given in UTC.*

The volume mixing ratios of the first days of data shown in **Figure 4-11** reflect roughly the atmospheric CFC-12 background of 492 pptv as reported by AGAGE within the range of error (Hossaini et al., 2019; Prinn et al., 2018). However, there is an increase from ~480 pptv up to more than 700 pptv CFC-12, parallel to the reported increase in the chloromethane data shown above. The production and usage of the exclusively anthropogenic CFC-12 are regulated in compliance with the Montreal Protocol. Any local sources would therefore be illegal, and the lack of residential and industrial areas upstream of ATTO makes these even more unlikely. Combined with the fact that no natural sources are known for CFC-12, the assumption to exclude local sources is justified, which leads to the conclusion that the observed increase in CFC-12 is highly likely due to a systematic error.

4.5.2 Potential Sources of Error

The underlying source of the observed error could be either the instrumental setup, the inlet system, or a change in natural conditions that affected the measurement results in a yet unknown way. First of all, no physical changes to the analytical setup were made in the corresponding period, nor were any changes made to the hardware and software method. Any variations in the data caused by such changes would anyway lead to a more abrupt change in the data, rather than the gradual increase one can see in this data. However, several factors regarding the analytical setup could lead to variations in the measurements. In terms of the Entech 7200CTS preconcentration system, one of these factors could be the temperature of the system's surroundings, i.e., the laboratory container. A temperature change could impact the volume of the stainless steel canister from which the sampled volume is derived during the preconcentration process (see Chapter 4.3.2). Lower temperatures could lead to a shrinking of this canister, while higher temperatures could cause an expansion. The lab container's

temperature is controlled by two air conditioning units, which are positioned directly above the described instrumentation. The set temperature is usually 27 °C. The two major influences on the lab container temperature are the frequency of opening of the container entrance door due to colleagues entering, and the exhaust of the GC, especially when the GC cools down from its final method temperature of 250 °C to its initial method temperature of 35 °C. The lab container's temperature is monitored and would alarm the site engineer if it exceeded a certain threshold temperature. The usual changes in temperature are about 1.5 °C. To evaluate the impact of usual lab air temperature changes, the thermal expansion of the canister can be calculated with Equation 10:

$$\Delta A = A_0 \cdot 2\alpha \cdot \Delta T \qquad \text{Equation 10}$$

Where:

ΔA = change in surface area

A_0 = original surface area

α = Coefficient of linear thermal expansion

ΔT = Change in temperature (in K)

Considering that the canister is a hollow object made of thin stainless steel, it makes sense to treat it as a surface when calculating thermal expansion. For an original surface area of the canister of about 660 cm^2 and a thermal expansion coefficient for stainless steel of $15 \cdot 10^{-6}$ K^{-1} ("Thermal Expansion - Linear Expansion Coefficients," 2003), the change in surface area would be 0.02 cm^2 K^{-1}, corresponding to a change of canister volume of 0.003 % per °C. It can therefore be ruled out that this effect is responsible for the observed change in the CFC-12 mixing ratios.

The GC itself is a very basic functioning instrument compared to the preconcentrating system and the MS. Its only tasks are to control the temperature of the oven and the AUX, as well as the flow through the GC column. All these parameters were monitored and didn't show any anomalies during the corresponding measurements.

As described in Chapter 4.3.5, there was only one calibration carried out for the whole measurement period. This is suboptimal because the MS sensitivity can slowly decrease over time due to several reasons, e.g., ion source contamination, detector degradation, alignment drifts of the ion optics, or degradation of the electric field. This is why regular tuning of the MS and consequently regular calibration is crucial to maintain optimal performance. However, the described issues would lead to a sensitivity decrease, and not to an increase. Fixing an initially wrong tuning by retuning the system could lead to a sensitivity increase but again, this increase would then be abrupt and not ramped.

One common issue there is at ATTO is power fluctuations. Within the MS, the filament is a critical component of the system that directly influences the system's sensitivity and is theoretically sensitive to power fluctuations. To manage these, uninterruptible power supplies (UPS) are used on-site not only to protect against power outages but also to smooth out fluctuations and spikes in the power supply. This ensures that the voltage delivered to the device remains stable. Even if assuming these UPS would fail, mass spectrometers are equipped with stabilized power supplies and precise power sources specifically designed to compensate for fluctuations in the mains voltage including transformers, rectifiers, capacitors, and voltage regulators.

In summary, it hasn't been possible to connect the increased chloromethane and CFC-12 VMRs with a systematic error in the analytical instrumentation. Potential wall effects of the inlet lines need to be investigated for the analytes and can't be fully excluded from this discussion. However, wall effects would lead to a permanent misestimation of the ratio of analytes rather than an error that varies over time for a particular connection. Another aspect of the inlet lines that is subject to fluctuations is the total line flows, which depend on the performance of the respective main pumps. This parameter was not monitored but due to the setup of the whole inlet system, it is unlikely that this is the reason for the observed issue. The bypass that connects the main inlet line with the 7200CTS inlet is probably independent of fluctuations in the pump performance, as its flow is regulated by the preconcentration system. The sampled volume, and also the final sampling flow, is determined by the pressure change within the evacuated canister inside the 7200CTS. It therefore is independent of external factors. If desired sampling flow speeds couldn't be established, the system would compensate for that automatically by increasing the sampling time, which in turn doesn't affect the system's sensitivity.

A similar justification, i.e., the pressure insensitivity of the 7200CTS, can be used to rule out variations in ambient air pressure to be the reason for the large detected chloromethane and CFC-12 VMR increase, at least from an instrumental point of view. Local ambient conditions are in general crucial factors in gas analytics: ambient temperature can affect the volatility of compounds, humidity can influence the adsorption and desorption behavior of gases on surfaces, rain or fog can lead to wet deposition, and sunlight drives photochemical reactions. However, experience shows that it is unlikely that the fluctuations in natural conditions are responsible for the measurement inaccuracies of more than 100 % that we observed here. Nevertheless, all these factors need to be taken into account when evaluating also future data, even though for this work, no connection between variations of ambient conditions and variations in the data was obvious. Therefore, we need long-term data sets to obtain more statistics on such potential correlations.

4.5.3 Correction Method

Drifts or slow system changes that lead to systematic errors can never be completely avoided in long-term measurements. Usually, measures are taken to correct the data for these errors. This can be achieved, for example, by regular calibrations, by measuring a calibration standard at least once a day to monitor its changes over time, or by using an internal standard that is measured together with each individual measurement. Since there hasn't been a permanent calibration setup implemented yet because of external circumstances, calibrations could only be carried out on-site, which is why there has been only one calibration used for the whole measurement period from mid-December to mid-January. In addition, there was no internal standard available during this time. There is no possibility to calibrate the system retrospectively. This requires a different correction method if the available data is nevertheless to be evaluated and discussed. Such a correction has been developed in the scope of this work and applied to the presented data. The basic assumption of this correction method is that the CFC-12 measured in ambient air is constant and that any increase or decrease in the VMR data of this compound must be a systematic error. Under this assumption, CFC-12 can be used as an internal standard, and all other compounds can be normalized by this CFC.

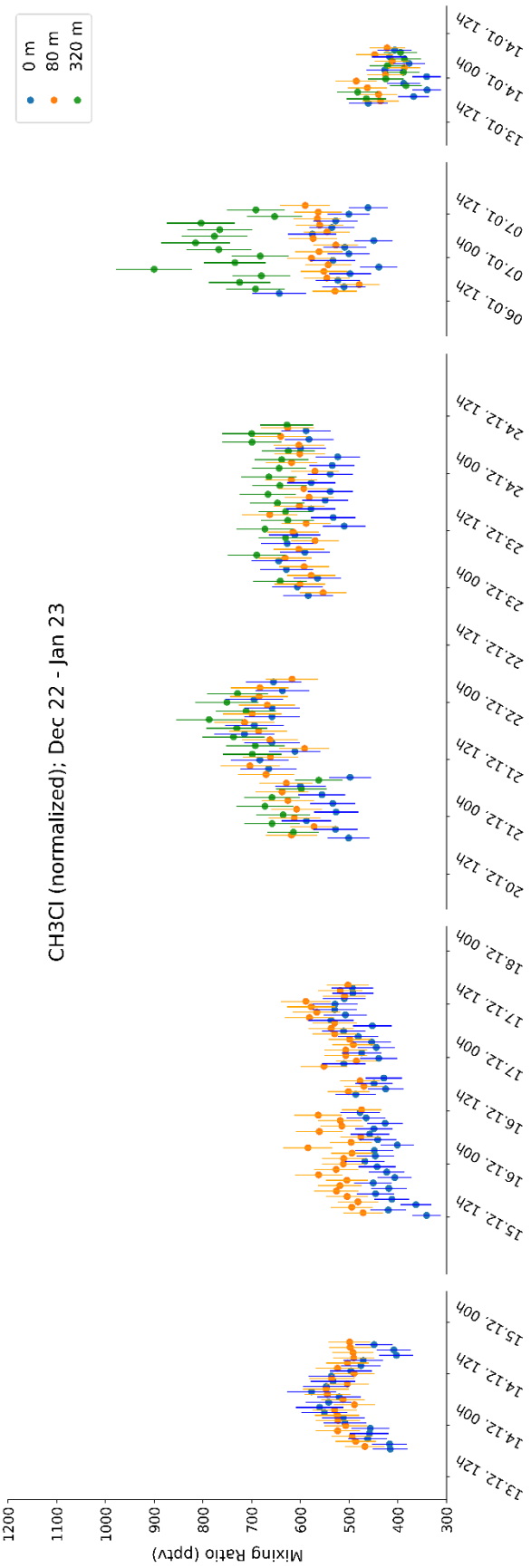

Figure 4-12. *Chloromethane mixing ratios of ambient air, normalized by CFC-12, measured at the ATTO tower at ground level ("0 m"), 80 m, and 320 m, respectively, between mid-December 2022 and mid-January 2023. Error bars indicate a systematic uncertainty of 8.66 % for each data point. All times are given in UTC.*

Figure 4-12 shows the same data as **Figure 4-10**, only this time after being corrected with CFC-12 as described above. Compared to the uncorrected data, chloromethane VMRs now show less extreme changes. An increase between 20.12. and 22.12., however, is still visible, as well as the decrease between 07.01. and 13.01. Overall, this correction method seems to be a good start but also not perfect. If a similar correction is needed in the future, it might be more precise if not only one CFC, but many other CFCs or similarly inert compounds would be included in the correction, resulting in some kind of mean value which then could be used as the correction factor. If used for longer periods or even permanently, more robust and detailed method validation needs to be carried out to make the method "fool-proof". For example, it is not certain whether the relative changes between CFCs and the target analytes such as chloromethane are constant or whether they may vary over time due to changes in detector sensitivity (Stephen Montzka, NOAA, personal communication).

By design, the applied correction method changes absolute VMR values but the qualitative differences between the different datasets (0 m, 80 m, and 320 m) remain. In this matter, it is striking that the 80 m VMRs tended to have slightly higher values than at 0 m for most of the measurement period. 320 m, when measured, showed overall highest values. Especially during 06.01. and 07.01., chloromethane VMRs at 320 m are in a range between 650 and 900 pptv, while 80 m and ground level values are about 550 pptv.

This observation of an apparent height gradient for chloromethane VMRs could be seen as a first hint of the interplay between local sources and sinks on one side and long-range transport on the other. Measurements at ground level and at 80 m are most strongly characterized by local influences, i.e., potential sources and sinks within the canopy or the soil. The data from 320 m are

influenced by a larger footprint region, it therefore is expected to be less sensitive to single or locally restricted sources and sinks. It also represents the influence of long-range transported air masses, as well as regional biomass burning which could influence the local VMR (Lobert et al., 1999; Rudolph et al., 1995).

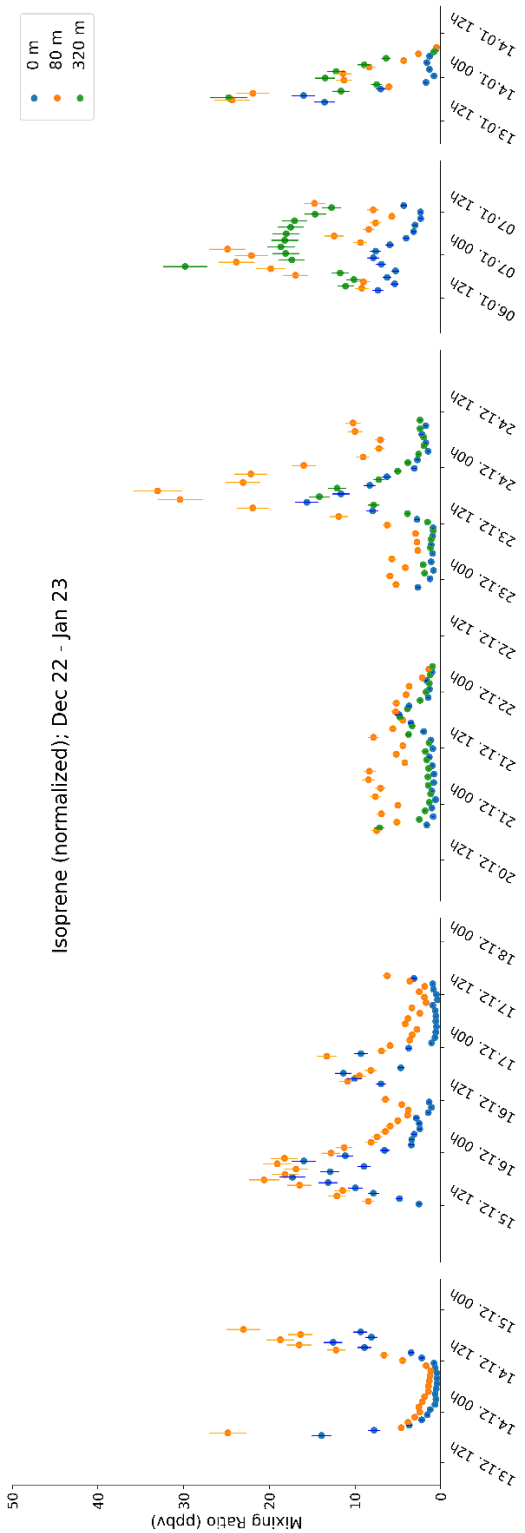

***Figure 4-13**. Isoprene mixing ratios of ambient air, normalized by CFC-12, measured at the ATTO tower at ground level ("0 m"), 80 m, and 320 m, respectively, between mid-December 2022 and mid-January 2023. Error bars indicate a systematic uncertainty of 8.66 % for each data point. All times are given in UTC.*

4.5.4 Isoprene Data Validates the Resolution of Potential Diel Fluctuations

Chloromethane, with an atmospheric lifetime of 0.9 years (WMO, 2022), is not classified as a Very Short-Lived Substance (VSLS). This extended lifetime makes it more challenging to pinpoint potential sources and sinks using only temporal data. For instance, even if chloromethane emissions were higher during the day due to light or temperature-dependent sources, this wouldn't necessarily result in a clear diel pattern in the dataset. Unlike other trace gases that may show significant nighttime decreases as daytime production ceases and removal processes take over, chloromethane's persistence in the atmosphere leads to a more uniform distribution of emissions throughout the 24-hour cycle. To confirm this presumption, we compared the chloromethane dataset with a compound known to show clear diel cycles, i.e., isoprene (Yáñez-Serrano et al., 2015).

Figure 4-13 shows overall clear diel patterns for isoprene, spiking over the day and flat at night. The absolute values are in a realistic order of magnitude but must be critically scrutinized, even though they are based on calibration because the method is not optimized for measuring hydrocarbons such as isoprene. However, isoprene is not part of the compound class of halogenated VOCs and therefore will not be discussed in more detail in this work. This data is only intended for a qualitative assessment and therefore fulfills its purpose. It proves that if there were diel cycles for chloromethane, this system would be able to resolve them.

4.6 Analytical Outlook

Over the last pages, the instrumental setup and the method of an Entech 7200CTS preconcentrator coupled with a GC-MS were described. The first results demonstrated the overall functioning of this setup, proving that it enables long-term in situ measurements of halogenated VOCs like chloromethane. As previously mentioned, the described setup is a current version, but it is subject to ongoing refinement and will continue to evolve in the future. Some of these future improvements are evident or even necessary and can therefore be suggested in this analytical outlook.

A first measure for future long-term observations would be to exchange the funnels regularly, i.e., every few weeks or months. The funnels are exposed to harsh conditions, being degraded by sunlight and worn out by thunderstorms. The inlet lines could be improved overall, e.g., by properly reattaching the tube insulation. The inlet tubing of the tower inlet lines could also be shortened by several meters between the tower base and the lab container inlet. This hasn't been done so far because it hasn't been clear if the same tubing would be needed for other experiments or analytical setups. These measures can be seen as optional, as so far, there haven't been any major issues with the inlet line like condensation, rainwater intake, or insect infestation.

One necessary future task would be to measure potential line loss and confirm the residue time of the target analytes within the inlet system. Both can be achieved by attaching the CalGas or any other gas mixture with a known concentration of the target analytes to the inlets while measuring. A study on losses of different atmospheric trace gases using a tall tower PFA inlet line showed no significant losses for most compounds (Li et al., 2023).

Also, as elaborated in Chapter 4.3.5, a permanent calibration setup needs to be implemented to enable remote calibration, as well as the possibility of measuring the CalGas in between the ambient measurements to obtain a day-factor correction. Hereby, the nitrogen MFC should be kept constant while the CalGas MFC would be adjusted for every dilution step to achieve more precise results.

Finally, the change from full-scan method in TIC mode to target analysis in SIM mode should be performed to improve the sensitivity and, in turn, the LODs of the setup and to detect compounds with lower VMRs like chloroform or even brominated compounds.

4.7 Scientific Outlook

The headline of this chapter underscores the essential next step for this project: long-term measurements. This approach is both straightforward and critical. The questions this analytical setup was designed to address can only be answered through sustained, long-term data collection. Such data is essential for reliably capturing diel patterns and understanding how local conditions affect the emission or uptake of halogenated VOCs. Furthermore, accurate assumptions about seasonal variations in the VMRs of these compounds can only be made by analyzing extended datasets. Finally, predicting the net fluxes of the Amazon rainforest in response to ecosystem changes will require robust, long-term data.

One detail that should be considered regarding the tower measurements is the balance between temporal resolution and the resolution of potential height gradients. The first data shows that it might be worth it to include the 150 m inlet line into the ATTO profile measurements, generating data from four different heights, even if this is at the expense of the temporal resolution. This approach applies at least to compounds like chloromethane. For more reactive compounds like

chloroform or bromoform, the opposite might be better: pushing the temporal resolution at the expense of the height profile.

However, this analytical setup can be used for even more versatile approaches than the tower profile measurements. It can also be attached to a soil chamber measurement system, that measures VOCs emitted or taken up by soil. A more campaign-based approach would be to use the instrumental setup to measure halogenated VOC emission from single sources like plants, either in situ or incubated. Also, insect nests such as from termites are interesting in this regard and could be examined for emissions of halogenated VOCs.

Both long-term and campaign-based measurements of single sources are complementary approaches for the same goal: a better understanding of the processes that affect halogenated VOCs in the Amazon rainforest.

4.8 References

5973N MSD Hardware Manual (No. G2589-90001), 1999. Agilent Technologies, Inc., USA.

Carpenter, L.J., Reimann, S., BURKHOLDER, J.B., Clerbaux, C., Hall, B., Hossaini, R., Laube, J., Yvon-Lewis, S., 2014. Chapter 1: Update on Ozone-Depleting Substances (ODSs) and Other Gases of Interest to the Montreal Protocol, in: Ennis, C.A. (Ed.), Scientific Assessment of Ozone Depletion, Global Ozone Research and Monitoring Project Report. World Meteorological Organization (WMO), Geneva, pp. 21–125.

EPA, 1999. Air Method, Toxic Organics-15 (TO-15): Compendium of Methods for the Determination of Toxic Organic Compounds in Ambient Air, Second Edition: Determination of Volatile Organic Compounds (VOCs) in Air Collected in Specially-Prepared Canisters and Analyzed by Gas Chromatography/Mass Spectrometry (GC/MS).

Ganeff, J.M., Jungers, J.C., 1948. Tensions de vapeur du système CH3Cl - CH2Cl2. Bulletin des Soc Chimique 57, 82–87. https://doi.org/10.1002/bscb.19480570109

Gebhardt, S., Colomb, A., Hofmann, R., Williams, J., Lelieveld, J., 2008. Halogenated organic species over the tropical South American rainforest. Atmospheric Chemistry and Physics 8, 3185–3197. https://doi.org/10.5194/acp-8-3185-2008

Gloor, M., Bakwin, P., Hurst, D., Lock, L., Draxler, R., Tans, P., 2001. What is the concentration footprint of a tall tower? Journal of Geophysical Research: Atmospheres 106, 17831–17840. https://doi.org/10.1029/2001JD900021

Heard, D.E. (Ed.), 2007. Analytical techniques for atmospheric measurement, 2. print. ed. Blackwell, Oxford.

Hossaini, R., Atlas, E., Dhomse, S.S., Chipperfield, M.P., Bernath, P.F., Fernando, A.M., Mühle, J., Leeson, A.A., Montzka, S.A., Feng, W., Harrison, J.J., Krummel, P., Vollmer, M.K., Reimann, S., O'Doherty, S., Young, D., Maione, M., Arduini, J., Lunder, C.R., 2019. Recent Trends in Stratospheric Chlorine From Very Short-Lived Substances. Journal of Geophysical Research: Atmospheres 124, 2318–2335. https://doi.org/10.1029/2018JD029400

Li, X.-B., Zhang, C., Liu, A., Yuan, B., Yang, H., Liu, C., Wang, S., Huangfu, Y., Qi, J., Liu, Z., He, X., Song, X., Chen, Y., Peng, Y., Zhang, X., Zheng, E., Yang, L., Yang, Q., Qin, G., Zhou, J., Shao, M., 2023. Assessment of long tubing in measuring atmospheric trace gases: applications on tall towers. Environ. Sci.: Atmos. 3, 506–520. https://doi.org/10.1039/D2EA00110A

Lobert, J.M., Keene, W.C., Logan, J.A., Yevich, R., 1999. Global chlorine emissions from biomass burning: Reactive Chlorine Emissions Inventory. Journal of Geophysical Research: Atmospheres 104, 8373–8389. https://doi.org/10.1029/1998JD100077

Ort, L., Röder, L.L., Parchatka, U., Königstedt, R., Crowley, D., Kunz, F., Wittkowski, R., Lelieveld, J., Fischer, H., 2024. In-flight characterization of a compact airborne quantum cascade laser absorption spectrometer. Atmos. Meas. Tech. 17, 3553–3565. https://doi.org/10.5194/amt-17-3553-2024

Prinn, R.G., Weiss, R.F., Arduini, J., Arnold, T., DeWitt, H.L., Fraser, P.J., Ganesan, A.L., Gasore, J., Harth, C.M., Hermansen, O., Kim, J., Krummel, P.B., Li, S., Loh, Z.M., Lunder, C.R., Maione,

M., Manning, A.J., Miller, B.R., Mitrevski, B., Mühle, J., O'Doherty, S., Park, S., Reimann, S., Rigby, M., Saito, T., Salameh, P.K., Schmidt, R., Simmonds, P.G., Steele, L.P., Vollmer, M.K., Wang, R.H., Yao, B., Yokouchi, Y., Young, D., Zhou, L., 2018. History of chemically and radiatively important atmospheric gases from the Advanced Global Atmospheric Gases Experiment (AGAGE). Earth Syst. Sci. Data 10, 985–1018. https://doi.org/10.5194/essd-10-985-2018

Rudolph, J., Khedim, A., Koppmann, R., Bonsang, B., 1995. Field study of the emissions of methyl chloride and other halocarbons from biomass burning in Western Africa. J Atmos Chem 22, 67–80. https://doi.org/10.1007/BF00708182

Scheeren, H.A., 2003. Reactive hydro- end chlorocarbons in the troposphere and lower stratosphere : sources, distributions, and chemical impact. Ph.D. Thesis.

Schwandner, F.M., Seward, T.M., Giże, A.P., Hall, K., Dietrich, V.J., 2013. Halocarbons and other trace heteroatomic organic compounds in volcanic gases from Vulcano (Aeolian Islands, Italy). Geochimica et Cosmochimica Acta 101, 191–221. https://doi.org/10.1016/j.gca.2012.10.004

Thermal Expansion - Linear Expansion Coefficients [WWW Document], 2003. . The Engineering ToolBox. URL https://www.engineeringtoolbox.com/linear-expansion-coefficients-d_95.html (accessed 9.11.24).

World Meteorological Organization (WMO) (Ed.), 2022. Scientific Assessment of Ozone Depletion: 2022. Geneva.

Yáñez-Serrano, A.M., Nölscher, A.C., Williams, J., Wolff, S., Alves, E., Martins, G.A., Bourtsoukidis, E., Brito, J., Jardine, K., Artaxo, P., Kesselmeier, J., 2015. Diel and seasonal changes of biogenic volatile organic compounds within and above an Amazonian rainforest. Atmos. Chem. Phys. 15, 3359–3378. https://doi.org/10.5194/acp-15-3359-2015

Yokouchi, Y., Ikeda, M., Inuzuka, Y., Yukawa, T., 2002. Strong emission of methyl chloride from tropical plants. Nature 416, 163–165. https://doi.org/10.1038/416163a

5 Conclusions and Future Perspectives

Halogenated Volatile Organic Compounds (XVOCs) are of global relevance. This dissertation has investigated XVOCs in the Amazon rainforest from multiple angles, contributing to a deeper understanding of their sources, sinks, and atmospheric behavior. By integrating various analytical methods and perspectives, this research highlights the complexity and importance of XVOCs in atmospheric chemistry, particularly in the context of climate change and stratospheric ozone depletion.

Isotope ratio mass spectrometry unraveled the first triple-element isotopic fingerprint (^{2}H, ^{13}C, ^{37}Cl) of chloromethane plant emissions and degradations. Even though the investigated plants (royal fern *Osmunda regalis* and club moss *Selaginella kraussiana*) do not have their habitat in the tropics, their isotopic data offer valuable insights into the formation and degradation pathways of chloromethane, as the underlying processes are hypothesized to occur in the Amazon rainforest as well. The findings suggest the potential to use isotope-based models to differentiate between individual sources and sinks of chloromethane which represents a significant step toward resolving the uncertainties in the global chloromethane budget which remains unbalanced despite extensive research. The discovery of a previously unrecognized degradation mechanism further expands the scientific understanding of chloromethane's atmospheric fate. In the future, more experiments of this kind should be carried out to determine isotopic fingerprints of chloromethane formed and degraded by (hyperdominant) plant species of the Amazon rainforest.

The second study, focusing on the halogenated very short-lived substances (VSLSs) chloroform and bromoform, provided key insights into the local emissions and atmospheric behavior of these compounds in the Amazon rainforest. Seasonal and diel patterns of chloroform emissions were detected, with evidence suggesting ground-level sources, including soil, as the primary emitters. However, there are indications that soil is not the only compartment involved in local emission processes. In contrast, bromoform levels were influenced more by long-range transport from marine regions, with only occasional local source indications. The observed seasonal variations, especially during an El Niño Southern Oscillation (ENSO) event, emphasize the need for further studies to understand how such climatic phenomena and global climate change as a whole may affect local and regional VSLS emissions in the future. These studies should include a longer time series of data with better temporal and spatial resolution, both for canopy and soil measurements.

Finally, the implementation and validation of a cryogen-free preconcentration system coupled with a GC-MS at the Amazon Tall Tower Observatory (ATTO) marks a significant advancement in the ability to conduct long-term in situ measurements of XVOCs in the tropical rainforest. This setup, which allows for the continuous monitoring of XVOCs at different heights below and well above the canopy at the ATTO tall tower, complements other methods like adsorbent tube sampling in investigating local source and sink dynamics, as well as diel and seasonal trends. Even though within this doctoral project no long-term data series could be obtained due to unforeseen reasons, the first results presented in this work indicate that such data generated by this system will be crucial for better estimations of XVOC net fluxes from the Amazon rainforest and for understanding how these fluxes may evolve in response to ongoing ecosystem changes and climate variability. The system can also be used to measure suspected single sources or sinks in the form of plant incubation measurements or by being attached to soil chambers.

Overall, this dissertation provided new insights into formation and degradation processes that can mark one step towards improving our understanding of the global chloromethane budget. Measurements of chloroform and bromoform at the ATTO site indicated local sources, in particular for chloroform. These local sources seem to be seasonally dependent, raising questions on how they will evolve in times of global climate change with more frequently occurring ENSO anomalies that

impact the Amazon basin ecosystem. This work laid the foundation to answer this and many other questions in terms of the strength and variability of XVOC sources and sinks by implementing long-term on-line in situ measurements of XVOCs, from CFCs to VSLSs, in the remote Amazon rainforest.

Appendices

Supplementary Material

S.1 Back-Trajectories

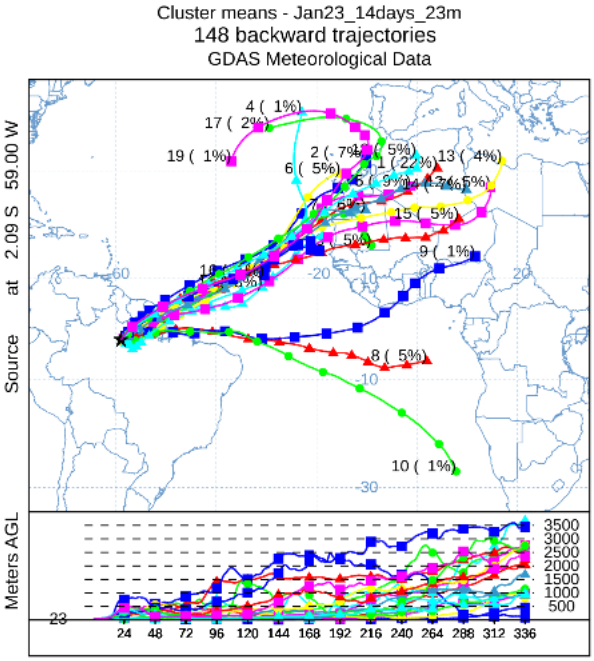

Figure 5-1: *14-day back-trajectories during the sampling period in January 2023 with ATTO coordinates as starting point at 23 m height above ground. Data based on HYSPLIT model (Draxler, 1999; Draxler and Hess, 1997, 1998; Stein et al., 2015).*

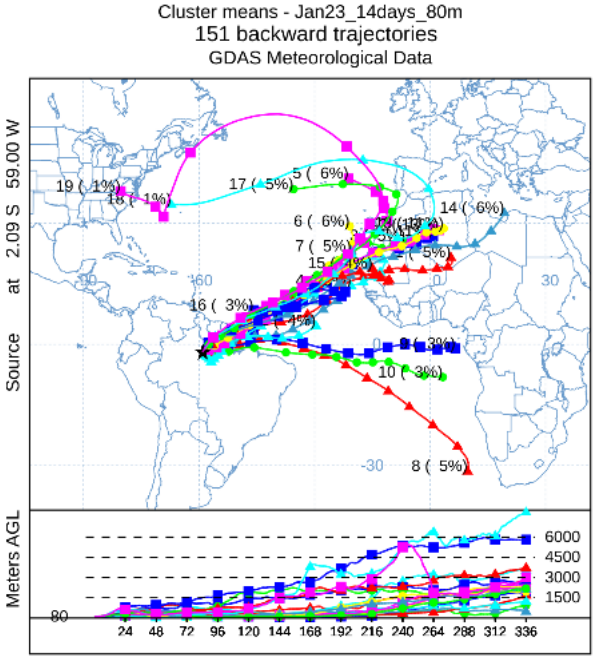

Figure 0-2: *14-day back-trajectories during the sampling period in January 2023 with ATTO coordinates as starting point at 80 m height above ground. Data based on HYSPLIT model (Draxler, 1999; Draxler and Hess, 1997, 1998; Stein et al., 2015).*

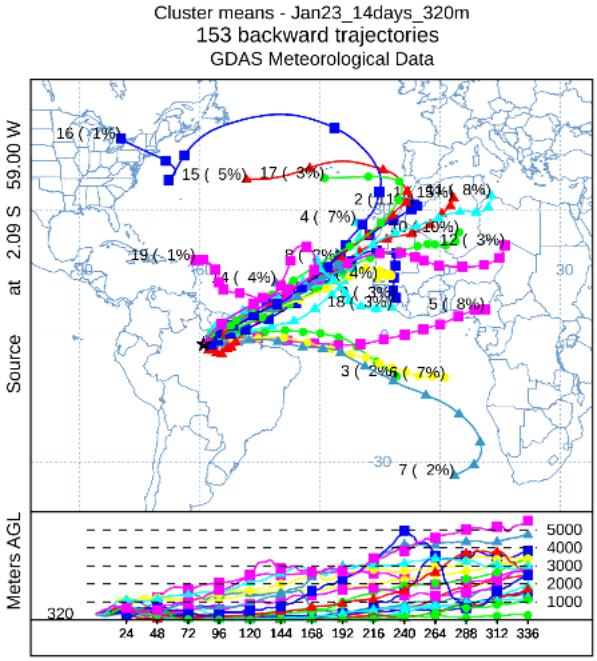

Figure 0-3: *14-day back-trajectories during the sampling period in January 2023 with ATTO coordinates as starting point at 320 m height above ground. Data based on HYSPLIT model (Draxler, 1999; Draxler and Hess, 1997, 1998; Stein et al., 2015).*

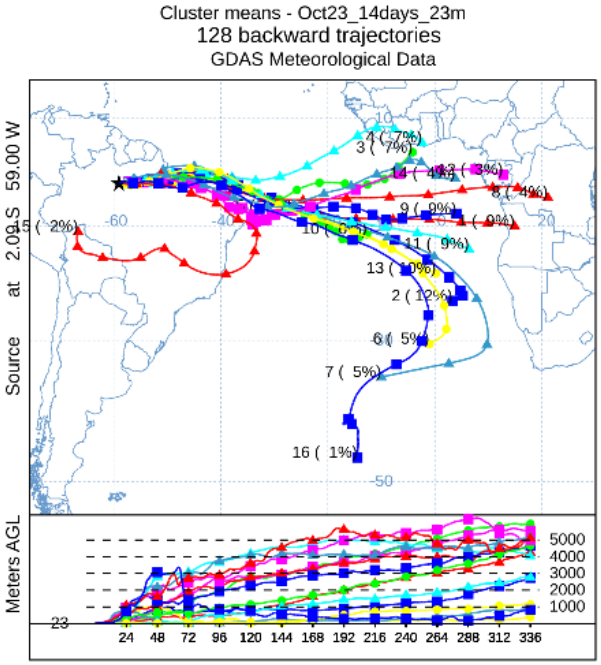

Figure 0-4: *14-day back-trajectories during the sampling period in October 2023 with ATTO coordinates as starting point at 23 m height above ground. Data based on HYSPLIT model (Draxler, 1999; Draxler and Hess, 1997, 1998; Stein et al., 2015).*

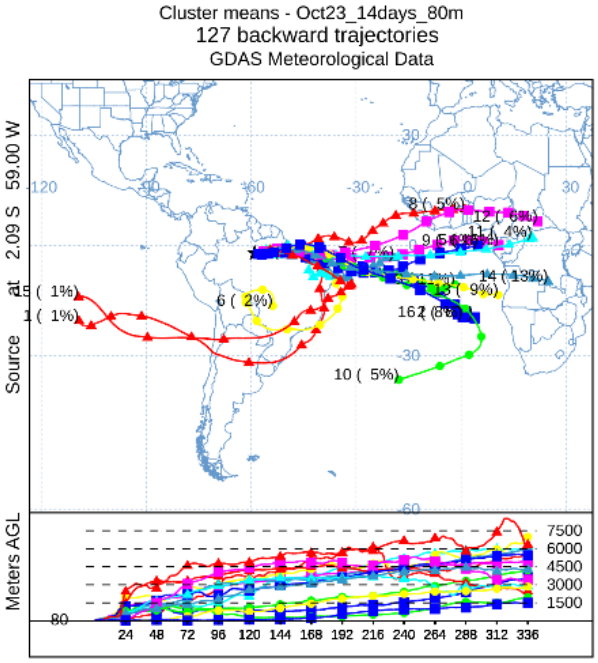

Figure 0-5: *14-day back-trajectories during the sampling period in October 2023 with ATTO coordinates as starting point at 80 m height above ground. Data based on HYSPLIT model (Draxler, 1999; Draxler and Hess, 1997, 1998; Stein et al., 2015).*

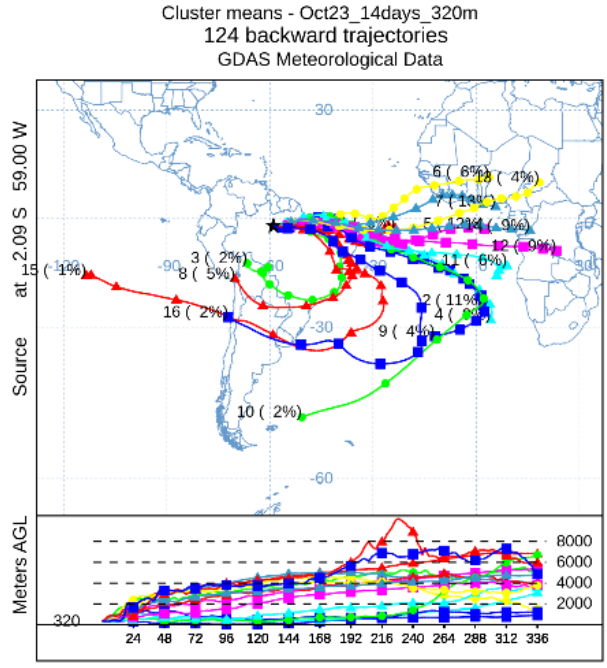

Figure 0-6: *14-day back-trajectories during the sampling period in October 2023 with ATTO coordinates as starting point at 320 m height above ground. Data based on HYSPLIT model (Draxler, 1999; Draxler and Hess, 1997, 1998; Stein et al., 2015).*

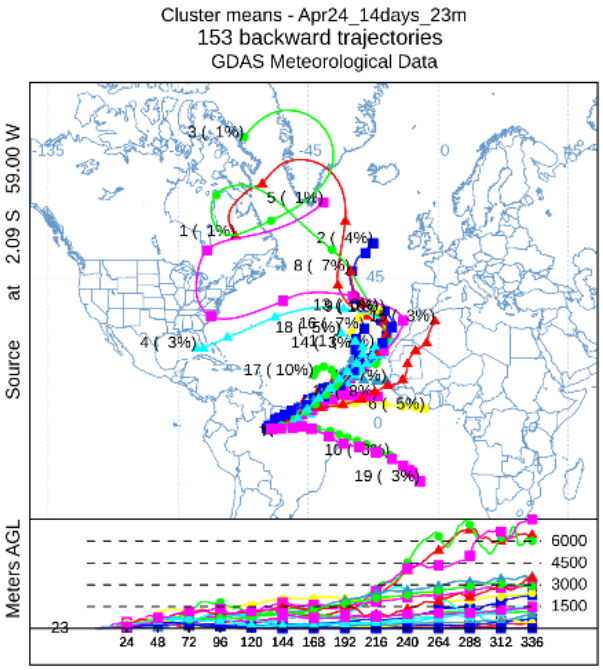

Figure 0-7: *14-day back-trajectories during the sampling period in April/May 2024 with ATTO coordinates as starting point at 23 m height above ground. Data based on HYSPLIT model (Draxler, 1999; Draxler and Hess, 1997, 1998; Stein et al., 2015).*

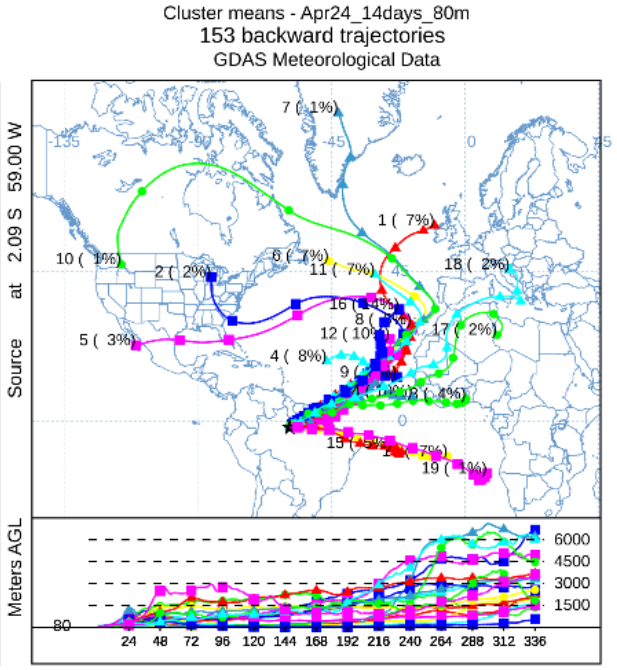

Figure 0-8: *14-day back-trajectories during the sampling period in April/May 2024 with ATTO coordinates as starting point at 80 m height above ground. Data based on HYSPLIT model (Draxler, 1999; Draxler and Hess, 1997, 1998; Stein et al., 2015).*

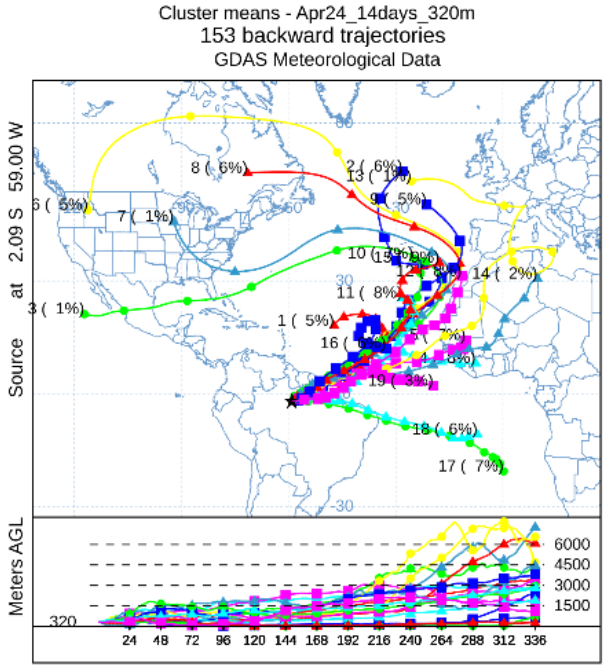

Figure 0-9: *14-day back-trajectories during the sampling period in April/May 2024 with ATTO coordinates as starting point at 320 m height above ground. Data based on HYSPLIT model (Draxler, 1999; Draxler and Hess, 1997, 1998; Stein et al., 2015).*

S.2 Incubation Experiments with *S. kraussiana* and *O. regalis*

Figure 0-10 to **Figure 0-13** show the development of CH_3Cl mixing ratios during the incubation experiments. As all incubation parameters (incubation vessels, amount of plant material, initial CH_3Cl mixing ratio, temperature) remained unchanged, the different emission and degradation rates may reflect a range of natural variability. The ranges of emission and degradation rates given in chapters 2.5.1.1 and 2.5.1.2, respectively, are determined by calculating the rate of the most and least productive incubation vessels of each experiment.

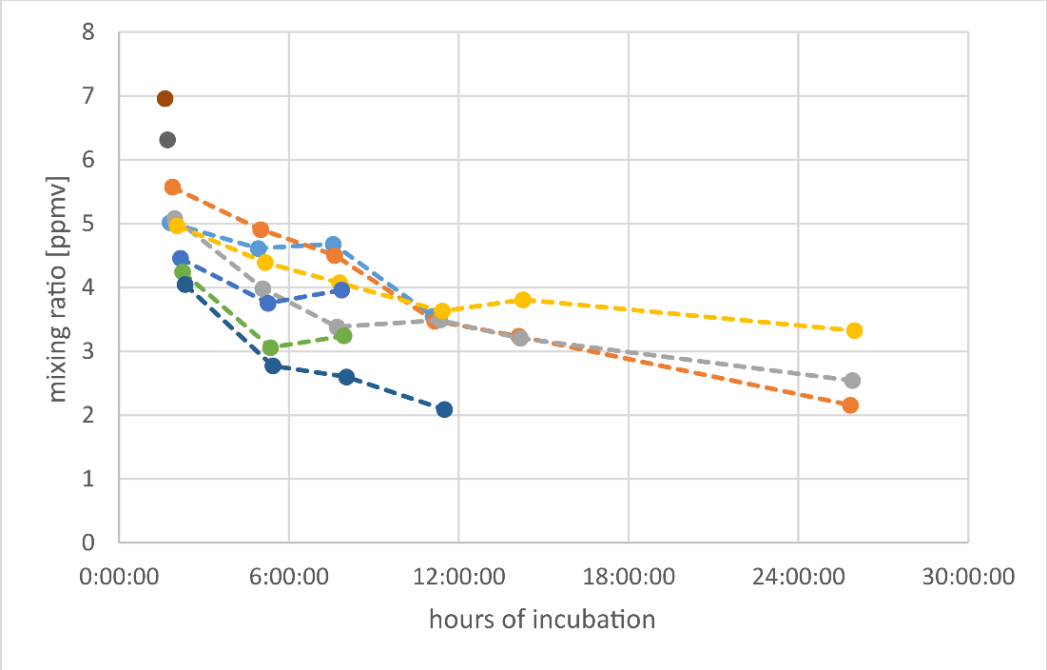

Figure 0-10. *Development of the mixing ratios over time during the first set of degradation experiments with* S. kraussiana. *Each color represents one of the 9 different incubation vessels. The last point of each data series indicates the sampling point for stable hydrogen and stable carbon isotope analysis as described in section 2.4.3.*

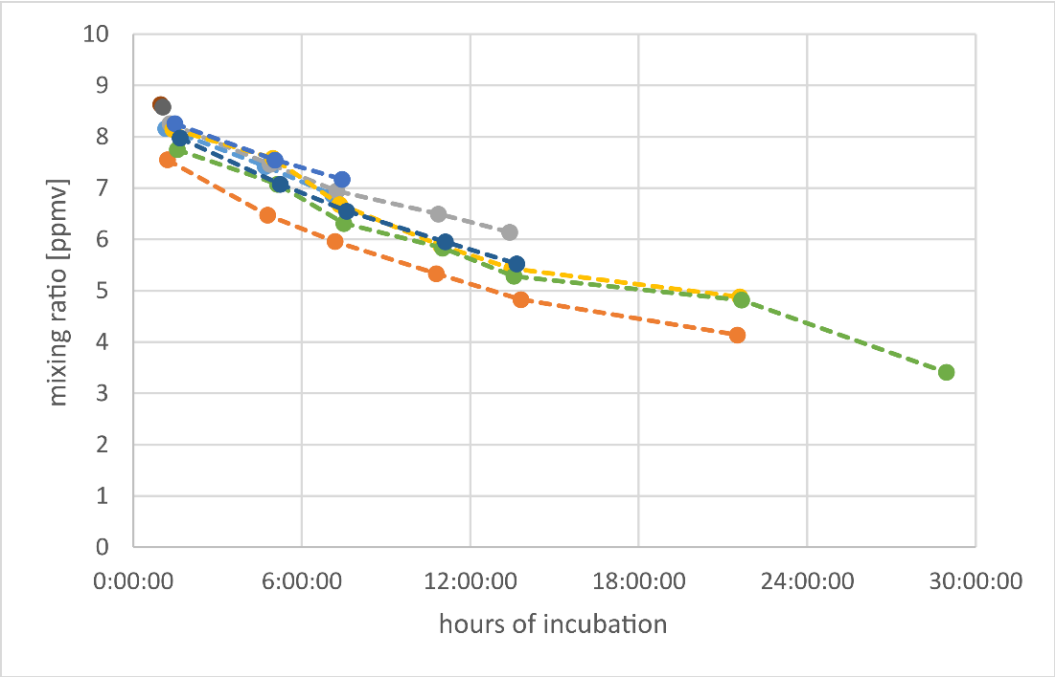

Figure 0-11. *Development of the mixing ratios over time during the second set of degradation experiments with* S. kraussiana. *Each color represents one of the 9 different incubation vessels. The last point of each data series indicates the sampling point for stable chlorine isotope analysis as described in 2.4.3.*

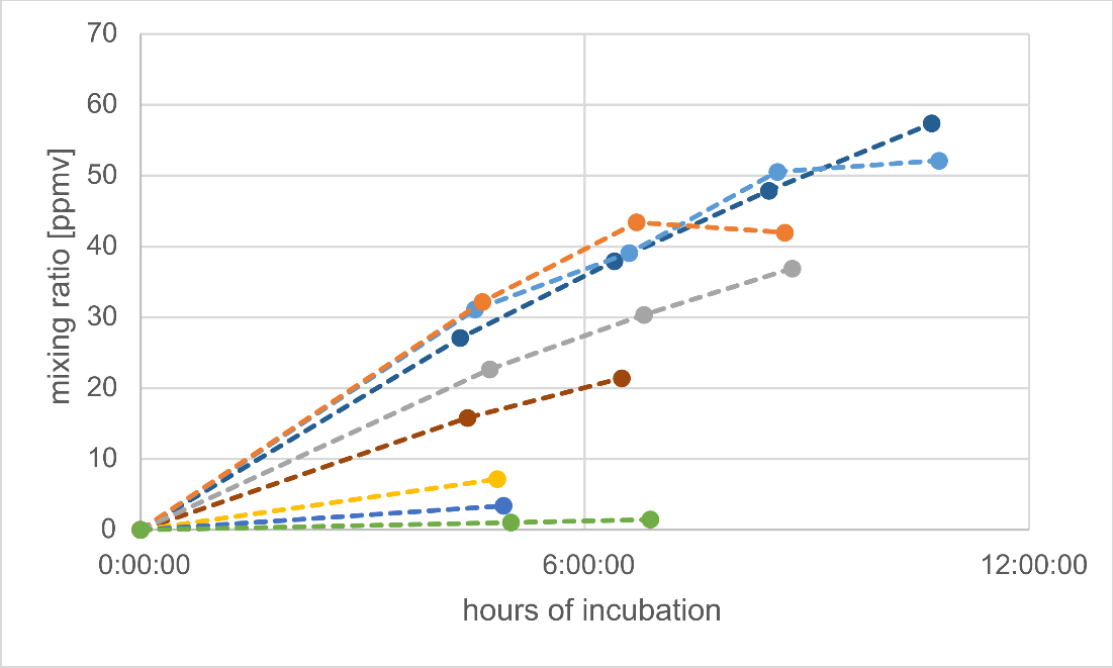

Figure 0-12. *Emission experiment with* O. regalis *carried out in September (2019). Each color represents one of 8 different incubation vessels. Last point of each data series represents extraction of gas samples for stable hydrogen isotope and stable carbon isotope analysis as described in 2.4.3.*

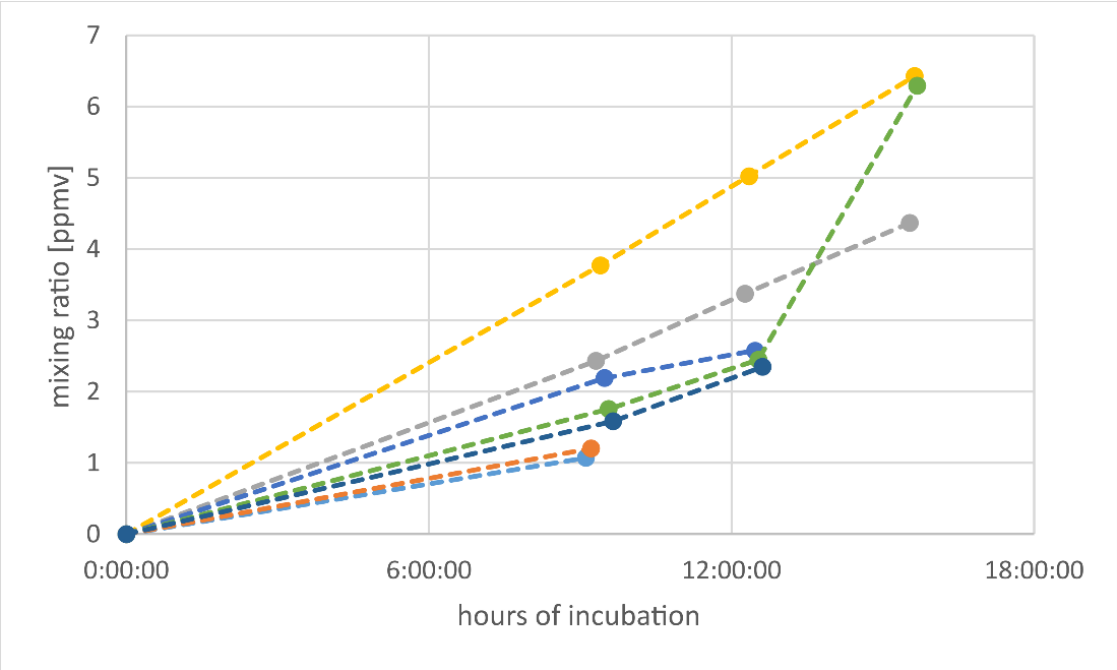

Figure 0-13. *Emission experiment with* O. regalis *carried out in July (2019). Each color represents one of 7 different incubation vessels. Last point of each data series represents extraction of headspace samples for stable chlorine isotope analysis as described in 2.4.3.*

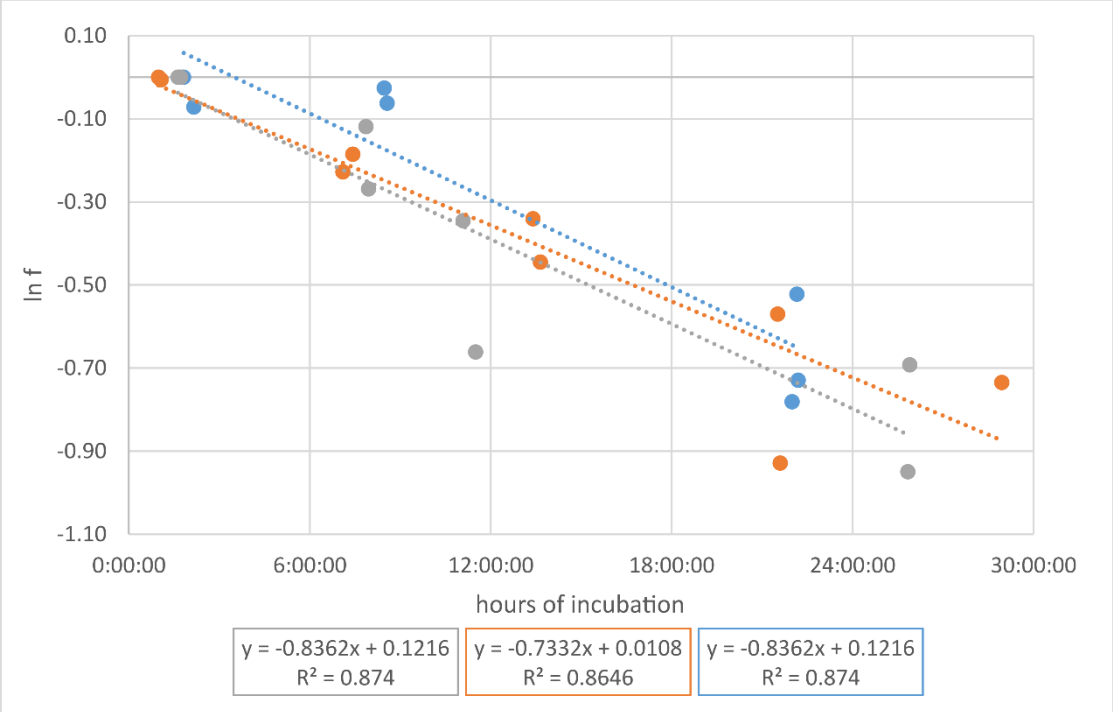

Figure 0-14. *Development of remaining fractions shown as natural logarithms during three degradation experiments* with S. kraussiana. *An overall linear trend is visible for all shown degradation experiments, indicating (pseudo-)first-order kinetics (van Breukelen et al. 2007). The slope of the regression is equivalent to the rate constant expressed in* h^{-1}

S.3 Stable Isotope Blank and Control Experiments

Stable chlorine isotope control measurements with reaction vessels only containing CH_3Cl and no plant material revealed that the CH_3Cl concentration did not change measurably over 25 hours remaining at a level of 9.5 ± 0.5 ppmv. For stable carbon isotopes a change of 0.47 ± 1.23 ‰ (n=3) was measured. The average value of this shift was within analytical uncertainty and hence stable carbon isotopic data was not corrected for this small change. For stable chlorine isotopes blank tests caused a slightly larger shift of $\delta^{37}Cl$ of 0.60 ± 0.07 ‰ (n=3) indicating a slight enrichment over 25 hours. Since this change is beyond the typical uncertainty of ±0.2 ‰ for $\delta^{37}Cl$-CH_3Cl measurements a linear correction was applied to all chlorine isotopic data. For stable hydrogen isotopes controls were not measured because stable carbon isotopes provide a more precise measure for such mass dependent isotope effects. This can be rationalized with the same mass difference between the heavy and light isotopologue of CH_3Cl which is 1 amu (50 for CH_3Cl and 51 for CDH_2Cl and $^{13}CH_3Cl$ respectively). Isotopic fractionation due to physical processes affect the entire molecule and it is irrelevant if the mass difference is caused by hydrogen or carbon. Therefore, carbon provides the more precise measurement of any potential mass dependent isotope effect because the analytical method is more precise (0.5 ‰ uncertainty instead of 5 ‰ for H).

In addition to blank experiments, we conducted control experiments to investigate whether any abiotic processes might change the concentration throughout our experiments. This test was carried out with dried and autoclaved plant material. We added CH_3Cl (~12 ppmv in 20 ml vials, 4 replicates) to 0.2-0.25 g dried biomass of *Selaginella kraussiana* (the same material that was used for previous experiments with living plants). Over an incubation period of 24 h a slight decrease of ~1.2 ppmv was detected in the incubation vessels. We observed a similar concentration decrease in a blank experiment without plant material to which the same amount of CH_3Cl was added. Thus, we assume that the slight decrease in concentration is due to the same loss processes and not related to the interaction with dead biomass. Furthermore, we measured the δ^2H_{CH3Cl} values during these experiments and did not observe any significant change for both dried biomass and control samples. This strongly indicates that no chemical reaction with CH_3Cl occurred during these additional experiments.

List of Figures

Figure 1-1. *Potential chloromethane sources and sinks in a forest ecosystem (atmosphere-plant-soil). Adapted from Keppler et al., 2020. References: [1]Keppler et al., 2000, [2]Nadalig et al., 2011, [3]Hamilton et al., 2003, [4]Jaeger et al., 2018b, [5]Blei et al., 2010, Anke and Weber, 2006, Berberich et al., 2017, [6]Jaeger et al., 2018a. Figure created in Biorender.com* 6

Figure 1-2. *Comparison of long-lived XVOCs and VSLSs concerning their respective sources and atmospheric fate. Taken from WMO, 2022 (Box 1-3 Figure 1).* 7

Figure 1-3. *ATTO site overview, including general key information derived from Andreae et al., 2015 and https://www.attoproject.org/. Figure created in Biorender.com* 9

Figure 1-4. *Sampling sites for XVOC source and product gases from the NOAA and AGAGE networks, together with their respective mean footprints. Taken from WMO, 2022* 10

Figure 2-1. *Isotopic values of hydrogen (a), carbon (b), and chlorine (c) of CH_3Cl emitted by O. regalis. Error bars indicate the overall uncertainty of the corresponding method which is usually 5 ‰ (δ^2H), 0.5 ‰ ($\delta^{13}C$), and 0.2 ‰ ($\delta^{37}Cl$) for a single analysis.* 28

Figure 2-2. *Rayleigh plots for stable hydrogen, stable carbon and stable chlorine isotopic fractionation in CH3Cl during degradation by club moss (S. kraussiana). The linear regressions result from the combination of two separate experiments for which the slopes were indistinguishable based on the standard error. Error bars indicate the analytical uncertainty and the dashed lines show the 95% confidence intervals.* 33

Figure 2-3. *Emission and degradation of CH_3Cl by the two plant species O. regalis and S. kraussiana and associated isotopic fingerprints and isotopic fractionation, respectively. δ_2H and $\delta_{13}C$ values for primary precursors (rain, CO_2) were estimated for the location (Heidelberg) or taken from the literature, respectively. The sizes of the blue arrows (emission, degradation) indicate the approximate relative importance of plant emissions in general.* 34

Figure 3-1. Flow path used for filling of calibration sorbent tubes. Figure created in Biorender.com 44

Figure 3-2. Violin plots of chloroform volume mixing ratios (VMR) from dry-to-wet transition season 2023 (Jan 23; n=80), dry season 2023 (Oct 23; n=112), and full-wet season 2024 (April-May 24; n=158). Samples taken from Instant Tower (23 m sampling height). Black horizontal bars represent the median values of the respective dataset. Limit of detection (LOD) and limit of quantification (LOQ) are displayed in dashed and dotted lines, respectively. 45

Figure 3-3. Violin plots of bromoform volume mixing ratios (VMR) from dry-to-wet transition season 2023 (Jan 23; n=80), dry season 2023 (Oct 23; n=112), and full-wet season 2024 (April-May 24; n=158). Samples taken from Instant Tower (23 m sampling height). Black horizontal bars represent the median values of the respective dataset. Limit of detection (LOD) and limit of quantification (LOQ) are displayed in dashed and dotted lines, respectively. 47

Figure 3-4. Volume mixing ratios (VMR) of chloroform (left) and bromoform (right) throughout the day at 320 m (a, c) and 80 m (b, d) sampling height, respectively. Black horizontal bars: median (n=12 per box for 80 m; n=10 per box for 320 m); boxes: interquartile range (25 to 75 percentiles); whiskers: extend to 1.5 times the IQR from the quartiles; black diamonds: outliers. Limit of

detection (LOD) and limit of quantification (LOQ) are displayed in dashed and dotted lines, respectively. Outliers exceeding the y-axis range are included in the data but not shown in the plot. 50

Figure 3-5. Violin plots of chloroform soil fluxes from dry-to-wet transition season 2023 (Jan 23; n=10), dry season 2023 (Oct 23; n=28), and full-wet season 2024 (April-May 24; n=23). Black horizontal bars represent the median values of the respective dataset. 52

Figure 4-1. Schematic design of the ATTO tall tower inlet system. Figure created in Biorender.com 67

Figure 4-2. Instrumental setup in a laboratory container at the ATTO site. Center: 7200CTS preconcentration unit with operating software (right) and attached GC (left). 68

Figure 4-3. Simplified flow path diagram of the Entech 7200CTS preconcentration system. Kindly provided by Entech Instruments Inc. 69

Figure 4-4. Compilation of 7200CTS method parameters used for the sampling of the ATTO tower inlet lines. The sample preflush duration for the ground-level inlet line is 60 sec; all other parameters are kept the same for both methods. Explanations for the temperatures: “Trapping” refers to the temperatures during the actual trapping of M1. “M1 preheat” refers to the heating of M1 to 90 °C at zero flow before the actual desorption step to allow faster desorption. “M1 Cool Purge” doesn’t apply to the method used. “M1->M2” are the temperatures during M1 desorption and sample transfer to M2. “M2 preheat” is comparable to the same step for M1. “M2 Inject” refers to the desorption temperature of M2 with the subsequent GC injection. “M1 & M2 Bakeout” are the temperatures during the bakeout of both traps which mobilizes any compounds remaining on the trap after regular desorption. 71

Figure 4-5. Temperature profile of the GC. 72

Figure 4-6. Flow path of the calibration setup. Figure created in Biorender.com 76

Figure 4-7. Chloromethane calibration curve derived from MFC setup shown in Figure 4-6. 77

Figure 4-8. Chromatogram of a tenfold diluted CalGas in TIC mode. 77

Figure 4-9. Comparison of two chromatograms of ambient air, one with PFA tubing (black) and one with SilcoNert®-coated stainless steel tubing (blue). Both images show the same chromatograms, whereby the lower image has only been zoomed. 79

Figure 4-10. Chloromethane mixing ratios of ambient air measured at the ATTO tower at ground level (“0 m”), 80 m, and 320 m, respectively, between mid-December 2022 and mid-January 2023. Error bars indicate a systematic uncertainty of 8.66 % for each data point. All times are given in UTC. 80

Figure 4-11. CFC-12 mixing ratios of ambient air measured at the ATTO tower at ground level (“0 m”), 80 m, and 320 m, respectively, between mid-December 2022 and mid-January 2023. Error bars indicate a systematic uncertainty of 8.66 % for each data point. All times are given in UTC. 81

Figure 4-12. Chloromethane mixing ratios of ambient air, normalized by CFC-12, measured at the ATTO tower at ground level (“0 m”), 80 m, and 320 m, respectively, between mid-December 2022

and mid-January 2023. Error bars indicate a systematic uncertainty of 8.66 % for each data point. All times are given in UTC. 84

Figure 4-13. Isoprene mixing ratios of ambient air, normalized by CFC-12, measured at the ATTO tower at ground level ("0 m"), 80 m, and 320 m, respectively, between mid-December 2022 and mid-January 2023. Error bars indicate a systematic uncertainty of 8.66 % for each data point. All times are given in UTC. 85

Figure 0-1: *14-day back-trajectories during the sampling period in January 2023 with ATTO coordinates as starting point at 23 m height above ground. Data based on HYSPLIT model (Draxler, 1999; Draxler and Hess, 1997, 1998; Stein et al., 2015).* 93

Figure 0-2: 14-day back-trajectories during the sampling period in January 2023 with ATTO coordinates as starting point at 80 m height above ground. Data based on HYSPLIT model (Draxler, 1999; Draxler and Hess, 1997, 1998; Stein et al., 2015). 93

Figure 0-3: 14-day back-trajectories during the sampling period in January 2023 with ATTO coordinates as starting point at 320 m height above ground. Data based on HYSPLIT model (Draxler, 1999; Draxler and Hess, 1997, 1998; Stein et al., 2015). 93

Figure 0-4: 14-day back-trajectories during the sampling period in October 2023 with ATTO coordinates as starting point at 23 m height above ground. Data based on HYSPLIT model (Draxler, 1999; Draxler and Hess, 1997, 1998; Stein et al., 2015). 94

Figure 0-5: 14-day back-trajectories during the sampling period in October 2023 with ATTO coordinates as starting point at 80 m height above ground. Data based on HYSPLIT model (Draxler, 1999; Draxler and Hess, 1997, 1998; Stein et al., 2015). 94

Figure 0-6: 14-day back-trajectories during the sampling period in October 2023 with ATTO coordinates as starting point at 320 m height above ground. Data based on HYSPLIT model (Draxler, 1999; Draxler and Hess, 1997, 1998; Stein et al., 2015). 94

Figure 0-7: 14-day back-trajectories during the sampling period in April/May 2024 with ATTO coordinates as starting point at 23 m height above ground. Data based on HYSPLIT model (Draxler, 1999; Draxler and Hess, 1997, 1998; Stein et al., 2015). 95

Figure 0-8: 14-day back-trajectories during the sampling period in April/May 2024 with ATTO coordinates as starting point at 80 m height above ground. Data based on HYSPLIT model (Draxler, 1999; Draxler and Hess, 1997, 1998; Stein et al., 2015). 95

Figure 0-9: 14-day back-trajectories during the sampling period in April/May 2024 with ATTO coordinates as starting point at 320 m height above ground. Data based on HYSPLIT model (Draxler, 1999; Draxler and Hess, 1997, 1998; Stein et al., 2015). 95

Figure 0-10. Development of the mixing ratios over time during the first set of degradation experiments with S. kraussiana. Each color represents one of the 9 different incubation vessels. The last point of each data series indicates the sampling point for stable hydrogen and stable carbon isotope analysis as described in section 2.4.3 96

Figure 0-11. Development of the mixing ratios over time during the second set of degradation experiments with S. kraussiana. Each color represents one of the 9 different incubation vessels. The

last point of each data series indicates the sampling point for stable chlorine isotope analysis as described in 2.4.3. 97

Figure 0-12. Emission experiment with O. regalis carried out in September (2019). Each color represents one of 8 different incubation vessels. Last point of each data series represents extraction of gas samples for stable hydrogen isotope and stable carbon isotope analysis as described in 2.4.3. 97

Figure 0-13. Emission experiment with O. regalis carried out in July (2019). Each color represents one of 7 different incubation vessels. Last point of each data series represents extraction of headspace samples for stable chlorine isotope analysis as described in 2.4.3. 98

Figure 0-14. Development of remaining fractions shown as natural logarithms during three degradation experiments with S. kraussiana. An overall linear trend is visible for all shown degradation experiments, indicating (pseudo-)first-order kinetics (van Breukelen et al. 2007). The slope of the regression is equivalent to the rate constant expressed in h^{-1} 98

List of Tables

Table 1-1. *Principal gas composition of dry air at sea level* 2

Table 2-1. *$\delta^{37}Cl$ Values of Chloride in Rainwater Samples Taken at Three Different Sites in Germany Between April and June 2021* 29

Table 2-2. *$\delta^{33}C$ and $\delta^{2}H$ Values of Methoxy Groups of the two Selected Plant Species* 30

Table 2-3. *Overview of Isotopic Data of CH_3Cl Obtained from Previous Emission and Degradation Experiments* 31

Table 3-1. Pearson correlation coefficients for chloroform and bromoform VMRs and other environmental parameters. 49

Table 4-1. Mass Spec parameters for TIC mode. 73

Table 4-2. Mass Spec parameters for SIM mode 74

Table 4-3. Multi-component calibration mixture in ultra-pure nitrogen. 75

Abbreviations and Acronyms

AGAGE	Advanced Global Atmospheric Gases Experiment
ATTO	Amazon Tall Tower Observatory
AVOCs	Anthropogenic volatile organic compounds
BP	Boiling point
BVOCs	Biogenic volatile organic compounds
CFCs	Chlorofluorocarbons
DMS	Dimethyl sulfide
ENSO	El Niño-Southern Oscillation
FCKW	Fluorchlorkohlenwasserstoffe
GC-MC-ICPMS	Multiple-collector inductively coupled plasma mass spectrometry
GC-MS	Gas chromatography-mass spectrometer
GC-ToF-MS	Gas chromatography-time of flight-mass spectrometer
GWP	Global warming potential
HCFCs	Hydrochlorofluorocarbons
HFCs	Hydrofluorocarbons
IAEA	International Atomic Energy Agency
IPCC	Intergovernmental Panel on Climate Change
IRMS	Isotope ratio-mass spectrometer
ITCZ	Inter-Tropical Convergence Zone
LN	Liquid nitrogen
LOD	Limit of detection
LOQ	Limit of quantification
MBL	Marine boundary layer
MCCTS	Multi-capillary column trapping system
MFC	Mass flow controller
MPIC	Max Planck Institute for Chemistry
MSD	Mass Selective Detector
NMVOCs	non-methane volatile organic compounds
NOAA	National Oceanic and Atmospheric Administration
ODSs	Ozone-depleting substances

ONI	Oceanic Niño Index
OVOCs	Oxygenated volatile organic compounds
PAR	Photosynthetically active radiation
PE	Polyethylene
PFA	Perfluoroalkoxy alkanes
PGI	Product gas injection
ppbv	Parts-per-billion (volume fraction)
ppmv	Parts-per-million (volume fraction)
pptv	Parts-per-trillion (volume fraction)
PTFE	Polytetrafluoroethylene
RH	Relative humidity
ROS	Reactive oxygen species
SAM	S-adenosyl methionine
SGI	Source gas injection
SIM	Selected ion monitoring
SMOC	Standard Mean Ocean Chloride
SVOCs	Semi-volatile organic compounds
TC/EA-IRMS	Thermal combustion/elemental analyzer-isotopic ratio mass spectrometry
TIC	Total ion current
TVOCs	total volatile organic compounds
UPS	Uninterruptible Power Supply
UV	Ultraviolet
VMR	Volume mixing ratio
VOCs	Volatile organic compounds
VPDB	Vienna Pee Dee Belemnite
VSLSs	Halogenated very short-lived substances
VSMOW	Vienna Standard Mean Ocean Water
VVOCs	Very volatile organic compounds
WHO	World Health Organization
WMO	World Meteorological Organization
XVOCs	Halogenated volatile organic compounds

List of Publications: S. C. Hartmann

Publications:

Gomes Alves, E., Taylor, T., Robin, M., Pinheiro Oliveira, D., Schietti, J., Duvoisin Júnior, S., Zannoni, N., Williams, J., Hartmann, S. C., Gonçalves, J. F. C., Schöngart, J., Wittmann, F., and Piedade, M. T. F.: Seasonal shifts in isoprenoid emission composition from three hyperdominant tree species in central Amazonia, Plant Biol J, 24, 721–733, https://doi.org/10.1111/plb.13419, 2022.

Hartmann, S. C., Keppler, F., Greule, M., Lauer, R., and Horst, A.: Triple-Element Stable Isotope Analysis of Chloromethane Emitted by Royal Fern and Degraded by Club Moss, Journal of Geophysical Research: Biogeosciences, 128, e2022JG007256, https://doi.org/10.1029/2022JG007256, 2023.

Keppler, F., Barnes, J. D., Horst, A., Bahlmann, E., Luo, J., Nadalig, T., Greule, M., Hartmann, S. C., and Vuilleumier, S.: Chlorine Isotope Fractionation of the Major Chloromethane Degradation Processes in the Environment, Environ. Sci. Technol., 54, 1634–1645, https://doi.org/10.1021/acs.est.9b06139, 2020a.

Keppler, F., Röhling, A. N., Jaeger, N., Schroll, M., Hartmann, S. C., and Greule, M.: Sources and sinks of chloromethane in a salt marsh ecosystem: constraints from concentration and stable isotope measurements of laboratory incubation experiments, Environ. Sci.: Processes Impacts, 22, 627–641, https://doi.org/10.1039/C9EM00540D, 2020b.

Liu, J., Hartmann, S. C., Keppler, F., and Lai, D. Y. F.: Simultaneous Abiotic Production of Greenhouse Gases (CO_2, CH_4, and N_2O) in Subtropical Soils, JGR Biogeosciences, 124, 1977–1987, https://doi.org/10.1029/2019JG005154, 2019.

Publications in preparation:

Zannoni, N., Hartmann, S. C., Wolff, S., Tsokankunku, A., Soergel, M., Edtbauer, A., Ringsdorf, A., Pfannerstill, E., Ostermann, C., Vega, O., Assis, P., Sà, M., Rodrigues, R., Quaresma, C., Araujò, A., Williams, J.: Atmospheric impact of monoterpenes and sesquiterpenes mixing ratios measured in central Amazonia during 2018-2021 dry and wet seasons, Atmospheric Chemistry and Physics, (*in preparation*), 2024

Zannoni, N., Hartmann, S. C., Tsokankunku, A., Kuhn, U., Ringsdorf, A., Edtbauer, A., Gomes Alves, E., Pinheiro, D., Caetano, M., Assis, P., Williams, J.: Investigating the atmospheric impact of sesquiterpenes emitted from dominant tree species in the Amazon rainforest, Atmospheric Chemistry and Physics, (*in preparation*), 2024

Hartmann, S. C., Byron, J., Pugliese, G., Schüttler, J., Brill, S., Quaresma, C., Monteiro, C., Finck, J., Pöhlker, C., Hoffmann, T., Lelieveld, J., Williams, J.: Investigation of local sources of Chloroform and Bromoform in the Amazon rainforest, Biogeosciences, (*in preparation*), 2024